

## **S-Bos Assessment of Floating offshore wind turbine-Coupled Analysis**

**Auteur** : Malik, Qamar Hassan

**Promoteur(s)** : 15000

**Faculté** : Faculté des Sciences appliquées

**Diplôme** : Master : ingénieur civil mécanicien, à finalité spécialisée en "Advanced Ship Design"

**Année académique** : 2020-2021

**URI/URL** : <http://hdl.handle.net/2268.2/13267>

---

### *Avertissement à l'attention des usagers :*

*Tous les documents placés en accès ouvert sur le site le site MatheO sont protégés par le droit d'auteur. Conformément aux principes énoncés par la "Budapest Open Access Initiative"(BOAI, 2002), l'utilisateur du site peut lire, télécharger, copier, transmettre, imprimer, chercher ou faire un lien vers le texte intégral de ces documents, les disséquer pour les indexer, s'en servir de données pour un logiciel, ou s'en servir à toute autre fin légale (ou prévue par la réglementation relative au droit d'auteur). Toute utilisation du document à des fins commerciales est strictement interdite.*

*Par ailleurs, l'utilisateur s'engage à respecter les droits moraux de l'auteur, principalement le droit à l'intégrité de l'oeuvre et le droit de paternité et ce dans toute utilisation que l'utilisateur entreprend. Ainsi, à titre d'exemple, lorsqu'il reproduira un document par extrait ou dans son intégralité, l'utilisateur citera de manière complète les sources telles que mentionnées ci-dessus. Toute utilisation non explicitement autorisée ci-avant (telle que par exemple, la modification du document ou son résumé) nécessite l'autorisation préalable et expresse des auteurs ou de leurs ayants droit.*

---



POLITÉCNICA



Universität  
Rostock



Traditio et Innovatio



SOLENT  
UNIVERSITY  
SOUTHAMPTON



Zachodniopomorski  
Uniwersytet  
Techniczny  
w Szczecinie



With the support of the  
Erasmus+ Programme  
of the European Union



# S-bos Assessment of Floating Offshore Wind Turbine-Coupled Analysis

Submitted on 25<sup>th</sup> August 2021

by

MALIK, QAMAR HASSAN | Akbar colony, Street No. 4 | 4000, Multan, PAKISTAN

[gamarmalik15@yahoo.com](mailto:gamarmalik15@yahoo.com)

Student ID No. S194322

## Supervisor:

Sergio Hernandez Blanco

Naval Architect & Marine Engineer

BLUENEWABLES

Greater Madrid Metropolitan Area.

Madrid, Spain

## Reviewer:

Professor Pierre Ferrant

École Centrale de Nantes (ECN), Nantes, France

LHEEA Lab.1 Rue de la Noë 92101

F-44321 Nantes Cedex 3

Nantes, France



## ABSTRACT

For large-scale electricity generation offshore wind power is becoming more popular around the world, and wind energy systems have emerged as a promising technology for using offshore wind resources. Large offshore wind energy systems have been installed and are being proposed for operation in offshore areas where environmental constraints are less stringent, large wind resources exist, and open sea areas are available for wind farm development, based on the maturity of wind turbine and floater technologies developed by the wind energy and oil and gas industries, respectively.

The BlueNewables designed S-bos floating wind platform which is a semi-submersible concept that aims to minimize installation, transportation, and maintenance costs while providing outstanding stability in harsh wind and wave environments. The primary goal of this thesis was to conduct a so-called coupled assessment of the S-bos platform. For the implementation, an Aero-Hydro-Servo-Elastic numerical model was used. The existence of diffraction, inertial, and viscous forces for various wave regimes makes modeling for the S-bos platform more difficult. By only applying hydrodynamic theories, are not enough to accurately predict the seakeeping of the structure to wave loading on their own as the main problem is aero/elasticity. Two hydrodynamic methodologies were studied in this thesis, first one was morison's equation approach and the other being a potential flow theory approach. The latter was accomplished with the help of ANSYS-AQWA, a wave interaction analysis software. The time domain calculations were performed in OrcaFlex software. Furthermore, experimental scaled tests are not done yet but they will be used to validate the numerical models. The numerical models were validated by comparing them to estimated values of the free decay testing with mooring lines. The linear damping coefficients and quadratic damping coefficients were calculated during the calibration procedure and quadratic terms were used for the numerical model. Finally, displacement response amplitude operators (RAOs) were calculated to reveal differences in wave loading modeling and behavior of the S-bos platform. The blades and tower were taken from the reference of IEA 15MW. Following the establishment of the fully coupled model, the analysis were carried out in OrcaFlex using a set of critical Design load cases (DLCs) in accordance with IEC international standards for the design of floating wind platforms.

## **ACKNOWLEDGEMENTS**

I'd like to express my gratitude to my supervisors, Sergio Hernandez Blanco and Bernardino Counago, for their superb guidance throughout this Master Thesis. They were the terrific source of advice as my thesis advisor and helped me better grasp how the coupled analysis of my work should be integrated into the whole project. Special thanks to the BlueNewables team especially Alfonso for enabling me to work on this amazing concept and for sharing their experience and encouragement throughout the process, even during the Covid\_19. My supervisor Bernardino Counago was not only my supervisor during my stay in Bluenewables but also he is a great team leader and his piece of advice gave me so much motivation that I am ready to enter in practical life with full dedication.

Secondly, I am thankful to the Erasmus Mundus Program (EMSHIP+) especially the Coordinator, Professor Philippe RIGO, who gave me the chance to prove my abilities on a different and high level.

Finally, I'd like to express my sincere affection and gratitude for my parents. During the time of pandemic their love and support was amazing. Their patience and encouragement have been crucial over the period I've been working on my research.

**Contents**

**ABSTRACT..... I**

**ACKNOWLEDGEMENTS..... II**

**DECLARATION OF AUTHORSHIP..... X**

**1. INTRODUCTION..... 1**

**1.1 Motivation.....1**

**1.2 Historical Development of FOWT.....2**

**1.3 Introduction to TLP, SPAR AND SEMI SUBMERSIBLE..... 3**

**1.4 AERO-HYDRO-SERVO-ELASTIC (ASHE) or Coupled Analysis.....6**

**2. THE S-BOS PLATFORM FROM BLUENEWABLES.....8**

**2.1 The S-bos Platform..... 8**

**2.2 Modes of motion of the platform..... 9**

**2.3 Moments caused on the platform..... 10**

*2.3.1 Wave loading on the platform..... 10*

*2.3.2 Forces and Moments on the Platform..... 11*

*2.3.3 Wind turbine..... 13*

*2.3.4 Coordinate System..... 15*

**2.4 Conditions of Loading..... 15**

**3. OCEANOLOGY.....17**

**3.1 Environmental Loads..... 17**

**3.2 Site of the project (Canary Islands)..... 17**

**3.3 Water Depth..... 18**

**3.4 Wave Height..... 18**

*3.4.1 Significant Wave Height (Hs)..... 19*

*3.4.2 Wave Rose..... 19*

**3.5 Wind Environment..... 20**

*3.5.1 Wind Data..... 20*

*3.5.2 Wind Profile Law.....21*

*3.5.3 Output from the Wind Turbine..... 23*

*3.5.4 Wind Rose..... 23*

**3.6 Currents..... 24**

**4. HYDRODYNAMIC MODEL..... 25**

**4.1 Statement of the Problem.....25**

4.2	Literature Review.....	25
4.3	Structural Description of the Model.....	26
4.4	Numerical Method.....	28
4.4.1	<i>Hydrodynamic Method Description</i> .....	29
4.4.2	<i>Morison Theory</i> .....	30
4.4.3	<i>Diffraction Theory</i> .....	31
4.4.4	<i>Simulation and Modelling Software's Description</i> .....	33
4.4.5	<i>Method Validation of hydrodynamics of S-bos Platform</i> .....	35
4.4.6	<i>Aerodynamic model description for S-bos Platform</i> .....	37
4.4.7	<i>Method Validation of Aerodynamics</i> .....	38
4.5	Numerical Analysis.....	39
4.6	Diffraction Analysis.....	40
4.6.1	<i>Motion RAOs</i> .....	40
4.6.2	<i>Heave</i> .....	41
4.6.3	<i>Roll</i> .....	42
4.6.4	<i>Pitch</i> .....	42
4.7	First order wave forces.....	43
4.8	Radiation damping and Additional Damping.....	45
5.	TURBINE CONTROLLER.....	47
6.	MOORING SYSTEM.....	48
7.	DEFINITION OF THE NUMERICAL MODEL.....	53
7.1	General Arrangement (G.A).....	54
7.2	S-bos Model Mesh.....	55
7.3	Rotor-Nacelle-Assembly (RNA).....	56
7.4	Tower.....	58
8.	TIME DOMAIN SIMULATIONS.....	60
8.1	Coupled Analysis.....	2
8.2	Design Load Cases.....	3
8.3	Parameters and Calculation for the DLCs.....	4
8.4	Results and Discussions.....	7
8.4.1	<i>DLC 1.2 NTM 7.5 m/s Hs 1.5m and Tp 8s</i> .....	7
8.4.2	<i>DLC 1.2 NTM 10.59 m/s, Hs 1.5m and Tp 8s</i> .....	10
8.4.3	<i>DLC 1.2 NTM 14.00 m/s, Hs 1.5m and Tp 8s</i> .....	12
8.4.4	<i>DLC 1.6 NTM 10.59 m/s, Hs 5.11m and Tp 11.08s</i> .....	15

<b>8.4.5</b>	<b><i>DLC 6.1 EWM 37.41 m/s, Hs 5.11m and Tp 11.08s</i></b> .....	<b>17</b>
<b>8.4.6</b>	<b><i>Discussion of the Results</i></b> .....	<b>20</b>
<b>8.4.7</b>	<b><i>Generator power for DLCs 1.2, 1.6 and 6.1</i></b> .....	<b>22</b>
<b>9.</b>	<b>FUTURE WORK</b> .....	<b>24</b>
<b>10.</b>	<b>CONCLUSION</b> .....	<b>25</b>
	<b>REFERENCES</b> .....	<b>27</b>

## List of Figures

Figure 1: Nacelle of a FWOT (Source: pngitem.com).....	xii
Figure 2: Electricity System of a FWOT (Source: researchgate.net).....	xii
Figure 3: Control System of FWOT (Source: sciencedirect.com).....	xiii
Figure 4: Generator system of FWOT (Source: windpowermonthly.com).....	xiv
Figure 5: Rotor of a FWOT (Source: offshore-mag.com).....	xiv
Figure 6: Gear Box of FWOT (Source: wind power engineering).....	xv
Figure 7: Tower of FWOT (Source: Sciencedirect.com).....	xvi
Figure 8: Annual global wind capacity (source: Historical values based on IRENA’s renewable capacity statistics (IRENA, 2019d), and future projections based on IRENA analysis (IRENA, 2019a) .....	2
Figure 9: Types of floating wind turbines [Source: International Renewable Energy Agency [IRENA], 2016] [7].....	4
Figure 10: Sea-to-land ratios of ultimate loads from DLCs 1.1, 1.3, 1.4 and 1.5 for the MIT/NREL TLP, OC3-Hywind Spar and ITI Energy Barge (Source: NREL- Sea-to-land ratios of ultimate loads from DLCs 1.1, 1.3, 1.4, and 1.5).....	5
Figure 11: Description of coupled analysis (ASHE).....	6
Figure 12: AERO-HYDRO-SERVO-ELASTIC (ASHE) Coupled Analysis behaviors (Source: mdpi.com).....	7
Figure 13: S-bos platform.....	9
Figure 14: Stability of S-bos Platform.....	10
Figure 15: Platform Motion Nomenclature.....	12
Figure 16: Surge, sway, heave, roll, pitch, and yaw are the rigid-body movements of a floating structure. Source [11].....	13
Figure 17: Forces and moments on a stationary airfoil [Source: pilotfriend].....	14
Figure 18: Coordinate system used in the Analysis (Source: OrcaFlex).....	15
Figure 19: Pinned Location in the Gran Canaria (Source: SIMAR point 4038008, Puertos Del Estado) .....	18
Figure 20: Wave Rose of Hs in Gran Canaria (Source: Puertos Del Estado).....	20
Figure 21: Monthly wind speed and monthly maximum wind speed (Puertos Del Estado).....	22
Figure 22: Power curve for 15MW Wind turbine [25].....	23
Figure 23: Wind Rose in Gran Canaria (Puertos Del Estado).....	24
Figure 24: Multibody and FEM representations are depicted.....	27
Figure 25: RAO for heave motion of waves with -180 degree direction.....	41



Figure 26: RAO for roll motion of waves with 90 degree direction.....	42
Figure 27: RAO for Pitch motion of waves with -180 degree direction.....	43
Figure 28: Wave Excitation forces of S-bos.....	44
Figure 29: Total forces on the Platform.....	45
Figure 30: Frequency dependent Added Mass and Radiation Damping matrices.....	46
Figure 31: Quasi-static model's schematic diagram (source: MDPI).....	48
Figure 32: Description of dynamic mooring model.....	49
Figure 33: Mooring lines configuration schematic from OrcaFlex.....	50
Figure 34: Mooring Line analysis diagram (Source: CENER).....	50
Figure 35: Studless chain link illustration (Source: www.vicinaycadenas.com).....	52
Figure 36: Illustration of ASHE in OrcaFlex Model.....	53
Figure 37: Top-view and Side-view of the S-bos Platform.....	54
Figure 38: S-Bos model with Mesh.....	55
Figure 39: Decay test for the Heave.....	61
Figure 40: Decay test for the Roll.....	2
Figure 41: Decay test for Pitch.....	2
Figure 42: Submerged area consideration for S-bos Platform corner view.....	5
Figure 43: Drag coefficient consideration (Source: DNV-RP-C205).....	6
Figure 44: PITCH for DLC 1.2 NTM 7.5 m/s, Hs 1.5m and Tp 8s.....	7
Figure 45: MPME Heave for DLC 1.2 NTM 7.5 m/s, Hs 1.5m and Tp 8s.....	7
Figure 46: MPME Surge for DLC 1.2 NTM 7.5 m/s, Hs 1.5m and Tp 8s.....	8
Figure 47: Hub Acceleration for DLC 1.2 NTM 7.5 m/s, Hs 1.5m and Tp 8s.....	8
Figure 48: MPME Bending Moment (Tower Base) for DLC 1.2 NTM 7.5 m/s, Hs 1.5m and Tp 8s.....	8
Figure 49: MPME Line Tension for DLC 1.2 NTM 7.5 m/s, Hs 1.5m and Tp 8s.....	9
Figure 50: MPME Pitch for DLC 1.2 NTM 10.59 m/s, Hs 1.5m and Tp 8s.....	10
Figure 51: MPME Surge for DLC 1.2 NTM 10.59 m/s, Hs 1.5m and Tp 8s.....	10
Figure 52: MPME Heave for DLC 1.2 NTM 10.59 m/s, Hs 1.5m and Tp 8s.....	10
Figure 53: Hub Acceleration for DLC 1.2 NTM 10.59 m/s, Hs 1.5m and Tp 8s.....	11
Figure 54: MPME Bending Moment (Tower Base) for DLC 1.2 NTM 10.59 m/s, Hs 1.5m and Tp 8s .....	11
Figure 55: MPME Line Tension for DLC 1.2 NTM 10.59 m/s, Hs 1.5m and Tp 8s.....	11
Figure 56: MPME Pitch for DLC 1.2 NTM 14 m/s, Hs 1.5m and Tp 8s.....	12
Figure 57: MPME Surge for DLC 1.2 NTM 14 m/s, Hs 1.5m and Tp 8s.....	13
Figure 58: MPME Heave for DLC 1.2 NTM 14 m/s, Hs 1.5m and Tp 8s.....	13
Figure 59: Hub Acceleration for DLC 1.2 NTM 14 m/s, Hs 1.5m and Tp 8s.....	13

Figure 60: MPME Bending Moment (Tower Base) for DLC 1.2 NTM 14 m/s, Hs 1.5m and Tp 8s....	14
Figure 61: MPME Line Tension for DLC 1.2 NTM 14 m/s, Hs 1.5m and Tp 8s.....	14
Figure 62: MPME Pitch for DLC 1.6 NTM 10.59 m/s, Hs 5.11m and Tp 11.08s.....	15
Figure 63: MPME Surge for DLC 1.6 NTM 10.59 m/s, Hs 5.11m and Tp 11.08s.....	15
Figure 64: MPME Heave for DLC 1.6 NTM 10.59 m/s, Hs 5.11m and Tp 11.08s.....	15
Figure 65: Hub Acceleration for DLC 1.6 NTM 10.59 m/s, Hs 5.11m and Tp 11.08s.....	16
Figure 66: MPME Bending Moment (Tower Base) for DLC 1.6 NTM 10.59 m/s, Hs 5.11m and Tp 11.08s.....	16
Figure 67: MPME Line Tension for DLC 1.6 NTM 10.59 m/s, Hs 5.11m and Tp 11.08s.....	16
Figure 68: MPME Pitch for DLC 6.1 EWM 37.41 m/s, Hs 5.11m and Tp 11.08s.....	17
Figure 69: MPME Surge for DLC 6.1 EWM 37.41 m/s, Hs 5.11m and Tp 11.08s.....	18
Figure 70: MPME Heave for DLC 6.1 EWM 37.41 m/s, Hs 5.11m and Tp 11.08s.....	18
Figure 71: Hub Acceleration for DLC 6.1 EWM 37.41 m/s, Hs 5.11m and Tp 11.08s.....	18
Figure 72: MPME Bending Moment (Tower Base) for DLC 6.1 EWM 37.41 m/s, Hs 5.11m and Tp 11.08s.....	19
Figure 73: MPME Line Tension for DLC 6.1 EWM 37.41 m/s, Hs 5.11m and Tp 11.08s.....	19
Figure 74: Generator power for DLCs 1.2, 1.6 and 6.1 by showing Generator power.....	22

# List of Tables

Table 1: S-bos platform coordinates.....17

Table 2: Wave Data for the Location of Gran Canaria (Source: Flotant D.4.1 – STRUCTURAL AND NAVAL ARCHITECTURE DESIGN BASIS)..... 19

Table 3: Hs/Tp Scatter Diagram (Source: Puertos Del Estado)..... 19

Table 4: Normal and Extreme Wind Speed of Gran Canaria..... 22

Table 5: Current Induced by wind speed at sea surface at Gran Canaria (Flotant D.4.1, pg. 51)..... 24

Table 6: Mooring lines configuration main parameters and properties.....51

Table 7: Chain Link Diameters..... 52

Table 8: Mesh parameters in AQWA for S-bos Model.....56

Table 9: IEC 15 MW main parameters for RNA used for S-bos..... 57

Table 10: Inertia properties of the tower..... 58

Table 11: IEC 15 MW main parameters for reference Tower used for S-bos.....59

Table 12: Calculated Natural periods for S-bos..... 60

Table 13: Natural period comparison of the Estimated Values and OrcaFlex-AQWA models for the degrees of freedom of heave, pitch, and roll using decay tests..... 2

Table 14: DLCs (Design Load Cases) consideration for the Sbos Structure..... 4

Table 15: Ref. mean wind speed calculation for all considered DLCs..... 5

Table 16: Calculation of the force applied on the S-bos platform induced by currents for the DLCs 1.6 and 6.1..... 6

Table 17: Parameters calculated for DLC 1.2 NTM, 7.5 m/s, Hs 1.5m and Tp 8s..... 9

Table 18: Parameters calculated for DLC 1.2 NTM 10.59 m/s, Hs 1.5m and Tp 8s..... 12

Table 19: Parameters calculated for DLC 1.2 NTM 14 m/s, Hs 1.5m and Tp 8s..... 14

Table 20: Parameters calculated for DLC 1.6 NTM 10.59 m/s, Hs 5.11m and Tp 11.08s..... 17

Table 21: Parameters calculated for DLC 6.1 EWM 37.41 m/s, Hs 5.11m and Tp 11.08s.....19

## Declaration of Authorship

I declare that this thesis and the work presented in it are my own and have been generated by me as the result of my own original research.

Where I have consulted the published work of others, this is always clearly attributed.

Where I have quoted from the work of others, the source is always given. With the exception of such quotations, this thesis is entirely my own work.

I have acknowledged all main sources of help.

Where the thesis is based on work done by myself jointly with others, I have made clear exactly what was done by others and what I have contributed myself.

This thesis contains no material that has been submitted previously, in whole or in part, for the award of any other academic degree or diploma.

I cede copyright of the thesis in favor of the University of Liege, Belgium and University of Polytechnic de Madrid, Spain.

Date: 15, August 2021

Signature

A handwritten signature in black ink, consisting of a circular emblem on the left and a series of stylized, overlapping strokes extending to the right. The signature is written over a horizontal line.

## **Overview of Offshore Floating Wind Turbine Technology**

The offshore wind community is working to build efficient floating wind turbine technology that can take advantage of the abundant deep-water wind resource. To predict the coupled aero-hydro-servo-elastic behavior of such systems, validated numerical simulation tools are needed. The use of wind turbines to generate electricity has risen in popularity over the last decade.

### **Components of a Floating offshore wind turbine (FOWT)**

A wind turbine is a machine that transforms wind's kinetic energy into useful work output. Electrical power can be used as the output. An offshore wind farm is a power plant that includes all of the facilities necessary to collect wind energy, convert it to electricity, and distribute it to the main electricity grid. The wind turbines, cables, rotor, drive train, moorings, nacelle, generator, tower and turbine, control system, electrical power system and substations are the key components of a floating offshore wind turbine. The turbines are the most crucial component. Wind turbines are essentially generators that turn wind energy into electrical energy. Many wind turbines are built at the same time in one location for economic purposes, such as lowering planning, design, and maintenance costs. Horizontal Axis Wind Turbines (HAWT) are the most popular wind turbine design. The Horizontal Axis Wind Turbines (HAWT) output shaft is parallel to the level. There are seven main subsystems in a wind turbine which are as follows:

#### **Nacelle**

The nacelle of an offshore wind turbine varies from that of a land-based wind turbine in that it is sealed to prevent sea air from entering. The heat produced by the wind turbine machinery is transferred to the ocean air passing over the nacelle through a cooling system. The generator and drive train are located in the nacelle, which is a structure. The wind turbine equipment is protected from the elements by this arrangement. The nacelle's alignment is governed by the yaw mechanism. The nacelle is linked to the tower's top by this device. All upwind wind turbines must have their yaw orientation actively regulated so that the rotor faces the wind. Some downwind turbines have free yaw systems that automatically sync themselves with the

wind. The gyroscopic moment produced by a wind turbine is proportional to the rate of yaw and the rotational inertia of the rotor. As a consequence, the nacelle's yaw rate must be reduced. A pinion and bull gear arrangement is commonly used for active yaw control.



Figure 1: Nacelle of a FWOT (Source: pngitem.com)

### Electricity System

The generator's electrical output must be fed into the electric grid or into an electric load. Other electrical components that pass through the outlet include wires, transformers, power factor correction capacitors, solid state power converters, and switchgear. Solid state power converters are used in some wind turbine designs for improved flexibility. The output voltage is normally increased to 34.5 kilovolts. Offshore wind turbines usually transmit energy through cables buried beneath the seabed.

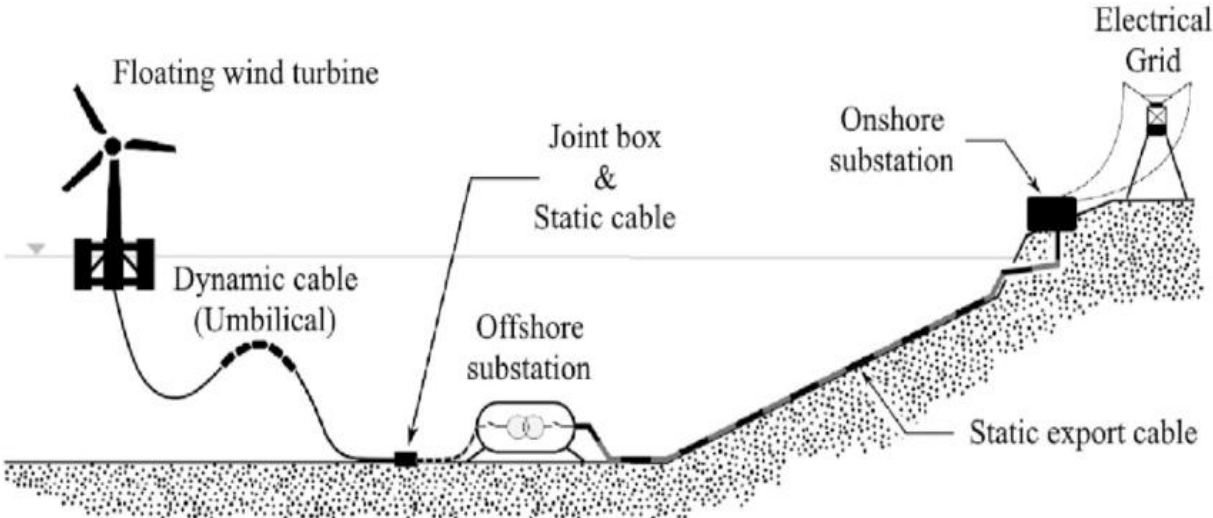


Figure 2: Electricity System of a FWOT (Source: researchgate.net)

## Control System

A wind turbine's blade pitch, nacelle yaw, and generator loading are all controlled by the control system. To adjust the amount of torque generated by the rotor, the control system may change the pitch of the blades. The control system's aim is to optimize power output while reducing fatigue. Manufacturers use a number of methods to achieve this goal.

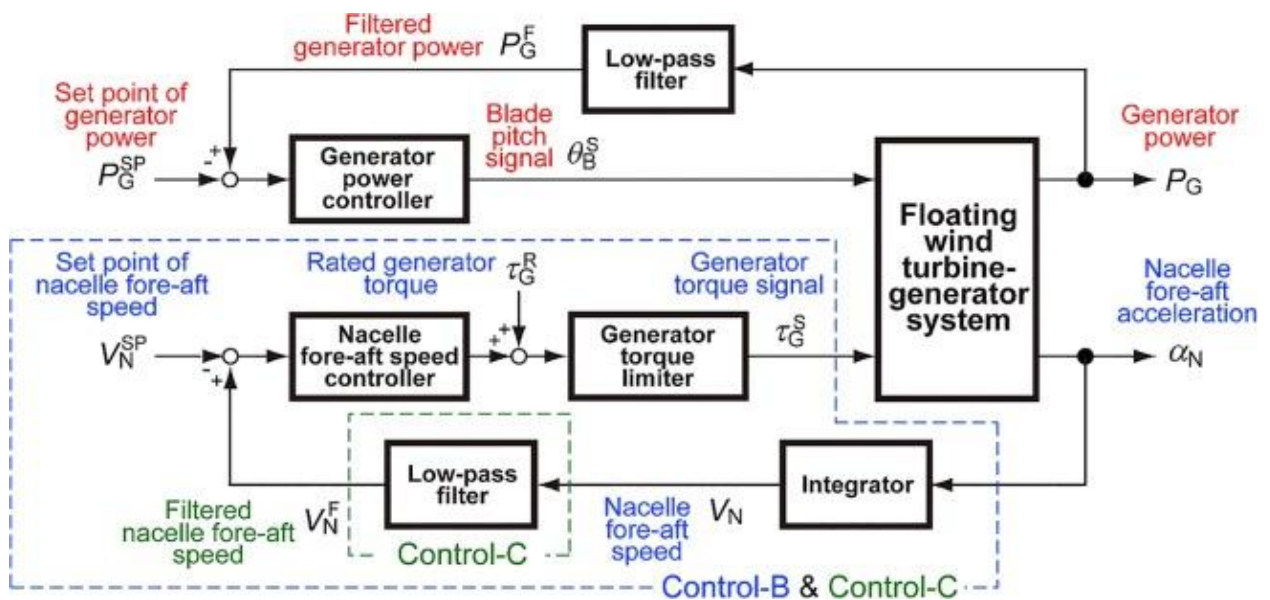


Figure 3: Control System of FWOT (Source: sciencedirect.com)

## Generator

Induction or synchronous generators are used in most wind turbines to accomplish this task. Induction generators are used in the majority of wind turbines. An induction generator's rotor spins slightly faster than the stator's spinning magnetic field. The generator transforms the wind turbine's mechanical work into usable electrical output. Slip is the difference between the rotor frequency of the generator and the moving magnetic field of the generator. The amount of power generated by an induction generator is determined by its slip.



Figure 4: Generator system of FWOT (Source: windpowermonthly.com)

## Rotor

The majority of wind turbines in operation today are three-bladed upwind designs. The blades may have either a constant pitch or a controllable pitch. Aerodynamic control which is also known as stall regulation or variable pitch blades control the rotor's power. A rotor is made up of two or three blades that are connected to a hub. The number, shape, and length of the blades determine the wind turbine's device output. The rotor can be designed to spin upwind or downwind.

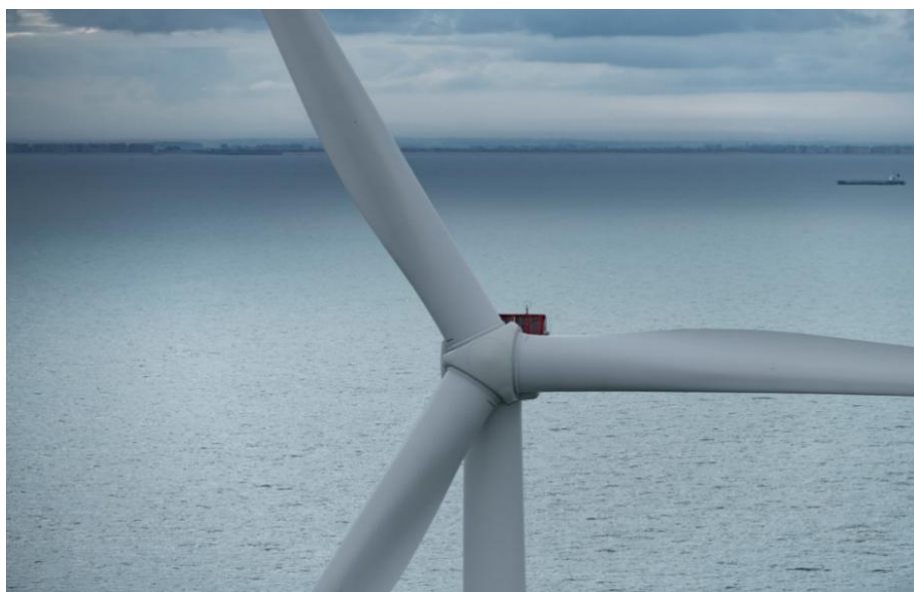


Figure 5: Rotor of a FWOT (Source: offshore-mag.com)



# Gear Box (Drive Train)

The wind turbine's output shaft spins slowly. The rotor output must be stepped to a higher speed in most electric generators. To spin the generator, a gearbox steps up the rotor output. Journal and thrust bearings support the shafts and restrict radial and axial movement of the drive train. Lift and drag are created by wind passing across the rotor blades. One of the most common causes of failure in wind turbines is the gearbox. As a result, some wind turbine generators are designed to run at the same speed as the rotor.

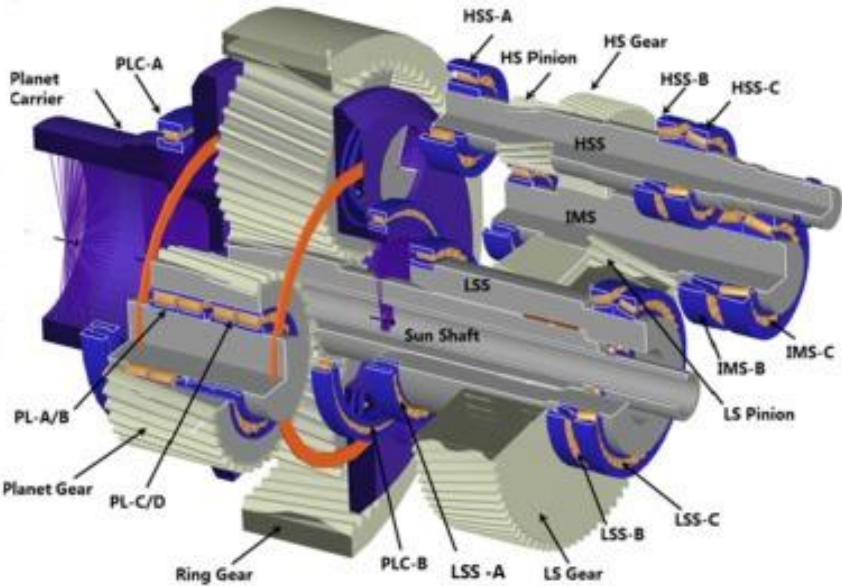


Figure 6: Gear Box of FWOT (Source: wind power engineering)

# Tower

The rotor diameter and the wind conditions at the site decide the tower's height. Wind shear causes the speed of the wind to rise with height above ground. Wind speeds that are higher result in more power output. To take advantage of this impact, it is preferable to lift the wind turbine nacelle off the ground.

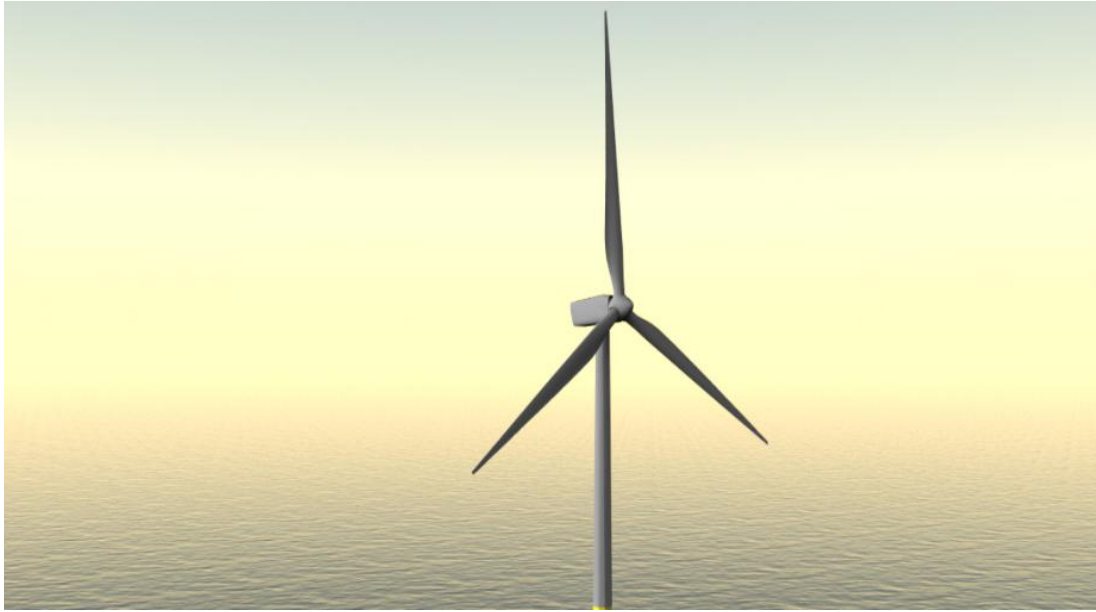


Figure 7: Tower of FWOT (Source: Sciencedirect.com)

The nacelle and rotor of a wind turbine must be supported at their operating height. The supporting tower will reach a height of more than 100 meters. The machine's fatigue life is shortened as a result of coupled vibrations. Downwind turbines must also contend with vortices ejected from the stack, known as tower shadow. This is just an overview of the floating offshore wind turbines in order to better understand the further process carried out in this study.

# 1. Introduction

## 1.1 Motivation

The use of wind turbines to generate electrical power has become a significant source of clean renewable energy all over the world. The average annual growth rate for the wind energy sector over the last five years has been 37% [1] and in 2019, the wind energy sector grew by 19%, adding about 60 GW of new power. Thanks to the long-established technological stability and widely available power that has yet to be control, wind energy has become one of the world's fastest-growing energy sources. Offshore wind energy is considered to have a high potential in the wind energy industry.

An offshore wind farm should be sited as near as possible to the place where it will be supplying load and with adequate wind speeds. On these locations, water depths are often too great for bottom-mounted wind turbines to be economically viable (example: wind farms of Hawaii). Coastal fishing, shipping, and recreational boating should not be harmed by a wind farm. Owing to the ocean's wide expanses, there is a lower visual impact and the opportunity for larger ventures and a wide open area. However, installing wind turbines offshore is more difficult than doing so on land. In addition, as we progress, turbine costs, multiple balance-of-station (BOS), and operating expenses which is the OPEX, has become more important. As a result, there is a constant attempt to improve features in deep water for the most affordable price.

The combination of declining costs due to ongoing changes in technology and supply chain, as well as the wind farms, proximity to coastal, mostly the densely populated areas, communities, has resulted in lower costs as well as the advantages of achieving economies of scale when constructing major projects on offshore and it enables them to become more cost-competitive while also generating employment and revitalizing ports [2].

Offshore energy power systems have come out as a promising technology for the large-scale production of electricity from offshore wind resources. Higher wind speeds are caused by the ocean's relatively low surface roughness. When wind turbines are relocated in the offshore,

some of the issues associated with them, such as taking up too much ground, are alleviated. Current projects for offshore wind power e.g. Horns Rev [3].

The S-bos Platform, a design owned by BlueNewables, is the subject of this master thesis. The model is a modified semi-submersible that is intended to provide better seakeeping while reducing material, installation, transportation, and maintenance costs. This platform is less demanding in terms of loads.

### 1.2 Historical Development of FOWT

In the past, research and study of floating wind turbines were minimal. In this area of study, European institutions have been the pioneers. The majority of the work has focused on potential floating support system designs and economic studies of different wind farms that use these designs. Let’s take an example of a group of Italian researchers who looked into the use of a toroidal-shaped floater [4]. In water depths ranging from 30 to 100 meters, this floater supports a single wind turbine. The support was kept in place by tensioned mooring lines. The floater had a unique design. Over the next three decades, the offshore market will expand dramatically, with total installed offshore wind capacity roughly ten-folding from 23 GW in 2018 to 228 GW in 2030 and near 1000 GW in 2050 as shown in Figure 8. In 2050, offshore wind would account for roughly 17% of the total world installed wind capacity of 6 044 GW (IRENA, 2019a). [7]

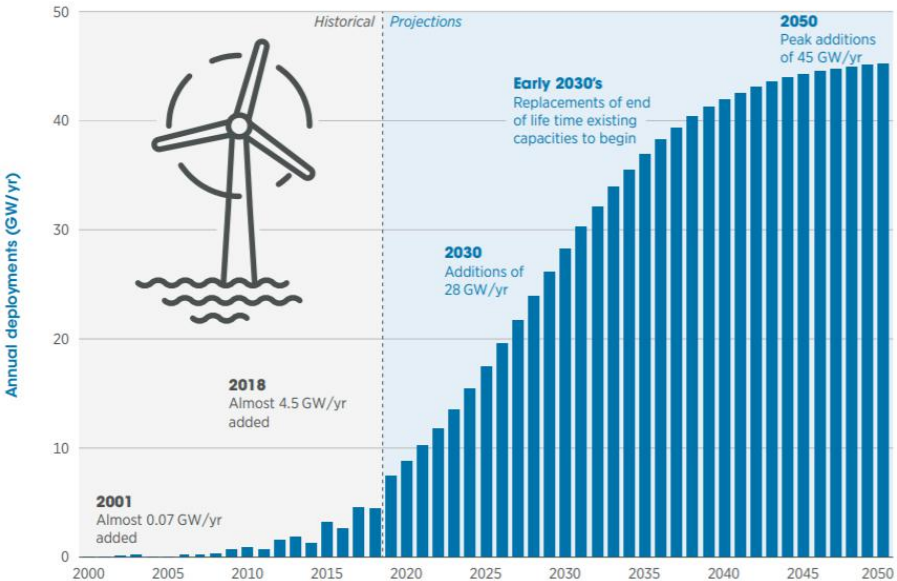


Figure 8: Annual global wind capacity (source: Historical values based on IRENA’s renewable capacity statistics (IRENA, 2019d), and future projections based on IRENA analysis (IRENA, 2019a))

### 1.3 Introduction to TLP, SPAR AND SEMI SUBMERSIBLE

The competitiveness of various foundation forms has been studied, and it has been discovered that it is highly dependent on the water depth [4]. For the water depth, there are three conditions:

- Shallow water conditions (0 m- 30 m)
- Transitional water conditions (30 m - 60 m)
- Deep water conditions (60 m - 1000 m)

These are the three water depth classes, with more than 53.6 % of the energy capacity estimated to be in areas with water depths greater than 50 m. The depth is vital when defining installation costs. Greater depths associates higher costs and the use of more complex and specialized technologies, something that is reflected in the final investment of the wind farm, reducing its profitability. Closed seas which are located within continental platforms, have an average depth significantly lower than oceans and open seas, being more convenient for this type of project [5].

To be able to replace the conventional bottom-fixed foundations, the floating platforms must be able to provide enough buoyancy to withstand the turbine's weight while also limiting pitch, roll, and heave motions [6]. Several substructure systems can be used for floating wind turbines including three most common types such as tension leg platform (TLP), Semi-submersible, and SPAR. The only difference is the mooring system among them and the different anchors can be used to maintain the position of floating wind turbines. These are especially competitive for relatively deep waters as mentioned previously.

- **TLP:** These are structures shaped by a central column with arms, the stability of which is accomplished by the lines of mooring. They are usually made of steel. It is anchored in the shape of a taut-leg. Its benefits, apart from good stability, are low structural mass and simple design. The disadvantages are its complicated installation and its mooring lines, and the need for an adequate floor.
- **Semi-submersible:** Wide plan dimensions, whose stability is accomplished by buoyancy, are considered in this form of structure. They can be made of steel, concrete or a combination of both. Its anchorage is typically made up of a catenary. The key benefits are the simplicity of installation and dismantling, since it is possible to assemble the turbine in

the port. The main drawbacks are the large amount of material required and its complex and expensive structure.

- **SPAR:** These are elongated cylindrical structures, the stability of which is achieved by ballasting. They can be made of steel, concrete or a combination of both. Typically the anchorage is by catenary, or by catenary and taut-leg mixtures. The major advantages are the flexibility of the design and its excellent stability. The main disadvantages are the restriction of depth and the need for a crane vessel to be mounted. In floating wind turbines the platform is normally connected to a mooring device that limits wind turbine displacements by adding additional restoring forces and moments. Some examples of floating platforms whose stability policy is based on the principles explained or a combination of them are shown in the Figure 9



Figure 9: Types of floating wind turbines [Source: International Renewable Energy Agency [IRENA], 2016] [7]

There is not a single theory behind any of the designs. Moreover all of these ideals are still in play to varying degrees. As a result, all these design of the floating offshore wind turbines are hybrid in nature. The floating platforms can be classified based on the basic theory or technique employed to maintain stability. The National Renewable Energy Laboratory (NREL) [8] conducted research to evaluate the dynamic response of six floating platform designs which are as follows:

- The MIT/NREL TLP
- The OC3-Hywind spar buoy

- ITI Energy barge
- UMaine Semi
- UMaine Hywind
- The UMaine TLP

The ITI Energy barge's platform motion-induced ultimate and fatigue loads for all turbine components were found to be the highest of the three concepts, with only small variations in ultimate and fatigue loads between the MIT/NREL [9] TLP system and the OC3-Hywind system. Figure 10 shows the sea-to-land ratios for ultimate loads for the six concepts based on separate design load cases (DLCs).

The ITI Energy barge's wind turbine was more influenced by the waves than by the wind. As a result, DLC 1.1 for the ITI Energy barge system dominated the load results more than DLC 1.3, which has more wind turbulence but the same wave conditions. The discussed findings could lead to the conclusion that TLP floaters are the most stable platforms, and that a spar concept would have comparable characteristics, which may be true in practice. However, buoys are expected to be heavier and more expensive to construct, and tension leg installation is complex and costly. In conclusion, all floating wind turbines have higher loads on turbine components than land-based systems, and thus must be reinforced.

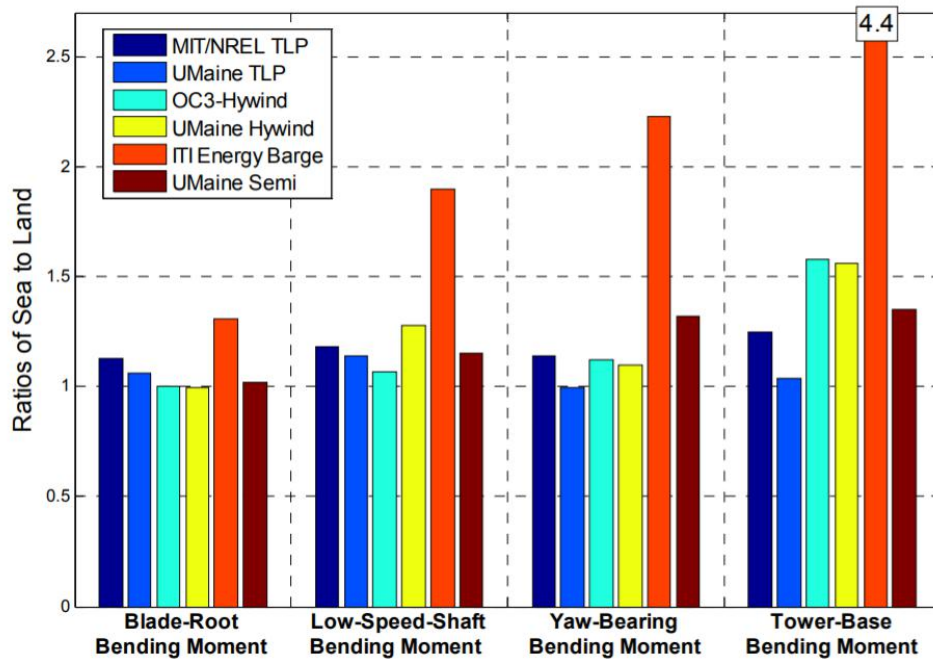


Figure 10: Sea-to-land ratios of ultimate loads from DLCs 1.1, 1.3, 1.4 and 1.5 for the MIT/NREL TLP, OC3-Hywind Spar and ITI Energy Barge (Source: [NREL](#)- Sea-to-land ratios of ultimate loads from DLCs 1.1, 1.3, 1.4, and 1.5)

## 1.4 AERO-HYDRO-SERVO-ELASTIC (ASHE) or Coupled Analysis

In the last few years, the offshore wind industry has been growing up and the engineers are focused on developing the powerful tools to access the combined behavior of Aero-Hydro-Servo-Elastic. The term aero-hydro-servo-elastic coupling refers to a connection between aerodynamic loads and responses, hydrodynamic loads and responses, the control system, and the structure's elasticity-induced deformation reaction. Typically, no coupling effects between the models of the external conditions are included in a given load simulation. All forcing and response equations are solved simultaneously in a coupled analysis, i.e. at each time step.

This analysis gives all the computational methodologies on the offshore wind turbine. On the other hand, more focused on the hydrodynamics and moorings assessment which have been in used for oil and gas industry so it is like a combination between them. To grow the solution in the time domain, various time stepping approaches exist. The components of a FOWT's complex multiphysics system are implicitly connected, resulting in holistic modeling. In terms of rotor aerodynamics, floater hydrodynamic loading, and mooring system dynamics, computational calculations are also described in this study using Diffraction and Morison equations. The fully couple assessment (ASHE) combines the effects of hydrodynamics, the blade pitch and the generator controllers (Part of Servo) which can be seen in the Figure 11 and it means that the aerodynamics of the loads produced by winds and also the pitch and surge motion of the platform. For the elasticity, one already knows that the materials have their own stiffness.

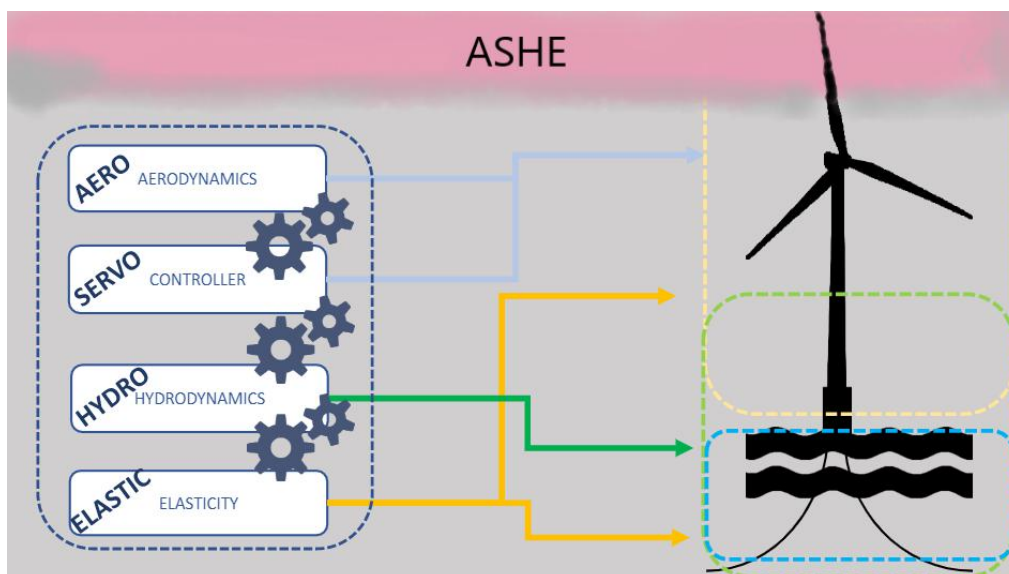


Figure 11: Description of coupled analysis (ASHE)



Regarding hydrodynamics one have to take into account the effects of waves and currents and later own it will be shown that two theories will be used which are the diffraction and morison theories or a combination of both of them. Preliminary mooring system will be used for this study. For the Servo part, one will use the FORTRAN compiler by using the dynamic library of a script by putting some parameters like the rotor angular speed or wind speed in order to calculate for e.g. the blade pitch.

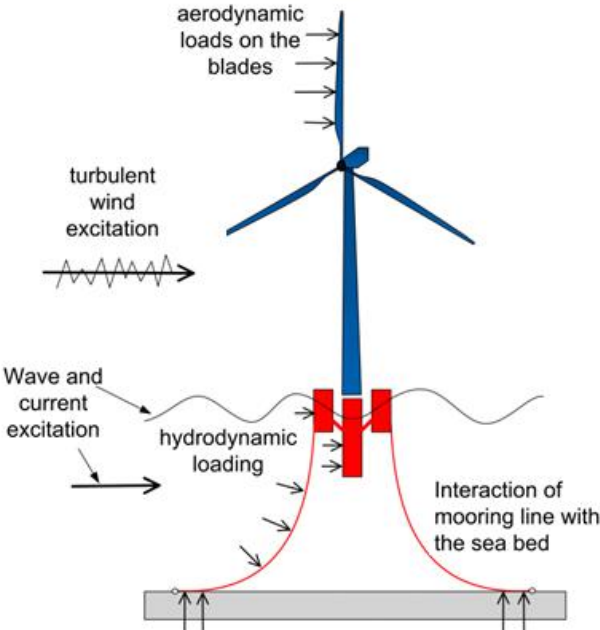


Figure 12: AERO-HYDRO-SERVO-ELASTIC (ASHE) Coupled Analysis behaviors (Source: [mdpi.com](http://mdpi.com))

In Figure 12 the blue color section shows the tower and RNA and most importantly for this project, nacelle elasticity is not taken into account and the red color shows the flexible components of the sub-structure and mooring lines. For the S-bos platform one must understand about the environmental conditions of the specific site described in chapter 3 on which the platform have to withstand loads.

For this structure one can define several conditions such as wave’s currents and winds and also the part of the servo, which will be defined mostly by the reference RNA and turbine. Later on it will be selected for the S-bos platform. One can combine the effects of wind, wave and currents by using different directions and alignments. This is the method which is being described and followed in this thesis and after combining all of the behaviors one can see how the model behaves under these conditions.

## **2. The S-bos Platform from BlueNewables**

### **2.1 The S-bos Platform**

BlueNewables is working on a floating platform called the S-bos platform, which is defined as a "one-of-a-kind" semi-submersible. The floater is made up of a concrete hull that is connected to a concrete counterweight (also known as keel) by a collection of concrete structure having four columns radially distributed each by 90 degrees. A catenary mooring mechanism is connected to the hull. The main purpose of the mooring system is to keep the platform in position and S-bos is stable itself. Since the floater is fabricated and built from common building materials and it is a kind of a compact design and it is more cost-efficient.

The S-bos low-motion platform concept, with the main structure positioned below the water line, where wave loads are decreased, station keeping is maintained using catenary moorings, and the water-plane cross-section area is kept low, resulting in low stiffness. The concept of the S-bos platform is based on buoyancy stabilization and floats semi-submerged on the water's surface. The platform is stabilized by scattered buoyancies and the righting moment is provided by the GM and GM depends on the KG, KB, and BM which further depends on water plane area. To ensure stability with complex structures requiring a more sophisticated construction process, the notion frequently necessitates a huge and hefty platform. Because of the low draft, it is easy to install and use, even in shallow seas. The concept might be used in as little as 25 meters of water and for this study the depth considered is 100 meters. At deeper water depths, however, the design of the catenary mooring system becomes more difficult because of reason that the tension increase on the fairlead due to increase in weight in deeper water levels, decrease in water temperature etc. The turbine may be readily built to the floating substructure in the port and moved to the offshore site by a tug boat, which speeds up the installation process.

Moreover, it can be manufactured by any reputable fabricator or shipyard. The transportation and installation is normally carried out at low wave heights but is should be analyzed. BlueNewables have designed a very concrete structure that the design has an excellent dynamic response to continuous wave and current motion, and it can withstand harsh environmental conditions especially during the transportation and installation while

supporting the largest wind turbine generators with a significant factor of protection. In this process as well, the floater can be wet towed in its transportation role, removing the need for a heavy lift.

For all the processes of the installation, the platform does not need advanced heavy lift machinery, and due to natural rules, these operations depend heavily on forces. The numerical validation of the dynamic behavior of the S-bos platform with the IEA 15 MW reference wind turbine installed on it, Also, the theoretical method used to construct the aero-hydro-servo-elastic analysis will be included in the later chapters.

## 2.2 Modes of motion of the platform

Wind and wave loadings cause the wind turbine's combined rigid body and floating support to oscillate in translation and rotation. Horizontal movements along the  $x$  and  $y$  axes are known as surge and sway. To have adequate water plane inertia, the system's horizontal axes are aligned with the four buoyancy columns. Figure 13 is the first figure of the S-bos:



Figure 13: S-bos platform

The floater's vertical motion is known as Heave. On the other hand, Roll, Pitch, and Yaw are the three oscillatory angular motions. On the calm waterline, the roots of the three axes are found in the middle of the floater. The global coordinate system's relation is a position in the tower's center where it attaches to one of the column's center.

### 2.3 Moments caused on the platform

The rotor of the wind turbine is mainly affected by wind forces and moments, while the floater is mainly affected by wave forces but the dry part of the floater can be affected by the wind but in this case it is negligible. Gravity, wind, and waves, all exert forces and moments on the wind turbine assembly and the platform. The platform receives the forces and moments produced by the wind turbine blades. The steel tower is also affected by the wind and it is very important for instance regarding DLC 6.1 where the wind speed will be around 40m/s to 50 m/s. The forces and moments operating on the combined system are discussed in the following section.

#### 2.3.1 Wave loading on the platform

The ability of a system to manage disturbances is characterized as stability. Waves, currents, and wind are examples of disturbances. Semi-submersibles have a center of gravity that is higher than the center of buoyancy and are stabilized by the restoring moment of the BM. Around the Z-axis, the floater is symmetrical. As a consequence, the hydrodynamic analysis just considers heave, roll, and pitch. The S-bos platform is made of a concrete squared block having four columns that provides buoyancy and enough water plane inertia as shown in the Figure 14:

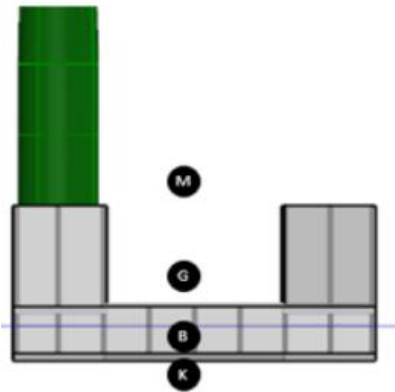


Figure 14: Stability of S-bos Platform

The structure's restoring forces are determined by a parameter known as the metacentric height of the structure. The meta-center is a made-up point that exists at the junction of the structure's center line and a vertical line drawn from the center of buoyancy. The metacenter, labeled M in the initial stability state, is shown in the Figure 14. The metacentric height is the distance between the structure's center of gravity and the point (M), which is known as (GM). It is considered to be constant for heel angles less than 10 degrees. Where (KB) denotes the distance from the keel to the (C.O.B), (KG) denotes the distance from the keel to the center of gravity (C.O.G), and (BM) denotes the distance from the metacenter to the center of buoyancy (C.O.B), as calculated in Eq. (2.1)

$$GM = BM + KB - KG \quad (2.1)$$

The columns provides enough water plane inertia and buoyancy as if one has more water plane inertia then the metacentric radius (BM) will be higher, and hence, if one has the more Metacentric height (GM) then the structure will have the more hydrostatic stiffness in the roll and pitch motions and less static pitch motions. The distance between the center of gravity and the center of buoyancy is known as (GZ) and this distance causes a moment that counteracts the disturbance. GZ is normally used for the large stability angles. The two forces will bring the system back to its original upright posture if the structure is not disturbed.

### ***2.3.2 Forces and Moments on the Platform***

Forces and moments produced by the wind turbine, on the other hand, can excite the platform's other modes of motion. Roll, pitch, and heave excitation are discussed in section 4.7. Since these modes are caused by horizontal forces on the submerged structure, sway and roll are close to surge and pitch. As a consequence, the discussion of surge and pitch relates to sway and roll as well. The pitch and surge motion equations are combined for a standard semi-submersible.

The platform's stiffness in heave and pitch can result in very small floater motions in these two modes. Some of the motion in the heave mode is due to the set-down induced by surge, since the mechanism behaves like an inverted pendulum. The floater's draft rises as it moves away from the rest place. As a consequence of this assumption, the platform produces no

major wave disruption. Both incoming wave and diffraction potential flow effects cause excitation forces.

The excitation forces and moments are measured using analytical expressions for the added mass terms and the incoming wave potential. The GI Taylor equations [10] are used to estimate the force induced by the incoming wave.

The floater's movements can have an effect on the wind turbine. Regular sinusoidal waves are thought to be the source of wave loading. To achieve realistic sea states, linearly superimposing the results from multiple normal waves can be used to calculate the motion of a floating structure in irregular waves. A floating wind turbine's action is complicated. Complex behaviors are generated when various modes of motion interact. A yaw moment on the floater is generated in two ways during normal operation of a floating wind turbine.

Because of the symmetry of the structure, waves do not often create large yaw motions on floating structures, but motion in all other degrees of freedom will be present. (Yaw motion may be present due to wind and wave interaction and misalignment). It's worth noting that the wind-turbine community uses the term "pitch" to refer to the rotation of the blade to modify the angle of attack, whereas the offshore community uses the term "nodding" to refer to vessel rotation. The nomenclature can be seen in Figure 15:

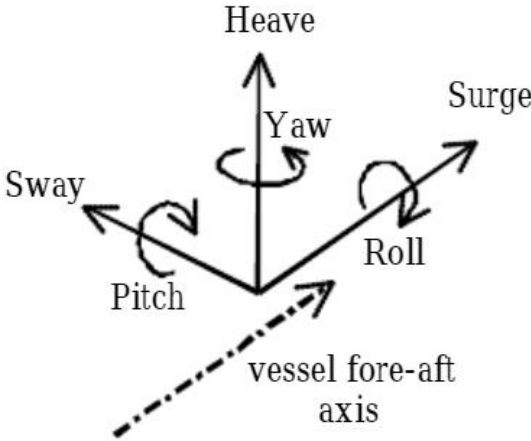


Figure 15: Platform Motion Nomenclature

Normally the first yaw moment cause by the oscillating yaw which is created by the rotor blades to rotate normally and it can change over time. The second yaw moment can cause by

the slight tilting of a floating wind turbine when under load. Also the generator torque can exert a roll moment on the floater when both wind and waves are aligned with the x-axis.

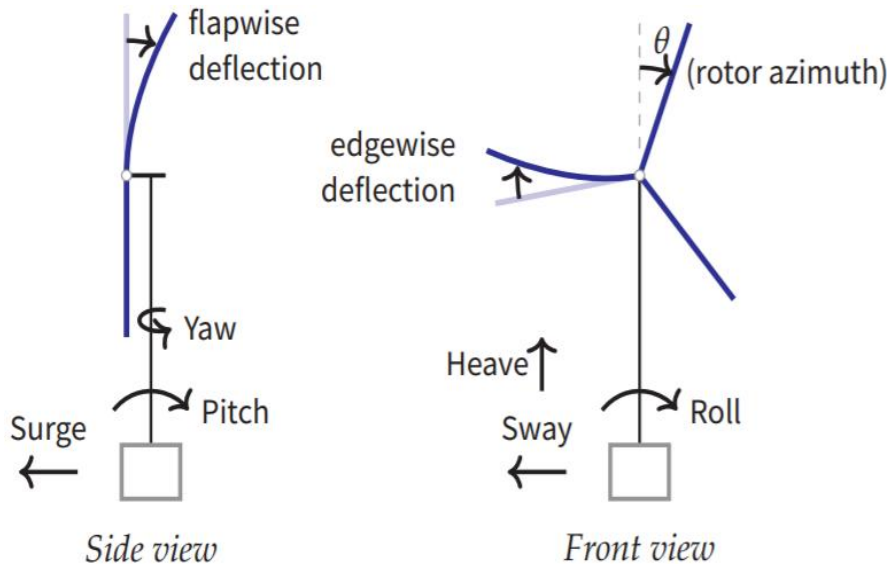


Figure 16: Surge, sway, heave, roll, pitch, and yaw are the rigid-body movements of a floating structure. Source [11]

The rotor thrust works on a moment arm formed by this movement along the x-axis. There is a yaw moment. It is important to note that, in most situations, this moment is small due to the low force along y-axis. Figure 16 depicts how the generator torque generates roll (amount of roll is exaggerated). One can see how a moment is created by blowing wind into the rotor.

### 2.3.3 Wind turbine

Wind creates lift and drag forces as it passes over the rotor blades. A torque on the rotor, a thrust along the rotor axis, and a pitching moment are all generated by these two forces. The tower and floater feel the thrust on the blades as well. These forces and moments function along the cord at a distance of approximately  $c/4$  from the leading edge for ideal non-separated flow [12], where  $c$  is the cord length. A diagram of forces and moments on a stationary airfoil in a wind stream is shown in Figure 17.

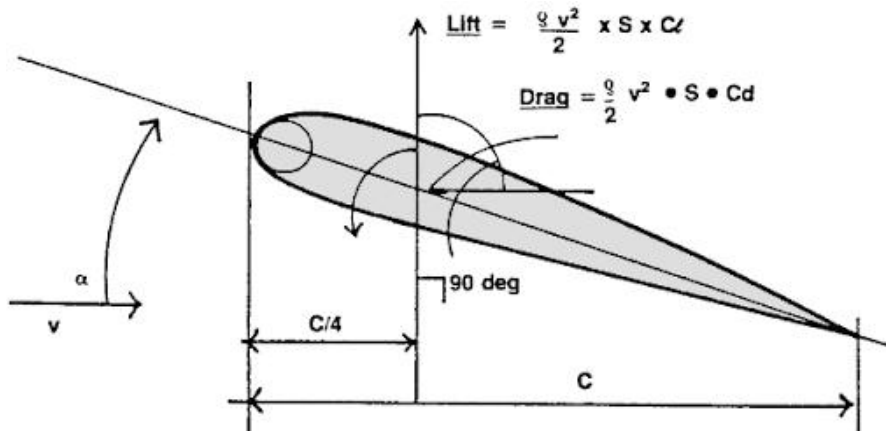


Figure 17: Forces and moments on a stationary airfoil [Source: pilotfriend]

The sum of the moments generated by the individual forces acting on the airfoil is the pitching moment. This moment is based on an axis perpendicular to the airfoil's cross-section. The rotation of the rotor in a wind turbine raises the inflow into the airfoil thereby changing the effective angle of attack.

The perpendicular force component of the lift force is defined as the force component perpendicular to the incoming air flow. The drag force is characterized as being parallel to the incoming airflow direction. Vortex shedding, viscous friction, and isolated wakes all contribute to drag. The pitching moment is perpendicular to the thrust on individual blades, which creates a moment at the blade base. These moments function about the y and z axes. (Rotor torque acts around the x-axis.) As the blades rotate, their orientations shift. As a result, cyclic moments are produced at the same frequency as the blade.

In both yaw and pitch, these moments are exciting for the floater. It's worth noting that the results of these moments would be minor in comparison to the rotor torque and rotor thrust moment at the tower's base. When a wind turbine is installed on a floating frame, gyroscopic moments are generated by the floater's yaw and pitch. A precession torque is generated when the plane of rotation of the wind turbine rotor is shifted.

This precession torque operates on an axis that is perpendicular to the rotor axis as well as the axis around which the plane of rotation is being shifted. Turbine fatigue is caused by the gyroscopic motion of the turbine. This is mainly caused by the wind turbine yawing in land-



based turbines. Since the plane of rotor rotation does not adjust during roll when the wind turbine, pitch motion will create a gyroscopic moment while roll motion will not do as such.

### 2.3.4 Coordinate System

To represent diverse coordinate systems, OrcaFlex employs a number of frames of reference, each of which consists of a reference origin and a set of axes directions. To begin with single global frame of reference, which is referred to as  $G_{XYZ}$ . The global origin is the reference point, and the global axis directions are  $G_X$ ,  $G_Y$ , and  $G_Z$ . The model thus has a number of local coordinate systems, one for each object, indicated by  $L_{xyz}$  and having axes directions  $L_x$ ,  $L_y$ , and  $L_z$ . Positive rotations are clockwise when looking in the direction of the axis of rotation in all coordinate systems, and they are all right-handed. The global axis and a vessel with its own local vessel frame are depicted in the illustration of Figure 18:

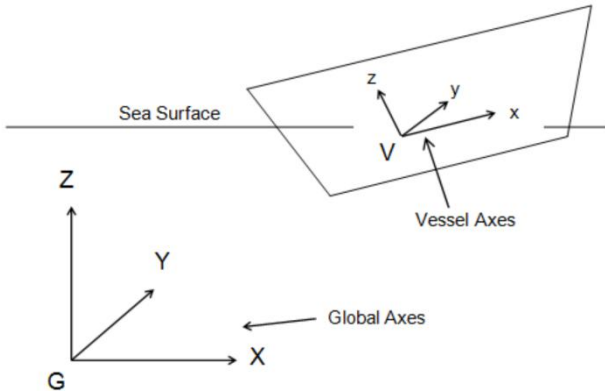


Figure 18: Coordinate system used in the Analysis (Source: OrcaFlex)

## 2.4 Conditions of Loading

The research provided in this study can be applied to five different loading conditions which are mentioned below:

- Wind or wave loading events that are incredibly high.
- There is no wind and the floater is subjected to static and dynamic loading.
- There is no wind or waves, so the load is static.
- Random wind and/or wave loading on the device, both static and dynamic.
- Static loading in the presence of a steady wind.

The rotor is aligned along the x-axis and the waves/wind is believed to blow in the x-direction as well for the majority of the following debate. This assumption is only made for the sake of this conversation. Variations in wind and wave paths are factored into the equations. Gravitational and buoyant forces and moments are accounted in the static loading state. The system's combined weight is supported by the floater. The floater is too buoyant, putting strain on the four columns. The floater's buoyancy is determined by its submerged depth.

The related buoyant force is greater than the total weight assisted as a result of this displacement. The four columns are stressed due to the excess buoyancy. A steady state wind with no waves is the second loading condition. The damping coefficients for the device benefit greatly from this loading state. Winds in a steady state exert nearly constant thrust and torque on the rotor. The wind inflow to the rotor is influenced by the rotation of the floater. The thrust and torque loading on the rotor are altered as a result of the change in wind inflow. For certain modes of device motion, the wind turbine functions as a damper.

When the turbine is not working and waves are acting on the floater, the third loading condition applies. In the surge, sway, roll, pitch, and heave modes of motion, waves acting on the floater create excitation forces and moments. Since the floater is a concrete based structure, the only source of yaw excitation is waves acting on the columns.

In the next loading state, the device is subjected to both random wind and waves. For different reference wind speeds and sea states, this condition is useful for evaluating expected device response during normal operations. The system's response to extreme wind and wave events is an important design feature that must be understood before a system's suitability can be determined. The numerical simulation makes use of wind and wave inputs that model extreme events. The component loading values are calculated after evaluating the fully coupled dynamic response.

### 3. Oceanology

#### 3.1 Environmental Loads

In the case of floating systems for wind turbines, it is important to ensure that wave loads are kept to a minimum and that the waves are as transparent as possible in order to keep the system's cost low. Wind, wave, current, tide, and ice loads are influenced by a number of factors, including the project's position and water depth. Environmental loads should be considered when choosing a foundation framework. All the data explained later has been extracted from Puertos Del Estado to get the environmental loads for the current project location.

#### 3.2 Site of the project (Canary Islands)

The project's chosen location is off the coast of Gran Canaria (GC) Island in Spain's Canary Islands. It's a place where the wind is very consistent, but the intense wind speed is poor. The wave, wind, and current data for this location were derived from the SIMAR point 4038008, *Puertos Del Estado*, given by the Spanish Authority as shown in the Figure 19. This is a grid of points at which models are run to generate numerical predictions. This point has the following coordinates as shown in Table 1:

Table 1: S-bos platform coordinates

Name of project	Sexagesimal System	
S-BOS	EAST	NORTH
	-15.390	28.050
	Longitude	Latitude



Figure 19: Pinned Location in the Gran Canaria (Source: SIMAR point 4038008, Puertos Del Estado)

### 3.3 Water Depth

The depth of water is one of the most critical factors to consider when selecting a floating platform. While current, wave, and wind loads normally increase with increasing water depth, this is not always the case. In addition, the platform height increases to keep the tower and turbine above the water's surface. Based on performance and cost, each foundation system is usually best suited for a specific range of water depths, which can differ depending on many geologic and environmental factors.

### 3.4 Wave Height

The Weibull distribution as shown in Eq. (3.1) extracted from the “Las Palmas Este” buoy which is the site location in Gran Canaria, is used to calculate the wave height of this location.

$$F_{HS}(h) = 1 - \exp\left(-\frac{h-\delta}{A}\right)^k \quad (3.1)$$

Whereas A is the scale coefficient and it is equal to 0.48,  $\delta$  is the location coefficient and it is equal to 2.02 and k is the shape parameter and it is equal to 1.02.

### 3.4.1 Significant Wave Height (Hs)

Significant wave heights associated with 50, 20, 10, and 1 year return periods are given in the Table 2, based on Weibull distribution and assuming 3-hour storms sea states. The wave peak time has been extrapolated as the most likely value associated with each of these heights, the following Table 2 and Table 3 shows significant wave heights correlated with 50, 20, 10, and 1 year return cycles, based on Weibull distribution and 3-hour storm sea states and scatter diagram for Hs/Tp for the above mentioned return periods. The most likely value associated with each of these heights has been extrapolated as the wave peak time.

Table 2: Wave Data for the Location of Gran Canaria (Source: Flotant D.4.1 – STRUCTURAL AND NAVAL ARCHITECTURE DESIGN BASIS)

Return Period	50	20	10	1
Hs(m)	5.11	4.69	4.40	3.35
Tp(s)	12	12	10	10

Table 3: Hs/Tp Scatter Diagram (Source: Puertos Del Estado)

			Significant Height (m)											Grand Total	
			<= 0.2	0.5	1.0	1.5	2.0	2.5	3.0	3.5	4.0	4.5	5.0		5.0 >
Dir °	N	0.0	0.000	1.311	13.497	19.881	17.886	6.179	0.889	0.353	0.205	0.000	0.000	0.000	60.203
	NE	45.0	0.000	0.080	7.524	14.626	9.679	1.642	0.479	0.068	0.011	0.000	0.000	0.000	34.109
	E	90.0	0.000	0.000	0.593	1.357	0.559	0.114	0.057	0.023	0.011	0.000	0.000	0.000	2.713
	SE	135.0	0.000	0.000	0.125	0.148	0.046	0.000	0.000	0.000	0.000	0.000	0.000	0.000	0.319
	S	180.0	0.000	0.080	0.171	0.000	0.000	0.000	0.000	0.000	0.000	0.000	0.000	0.000	0.251
	SW	225.0	0.000	0.239	0.855	0.171	0.000	0.000	0.000	0.000	0.000	0.000	0.000	0.000	1.265
	W	270.0	0.000	0.228	0.091	0.068	0.000	0.000	0.000	0.000	0.000	0.000	0.000	0.000	0.388
	NW	315.0	0.000	0.388	0.160	0.068	0.137	0.000	0.000	0.000	0.000	0.000	0.000	0.000	0.752
Grand Total			0.000	2.326	23.016	36.320	28.306	7.934	1.425	0.445	0.228	0.000	0.000	0.000	100.000

### 3.4.2 Wave Rose

The Graph of the wave rose extracted from Puertos Del Estado for the wind rose of the current location is as follows:

Rose of Significant Height (m) for Waves - SIMAR Point 4038008  
 Period: 1958 - 2021 - Efficiency: 98.52%

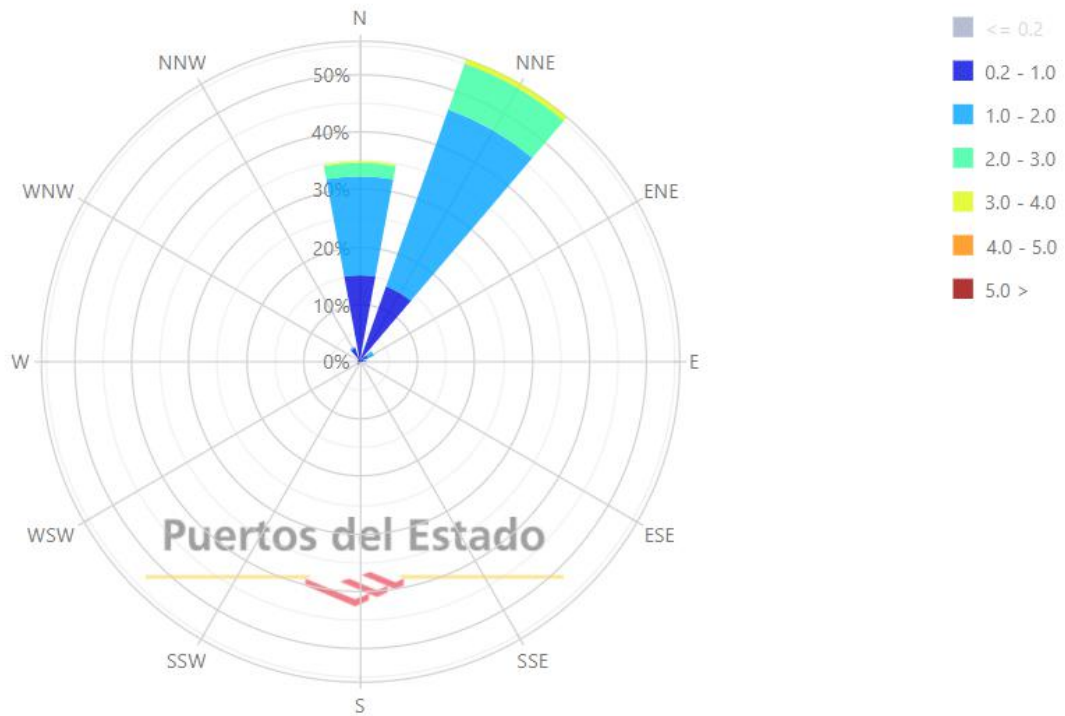


Figure 20: Wave Rose of Hs in Gran Canaria (Source: Puertos Del Estado)

### 3.5 Wind Environment

The low surface roughness of the sea is one of the advantages of constructing wind turbines offshore. Wind speeds near the surface are reduced when it passes through barriers such as trees, buildings, and hills. Wind speeds rise as you get higher above the ground. The power law profile or the profile in logarithm are widely used to model the wind profile.

#### 3.5.1 Wind Data

The wind data for this location was derived from the SIMAR point 4038008 data given by the Spanish Ports Authority. The same grid of points as mentioned in Table 1 where wave simulations and data are produced using models.

### 3.5.2 Wind Profile Law

The low surface roughness of the sea is one of the advantages of constructing wind turbines offshore. Wind speeds near the surface are reduced when it passes through barriers such as trees, buildings, and hills. Wind speeds rise as you get higher above the ground. The power law profile or the profile in logarithm are widely used to model the wind profile. The Eq. (3.2) for the power law is stated as:

$$\text{Power Law} = V(a) = V(a_r) * \left(\frac{a}{a_r}\right)^z \quad (3.2)$$

Where:

$z$ : Power law exponent

$a_0$ : Roughness length

$V(a_r)$ : Reference wind speed

$V(a)$ : Wind speed at height  $a$

$a$ : Height above ground

$a_r$ : For fitting the profile, a reference height above ground is used.

The power law profile or the profile in logarithm [9] are widely used to model the wind profile. For the assessment of S-bos platform, this method of calculating the wind environment is also considered but in DLC 6.1, if included the wind effect onto the tower, conservatively wind profile is not be considered but for the rest of the DLCs it is not important. Out at sea, the wind profile is such that, with the same height above the surface, wind speeds are usually higher than on land. The wind turbine's operation is enhanced by the difference in wind profiles. The rotor of an offshore wind turbine can be installed on a shorter tower and generate the same amount of energy as a land-based equivalent.

When you get higher above the water's surface, the wind speed rises up. Blades move through the wind profile as the rotor spins. This creates a periodic difference in the inflow speed to each blade. The blades generate oscillating thrusts and moments at a frequency equal to  $N$  times the rotor's rotational speed. For normal conditions, the logarithmic rule was chosen as the wind speed profile Eq. (3.3).

$$Profile\ in\ Logarithms = V(a) = V(a_r) * \frac{\ln(\frac{a}{a_0})}{\ln(\frac{a_r}{a_0})} \quad (3.3)$$

The Normal and Extreme wind speed profile for a return period of 50 years and different heights would be the following as shown in Table 4 and the monthly wind speed and monthly maximum wind speed is shown in Figure 21:

Table 4: Normal and Extreme Wind Speed of Gran Canaria

Normal Wind Profile	Height(m)	10	20	50	100	119
	Speed (m/s)	9.83	10.48	11.33	11.98	12.14
Extreme Wind Profile	Height(m)	10	20	50	100	119
	Speed (m/s)	20.75	22.55	25.17	27.35	27.93

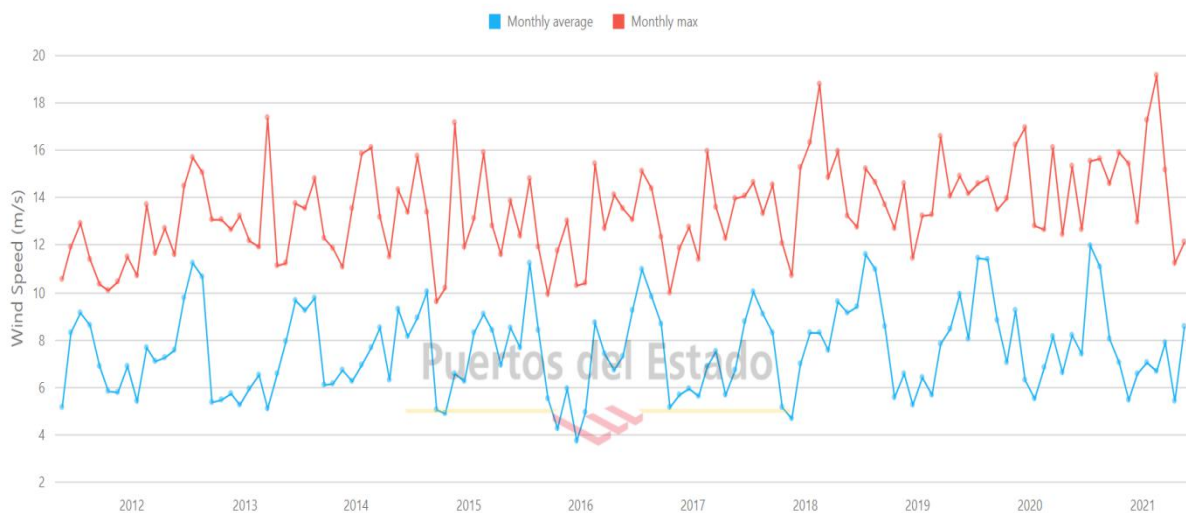


Figure 21: Monthly wind speed and monthly maximum wind speed (Puertos Del Estado)



**3.5.3 Output from the Wind Turbine**

The wind speed must be greater than the generator’s cut-in speed as shown in Figure 22 for the generator to achieve usable power output and lesser than the cut-out speed in order to prevent any damage. The wind turbine’s rated power output increases as the wind speed increases. Wind turbine power is controlled above the rated speed by adjusting the blade pitch or stalling a portion of the blade.

The cutout speed is the maximum speed at which a wind turbine can no longer run. Torque and thrust are produced by wind passing over the rotor blades. After that, the torque is converted to electrical power output. Wind speed increases the torque of the rotor. The power curve used for this study is taken from the IEA 15 MW for the rated wind speed 10.59m/s as shown in the Figure 22:

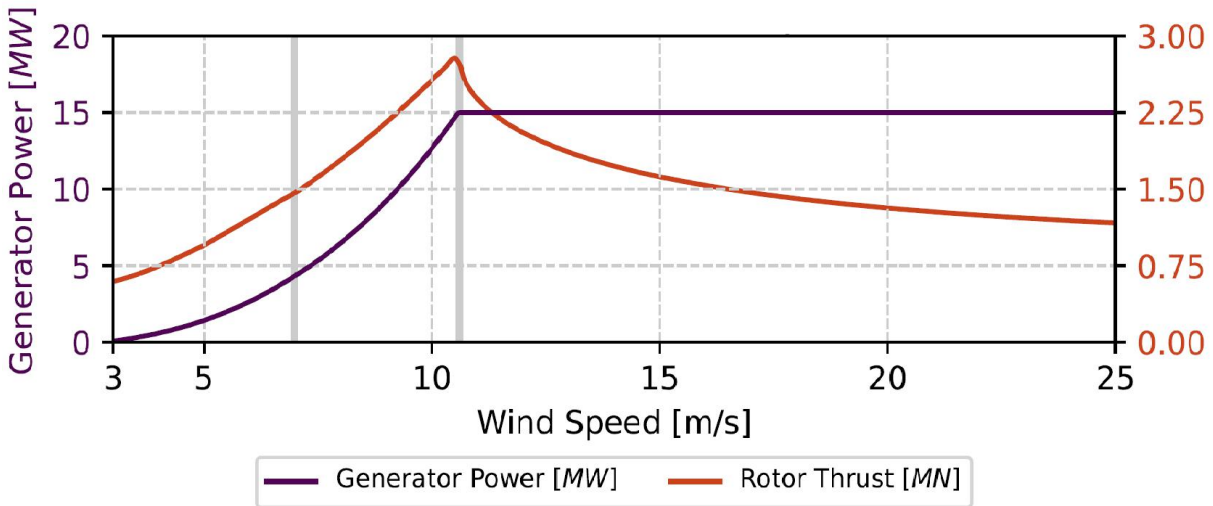


Figure 22: Power curve for 15MW Wind turbine [25]

**3.5.4 Wind Rose**

The Graph of the wind rose extracted from Puertos Del Estado is shown in the Figure 23:

Rose of Mean Speed (m/s) for Wind - SIMAR Point 4038008  
 Period: 1958 - 2021 - Efficiency: 98.52%

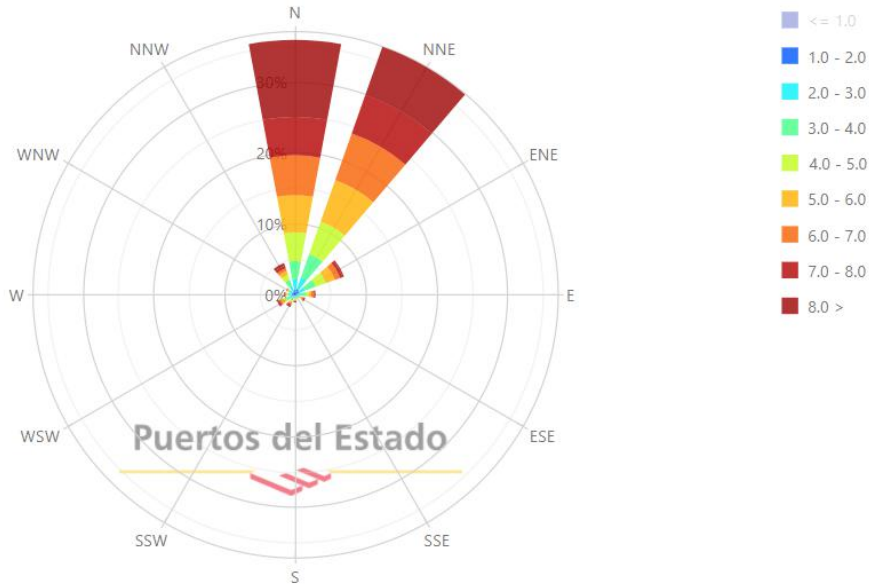


Figure 23: Wind Rose in Gran Canaria (Puertos Del Estado)

### 3.6 Currents

The value for the currents will be obtained using the as shown in Eq. (3.4):

$$V_{wind}(s_0) = k * U_{1Hr} \quad (3.4)$$

Where (k) coefficient will be taken as 0.03 in order to account for the worst-case scenario and obtain a safety side current speed value. The 50-year mean annual wind speed at 10m above sea level is 19.0m/s, so the current wind-induced speed for a  $T_R$  of 50 years is 0.57 m/s. The scatter diagram as shown in Table 3 most likely wind direction will be taken as the direction correlated with these current speed values. As a result, the wind-induced current path would be North-northeast (NNE) to South-southwest (SSW). The value calculated for the Current speed for a  $T_R$  of 50 years can be seen in the Table 6:

Table 5: Current Induced by wind speed at sea surface at Gran Canaria (Flotant D.4.1, pg. 51)

Current Induced by Wind data	
Current speed for a TR of 50 years ( $C_{50}$ )	0.57 m/s

## **4. Hydrodynamic Model**

### **4.1 Statement of the Problem**

To assess the viability of the S-bos platform, a range of issues must be addressed. The effect of aerodynamic analysis using the Blade-Element Momentum (BEM) is one aspect of the analysis. The hydrodynamic loading on the platform is also a critical part of the research.

Both waves and wind interact with the wind turbine/floater device. The study of a coupled analysis is achieved by combining the different components. The nacelle shifts with the floater as wave loads cause it to move. Changes in the inflow wind to the turbine rotor are caused by the nacelle's movement. Changes in rotor thrust loading can be caused by changes in rotor inflow. The floating support is influenced by the shift in thrust. Gyroscopic loads on the rotor can also be caused by the floater's angular motion.

Wind and wave loads on individual parts are determined using the body-based coordinate system for each part. In a total dynamics study relative to the global coordinate system, all of the forces and moments from the individual components of the system are integrated.

The motion of each component is calculated by analyzing the system's combined dynamic equations. The AQWA Solver is used to perform these calculations in the frequency domain. And time domain simulations are going to be calculated in OrcaFlex. The analysis will be based on both of the platforms used in this study.

### **4.2 Literature Review**

Researchers at Delft University of Technology (DTU) in the Netherlands recently conducted a study in 50 meters of water on the use of a floating support for wind power applications. A group of Italian researchers looked into the use of a toroidal-shaped floater. In water depths ranging from 30 to 100 meters, this floater supported a single wind turbine. The support was kept in place by catenary tensioned mooring lines.

The floater's shape was chosen to reduce wave interaction, but the concept was deemed too costly to build. This is a set of international projects overseen by the International Energy Agency (IEA) that focuses on validating tools used in the development of offshore wind systems. Offshore Code Collaboration (OC3), Offshore Code Comparison Collaboration Continuation (OC4), Offshore Code Comparison and Collaboration, Continued with Correlation (OC5), and Offshore Code Comparison and Collaboration, Continued with Correlation and Uncertainty (OC6) are among the Offshore Code Comparison ventures (OC6). The first two projects were successful in illuminating the gaps between the theoretical methods involved, but they were constrained in their ability to illustrate how well the models compared to experimental results. The OC5 project tackled this limitation by comparing the findings to real-world response data collected from the OC4 phase II project. A 1/50th-scale wind turbine based on the NREL 5-MW reference wind turbine [13] with a flexible tower affixed atop a semisubmersible was used for that project.

### 4.3 Structural Description of the Model

The first method treats the FOWT as a single rigid body subject to external loads, ignoring structural deflections and assuming infinite stiffness. This allows for a significant reduction in the model's complexity. The finite element method, which discretizes the structure into a number of finite elements and accounts for structural flexibility, is the second approach. The individual columns of an S-bos, can also be represented using rigid body models. Because rigid body motions, rather than elastic deformation, dominate the structural reaction and motions, the first approach is used to describe the FOWT with sufficient precision. The model performs a dynamic study of a FOWT by solving the equation of motion in the time domain. The Eq. (4.1) of motion is given which can be also referred as Newton second law of motion:

$$F_{ext}(t) = (M + A)\ddot{x}(t) + B\dot{x}(t) + Cx(t) \quad (4.1)$$

The FOWT's mass and additional mass are represented by  $M$  and  $A$ . The damping is  $B$ , while the hydrostatic stiffness is  $C$ . The derivatives reflect the corresponding velocities and accelerations (DOF). The motion vector which is  $x$  represents the displacements in each degree of freedom.

OrcaFlex structural module is based on a multibody approach, in which each body has a collection of geometric and structural properties that combine to form Timoshenko beam components. The bodies each have their own coordinate system, and they communicate with each other according to algebraic constraints that define the degrees of freedom.

The coupling constraints account for the nonlinear effects of body motion. As a result, the modeling method is well adapted to calculations involving versatile structures. A modal method, i.e. the linear superposition of a subset of the system's response shapes to a collection of local Timoshenko beam components, is used to describe nonlinear effects found in wind turbines. Furthermore, the aerodynamic loads are measured at the blades current location, resulting in a nonlinear loading. As a result, the response of the structure can be classified as nonlinear. This method has less fidelity than a completely nonlinear Finite Element Method (FEM) representation, but it allows for good agreement with experimental results while requiring less computational time. The multibody and FEM representation of the tower and turbine is shown in Figure 24:

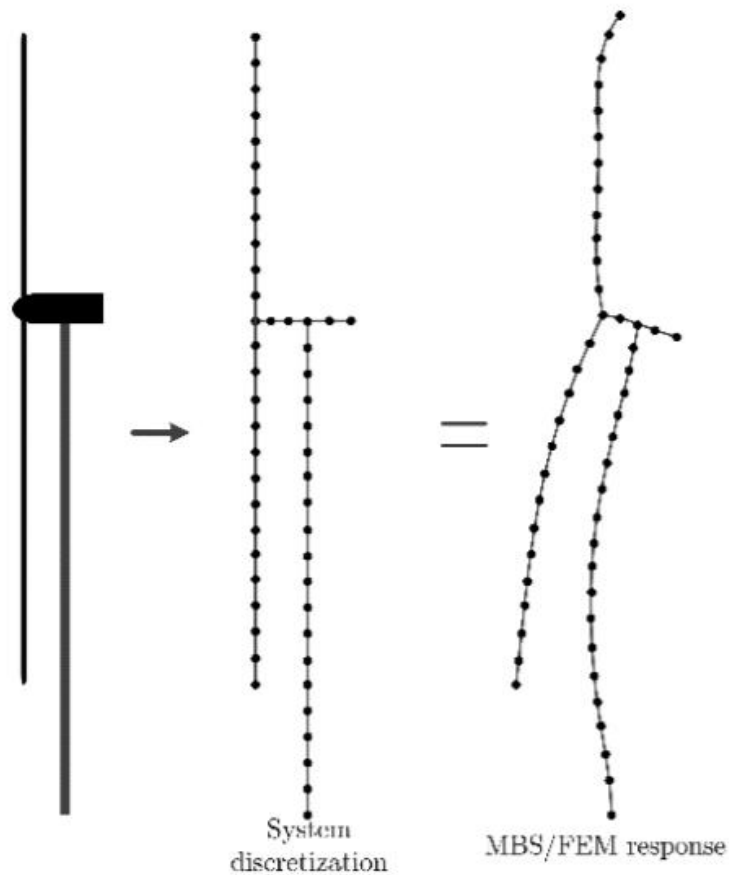


Figure 24: Multibody and FEM representations are depicted.

Using Morison's equation to compute hydrodynamic loads on the floater's Timoshenko beam components, a similar approach can be applied to the floating platform's bodies. However, since the hydrodynamic forces are obtained as bulk loads for the global rigid floater motion, using this method for possible flow models is difficult. Finally, if the bodies are carefully defined with enough beam components, the module can be used to solve complex nonlinear problems involving the behavior of highly flexible composite structures that can withstand massive deflections without reaching their elastic limits.

#### **4.4 Numerical Method**

The aerodynamics, hydrodynamics, and moorings sub-models used in the theoretical approaches taken by the participants can be divided into three categories. The aerodynamic sub-model is usually based on the Blade-Element Momentum (BEM) theory, but there are a number of other methods, including the 2-D Vortex Form, 2D/3D Actuator Line Theory, and 2D/3D Full CFD, to name a few. Improvements are possible such as a dynamic wake filter, which accounts for the lag in the induced velocities caused by vorticity being shed from the blades and convected downstream; or unsteady airfoil aerodynamics, which model flow hysteresis, unsteady attached flow, trailing-edge flow separation, dynamic stall, and flow reattachment. These findings showed that the more complex and detailed the model is, the better it is at capturing the system's dynamics. In the case of aerodynamics, including unsteady airfoil aerodynamics in BEM-based models aids in matching the dynamic response across a wider frequency spectrum.

A potential flow-based solution, a strip-theory solution based on Morrison's equation, or a combination of both is typically used to model the hydrodynamics. Radiation-diffraction matrices are used in potential flow models, but they do not account for viscous effects. As a consequence, viscous forces must be taken into account separately, such as an additional damping matrix or as a drag factor in Morrison's equation. The moorings can be modeled using either quasi-static or dynamic mooring line models, with additional features such as wave hydrodynamic excitation and seabed friction.

Quasi-static models are insufficient to predict ultimate and fatigue loads for moorings, dynamic models are much more accurate and can be enhanced by using hydrodynamic excitation from waves. In hydrodynamics, nonlinear forces beyond the wave excitation area trigger significant prediction errors and are best captured by second-order potential flow theory models and second-order or higher wave kinematics.

When the slenderness assumption is violated, Morison's equation-only models have been shown to be constrained. Due to the balance reached between precision and processor time, the participants in the OC projects used engineering or state-of-the-art methods to predict loads. Tools for numerical analysis (e.g. CFD) will be used in future, but mainly for results validation or cascading purposes, rather than for load measurement, due to the reason of computational resources requirements.

#### 4.4.1 Hydrodynamic Method Description

OrcaFlex measures buoyancy forces by combining external pressure forces, maintaining a proper force distribution in the structure's internal cross-sectional areas. The cross-sectional forces and moments are given by Eq. (4. 3) and Eq. (4. 4), respectively. The off-diagonal terms  $A_{3:1}$  and  $A_{3:2}$  are non-zero when the beam is not vertical, and  $A$  corresponds to the orientation matrix. The contribution of buoyancy is measured as follows:

$$F_{B,end} = \rho g S(z - z_0) + s p_{dyn} + 1/2 \rho C_{d,axial} * S * U_{rel} |U_{rel}| \quad (4.2)$$

$$\vec{F}_B = -g\rho \begin{cases} A_{3,1}S \\ A_{3,2}S \\ -\frac{\delta S}{\delta z}(z - z_0) + \frac{\delta S}{\delta z}P_{dyn} \end{cases} \quad (4.3)$$

$$\vec{M}_B = -g\rho \begin{cases} A_{3,2} \frac{\delta r}{\delta z} \pi r^3 \\ A_{3,1} \frac{\delta r}{\delta z} \pi r^3 \\ 0 \end{cases} \quad (4.4)$$

Eq. (4.2) involves concentrated forces at the ends of the beams or in places where the area changes. The axial drag coefficient is  $C_{d,axial}$ , and the relative velocity between the wave and the structure is  $U_{rel}$ .

#### 4.4.2 Morison Theory

Morrison's theory is useful for calculating preliminary estimates of a body's force magnitude. Morison is used for modelling the platform and to calculate the forces in the mooring. Also, the drag part of the Morison equation in order to calculate the current forces, or the quadratic damping term among other things. While defining the hydrodynamic module description of S-bos platform which is based on morison's equation, which predicts the force exerted on square structures extending from the bottom to above the crest by unbroken surface waves. A drag force proportional to the square of the horizontal wave velocity and the drag coefficient; and a virtual mass force proportional to the horizontal wave acceleration of the mass of water displaced by the structure [14]. In Eq. (4.5) and Eq. (4.6) the Morison's equation is presented as:

$$F_{ME} = \frac{1}{2}\rho C_d D |U_{rel}| U_{rel} + C_M \rho A \frac{dU_{rel}}{dt} \quad (4.5)$$

$$F_{ME} = \frac{1}{2}\rho C_d D |U_{rel}| U_{rel} + \rho C_a A \frac{dU_{rel}}{dt} + \rho A \frac{dU_{rel}}{dt} \quad (4.6)$$

Whereas:

$\rho$ : is the water density

$D$ : is the cross-sectional diameter

$\frac{dU_{rel}}{dt}$ : is the relative wave particle acceleration

$C_a$ : is the added mass coefficient, which is related to the shape-dependent cross-sectional area  $A$ ,

$C_M$ : is the inertia coefficient, which is defined as  $C_M = 1 + C_a$ ,

$C_d$ : is the drag coefficient.

Eq. (4.5) have the inertia concept which has been divided into two parts. The added mass effects are accounted for in the first term, while the Froude-Krylov force is accounted for in



the second. The implementation, which is based on strip theory, applies hydrodynamic loads to multiple interconnected elements derived directly from undisturbed wave and current kinematics at the displaced location of the sub-structure.

The cumulative forces and moments are calculated by integrating the force differentials at the calculation points along the structure. Currents, linear airy waves, irregular airy waves, deterministic irregular waves, stream function waves, and other wave kinematics can be produced in OrcaFlex, or the input can be read from the output of a wave interaction analysis program (e.g. OrcaWave). Load contributions from additional mass and drag effects from heave plates, as well as the impact of flooded members, can be included in addition to the hydrodynamic loads measured with morison's equation. A separate concentrated end effect based on the added mass of a column is used to achieve the added mass and drag from the inclusion of heave sections. The contribution of drag force is measured in Eq. (4.7):

$$F_{d,axial} = \frac{1}{2} \rho A C_{d,axial} U_{rel} |U_{rel}| \quad (4.7)$$

#### 4.4.3 Diffraction Theory

Regarding Potential flow theory also known as Diffraction theory. In order to assess the response of an offshore floating structure to motion. The diffraction potential theory uses the frequency domain to estimate wave stimulating forces on a floating body, and this method can be used to examine the motion of huge floating structures with acceptable precision. The strong diffraction effect that arises in large size structures in wave propagation accounts for the high accuracy of this diffraction theory when applied to huge structures. The equations described below in the frequency domain is given by potential flow theory, which assumes an equilibrium state for the floating body and the existence of a harmonic solution to the velocity potential. One can solve the Diffraction frequency domain problem by using the by using the Green 2<sup>nd</sup> theorem in Eq. (4.8) and Hskind Relation in Eq. (4.9) are expressed below:

$$\iiint_{V^*}^0 (\varphi_j * \nabla^2 \varphi_k - \varphi_k * \nabla^2 \varphi_j) * dV^* = \iint_{S^*}^0 (\varphi_j \frac{\partial \varphi_k}{\partial n} - \varphi_k \frac{\partial \varphi_j}{\partial n}) * dS^* \quad (4.8)$$

$$X_{Wk} = -i \rho e^{-i\omega t} \iint_{S^*}^0 (\varphi_\omega \frac{\partial \varphi_k}{\partial n} - \varphi_k \frac{\partial \varphi_j}{\partial n}) * dS^* \quad (for k = 1, \dots, 6) \quad (4.9)$$

One uses these equations to get the linear fluid velocity potential described in the Eq. (4.10). The velocity potential is expressed by the Laplace equation:

$$\varphi(x, y, z: t) = \varphi_{\omega} + \varphi_D + \varphi_R \quad (4.10)$$

$$\nabla^2 \varphi = 0 \quad (4.11)$$

The incident undisturbed wave potential is  $\varphi_{\omega}$ , the radiated wave potential is  $\varphi_R$  which is from the oscillatory motion of the body in still water and the diffracted wave potential of the waves about the restrained body is  $\varphi_D$ . After obtaining the wave fields, the force and moment contributions can be determined by using the Bernoulli Eq. (4.12).

$$P = -\rho \left( \frac{d\varphi_r}{dt} * \frac{d\varphi_{\omega}}{dt} * \frac{d\varphi_d}{dt} \right) - \rho g z = -\rho \frac{d\varphi}{dt} - \rho g z \quad (4.12)$$

The Force and moments equations can be calculated by using the Bernoulli equation and the Eq. (4.13) and Eq. (4.14) are expressed as follows:

$$\overline{F}_{PF} = \rho \iint \left( \frac{d\varphi}{dt} + g z \right) \vec{n} * dS \quad (4.13)$$

$$\overline{M}_{PF} = \rho \iint \left( \frac{d\varphi}{dt} + g z \right) \vec{r} \times \vec{n} * dS \quad (4.14)$$

Where:

$\vec{r}$  denotes the distance vector from the origin of the reference coordinate system.

$\vec{n}$  denotes the body surface normal vector

$\rho$  is the water density

$z$  denotes the vertical coordinate from mean sea level,

$S$  denotes the wet surface

$g$  denotes gravity's acceleration

Cummins' equation can also be used to obtain a time-domain solution. Potential flow solvers are more sophisticated hydrodynamic codes that can model scattered waves as well as the frequency-dependent variance of added mass and radiation damping. Cummins Eq. (4.15) is used to calculate the effects in the time domain:

$$F_{exc}(t) = (M + A_{\infty})\ddot{X}(t) + \int_{-\infty}^t K(t - \tau)\dot{X}(t)d\tau + CX(t) \quad (4.15)$$

Where:

$F_{exc}$  Is the exciting forces, taking into account the Froude-Krylov and wave scattering contributions.

$A_{\infty}$  Is the infinite frequency added mass matrix,

$K(t)$  is the impulse response function (IRF)

$M$  is the mass matrix

$C$  is the hydrostatic stiffness matrix

$X(t)$ ,  $\dot{X}(t)$  &  $\ddot{X}(t)$  Are the structure position, velocity, and acceleration vectors

An important point to be notice here is that while this method is appropriate for the application of low-order wave kinematics, then nonlinear potential flow fields must be considered in the case of more complex wave kinematics, suggesting that the linearization process discussed here will not be sufficient [15]. That is why this method is well preferred.

#### ***4.4.4 Simulation and Modelling Software's Description***

The added mass and damping due to radiated waves are captured by ANSYS-AQWA as a function of wave frequency. Since AQWA does not account for viscous forces as expected by theory, all damping would be provided by radiated waves if drag coefficients were not taken into account. It is possible to account for both viscous and radiation damping by defining viscous drag coefficients for the floater's bodies. The wave velocity potential has three components in AQWA, the incident wave potential, which is related to the Froude-Krylov power, the radiated wave potential, which is related to radiate wave forces, and the diffracted wave potential, which is related to scattered wave forces. OrcaFlex can be used in conjunction with a possible flow solver which is AQWA, with the output files from AQWA being read and used as direct inputs for OrcaFlex through an external file called .LIS. The AQWA program can describe a rigid body with six degrees of freedom (DOF), three translations, and three rotations. To link the floating structure and the wind turbine model, a set of constraints is specified, allowing for an integrated system representation. The following forces are used by ANSYS-AQWA:

- I. Hydrostatic pressure (from Ansys-AQWA output)
- II. Damping Forces, both linear and non-linear (specified by user)
- III. Frequency vs. Distance/Rotation (Heave RAOs)
- IV. Frequency vs. Distance/Rotation (Roll and Pitch RAOs)
- V. Forces of diffraction
- VI. The Law of Gravity (in COG)
- VII. Floatability (in COB)

The floating structure is in equilibrium when external forces interfere with it because buoyancy and gravity forces and centers are separate. The linear damping and stiffness forces specification is used to provide stability when modeling a system's interaction in a straightforward manner. Each DOF has six FRFs (frequency response function), one for each force part, for a total of 36 FRFs. The only driving parameter for diffraction forces is the wave elevation, which is dependent on six FRFs, one for each wave direction.

The FRFs of hydrodynamic forces driven by the movement of the system in all six DOFs are used to calculate radiation forces. The FRFs describe frequency domain powers, which are then translated to the time domain by convolution and it is defined in Eq. (4.16):

$$F(t) = \int_0^{\infty} K(t - \tau) X(\tau) d\tau \quad (4.16)$$

Where:  $X(\tau)$  is the driving parameter, which is either the structure's motion in the case of diffraction forces or the wave height in the case of exciting forces. Potential flow solvers allow for better modeling of the added mass since the frequency-dependent variance of the hydrodynamic coefficients is captured by solving the radiated wave potential on a 3D volumetric mesh with thousands of panels. Morison's equation is a very important engineering approach to a difficult physical problem involving a cylinder flow. A Morison equation implementation and a separate possible flow implementation, namely a coupling with wave analysis tools, are included in this work and the morison equation implementations are mentioned below:

- I. The forces' unpredictability is based solely on changes in horizontal velocity and acceleration, with no regard for three-dimensional effects. There is no axial pressure gradient or transverse force taken into account.
- II. Morison's equation refers only to inline forces for structures with a diameter-to-wave-length ratio, or diffraction parameter, of less than 0.2. If this condition is not met, the

sheltering effect produces dispersed wave fields that are impossible to model as a load at the structure's base and it is the most important implementation of morison equation.

- III. Morison's equation assumes a sinusoidally oscillating planar flow of particles, but it doesn't account for orbital motion, yaw, and body or free-surface proximity.
- IV. The Keulegan-Carpenter (KC) number is a measurement of the distance traveled by a particle on a wave. It can be seen Eq. (4.17):

$$\frac{F_{i,maximum}}{F_{d,minimum}} = \frac{20}{KC} \quad (4.17)$$

Where:

$F_{i,maximum}$  is the maximum inertial force

$F_{d,minimum}$  is the maximum drag force

As a result, the KC number represents the relative dominance of inertial or viscous effects. Inertial forces rule over drag forces for KC numbers below 20. As the KC number exceeds 20, drag forces win out over inertial forces. Morison's equation's inertia and drag components are based on empirical drag and inertia coefficients determined for particular flow conditions.

Just apply only morison equation model to situations with no major three-dimensional effects and sufficient KC numbers. The S-bos platform, or at least some of its members, could primarily violate the slenderness assumptions, rendering the implementation unsuitable unless a modification, such as the MacCamy-Fuchs correction, or a coupling with a possible flow solver, is used. As far as the correction is concerned for the flows with diameter to wave length ratios greater than 0.2, MacCamy-Fuchs suggested an enhancement derived from potential flow theory as a linear potential force acting on a cylinder including wave scattering effects.

#### ***4.4.5 Method Validation of hydrodynamics of S-bos Platform***

As previously mentioned, the hydrodynamic module can be based on a variety of theoretical methods, and their suitability is highly dependent on the structure's and flow regime's

characteristics. In conditions where inertia and drag effects dominate over diffraction and radiation effects, Morison's equation-based models are well adapted to predict loads.

DTU compared the results obtained in the IEA Annex 30 OC4 Phase II [16] to the results obtained in the IEA Annex 30 OC4 Phase I. The comparison of the results obtained with the HAWC2 standard version (Morison's only approach) was the emphasis. This method revealed that when the added mass is properly treated in the Morison's equation approach, including the added mass from heave plates and proper consideration of buoyancy, the natural frequencies observed provide an excellent agreement in terms of decay tests.

When the wave kinematics were used, it was discovered that the morison's equation model captured greater surge and pitch displacements, with increased pitch motion leading to an increase in tower bending moments and anchor line stress. This effect is amplified when the structure is made fully flexible, as the deformation of each node allows for additional displacements and rotations. The small wave non-linearity from wheeler stretching, which is only present in a morison's equation approach, is thought to be the primary cause of these inconsistencies in the results. The key drawback of this correction is that the low wave steepness expectation is not met for several wave regimes [17]. When modeling moderate to very steep waves in deep waters, where the waves cannot be closely approximated by sine waves, significant differences are observed, according to the experimental results. As for the S-bos, experimental tests are not yet taken, so the estimated results validate the numerical validation.

When the wave kinematics is taken into account, the Morison's equation model was found to capture greater surge and pitch displacements, with increased pitch motion leading to increased tower bending moments and anchor line stress.

As maximum versatility is applied to the structure, this effect is amplified because the deformation of each node allows for additional displacements and rotations. The small wave non-linearity from the wheeler stretching, which is only present in a Morison's equation approach, is thought to be the primary cause of the differences in the results. HydroDyn, the offshore hydrodynamics module of NREL's aero-hydro-servo-elastic code Quick, was compared to a more robust complete 3D CFD model in an article published in the ASME 2014 33rd International Conference on Ocean, Offshore, and Arctic Engineering [18]. To

predict loads on offshore structures, HydroDyn uses a combination of Morison's equation. As a result, it takes into account viscous and drag forces, as well as diffraction and radiation forces.

The OC4-DeepCwind semisubmersible studied in IEA annex 30 was used as the floating platform in that analysis. This platform is particularly well suited because it contains both large and small members, which are likely to be dominated by diffraction/radiation effects, and small members, which are likely to be dominated by inertia/viscous effects. OpenFOAM, a method that solves the incompressible Navier-Stokes equations for each cell in the mesh containing the semisubmersible geometry, was used to perform the complete 3D CFD simulations. There were three meshes used: one with the whole geometry, one with only the small members, and a third with only the big members. The wave case results revealed excellent agreement between FAST and OpenFOAM over a large range of wave heights. The semi-submersible is in a regime where diffraction effects are dominant in these situations. Furthermore, now that AQWA can involve member involvement, the shadowing effects can be treated.

In conclusion, neither a Morison nor a possible flow solution by themselves were expected to be suitable for modeling a floating platform such as the S-bos platform alone; instead, a combination of both was suspected to yield the best agreement with estimated results. Furthermore, none of these two methods sufficiently captures any 3D effects, so confirmation against experimental findings would almost certainly be needed to achieve physical results in future. Finally, it was anticipated that a careful selection of drag coefficients would boost the results for both the Morison's equation alone and the potential flow theory.

#### ***4.4.6 Aerodynamic model description for S-bos Platform***

Aside from the traditional approach, the module has been expanded to incorporate some modifications and corrections, such as dynamic inflows, which account for the phenomenon that occur when the loads exerted on the blades change suddenly. Another enhancement is the consideration of dynamic stall, which occurs when the angle of attack is quickly modified, causing the blade to stall and causing a delay until the flow returns to a stationary flow pattern. The aerodynamic module in OrcaFlex is based on a BEM theory that incorporates Blade

Element Theory and Momentum Theory, and solves the problem of simulating aerodynamic forces over a wind turbine rotor on two levels.

The rotor aerodynamics are modelled at the first degree, with the entire rotor region discretized into individual concentric annular components, or blade elements. The computation of the aerodynamic forces acting on each blade factor is thus reduced to a two-dimensional problem.

The aerodynamic module's second level consists of a model that describes the steady and unsteady aerodynamic forces on each blade element's 2D airfoil parts. The aerodynamic module is connected to a set of wind conditions that can be either deterministic or stochastic. Mean wind velocity, sudden acceleration, linear pattern, special gust events, and special shear are all deterministic inputs. Different methods are used to produce stochastic inputs from the outside.

#### ***4.4.7 Method Validation of Aerodynamics***

In this approach one have to calculate design loads on wind turbines using aero elastic codes based on BEM theory is known to produce strong agreement with estimated results while requiring little computational effort. However, some uncertainties exist, such as when dealing with scenarios that cannot be predicted by simple BEM theory, such as induced velocities for turbulent inflows and shear. A research by the Technical University of Denmark used experimental data to verify HAWC2's measured aerodynamic forces on a full-scale 2 MW wind turbine. EllipSys3D, a higher fidelity full 3D CFD model, was also used to compare the performance. The DANAERO experiment was the name of the project. The research used a turbulent inflow modelled in both codes with a Mann turbulence box fitted to the DANAERO experiment's estimated standard deviation and mean wind speed at hub height. [19]

The experiments were carried out by DTU in collaboration with industrial partners such as Siemens, Vestas, LM Wind Power, and DONG Energy between 2007 and 2010. Four radial positions of an NM80 2MW wind turbine blade with an 80-meter radius were measured for surface pressure. The power spectrum density of the measured and simulated force elements, tangential and regular to the chord, was compared to determine the results. But for a slightly lower spectrum at higher frequencies, where the effect of rotational sampling transfers energy



from the spectrum below the 1P to higher frequencies, the agreement was outstanding. For increasing radial positions, this effect is even more pronounced.

Except for the outboard and inboard parts, agreement was high throughout the entire blade span. The difference in the inboard section is due to stall in the CFD simulations, which is not visible in the estimated results.

## **4.5 Numerical Analysis**

The S-bos platform is a kind of semi-submersible platform having a concrete based structure. It is also having the eccentricity of steel tower with RNA compensated with ballast. The S-bos platform is robust and it has good seakeeping. The wind turbine is from the IEA 15MW reference wind turbine [25].

The platform is having four Columns which are providing excellent buoyancy and also provide enough waterplane inertia. The concrete base and the columns are the two major components of the S-bos platform. The concrete-based structure refers to the lowermost component of the platform. This component is deployed and filled with seawater to add the majority of the system's weight. The counterweight in the concrete foundation structure not only adds weight, but it also offers restoring forces, which counterbalance the overturning forces caused by wind, waves, currents, and the thrust force applied on the wind turbine.

The columns, which make up the upper half of the floater, are designed to provide the necessary positive buoyancy and water plane inertia to sustain the design wave and current loads. BlueNewables provided the structural properties of the floating platform with and without WTG, which were used to define the structural definition in both models. These properties are kept confidential for this version of the thesis as the project is still on going and experimental validation is yet to be done.

## 4.6 Diffraction Analysis

### 4.6.1 *Motion RAOs*

Response amplitude operators (RAOs) are used to analyze all six degrees of freedom for a platform, allowing the designer to better comprehend its movements and behavior. For the structure's motions as well as the loads on the cross sections, transfer functions are derived which are also known as response amplitude operators (RAOs). A platform's seakeeping results can be provided in two ways. Each displacement RAO is made up of two numbers that describe the vessel's response to a certain wave direction and period for one degree of freedom. The two numbers are amplitude and phase, which connect the amplitude of the vessel motion to the amplitude of the wave.

As mentioned above, a vessel has six degrees of freedom: three translations (surge, sway, heave) and three rotations (roll, pitch, yaw), therefore each wave period and direction has six amplitude and phase pairs in the RAO data [20]. The RAO amplitude and phase change depending on the type of vessel, and they also vary depending on draught, wave direction, forward speed, and wave period/frequency for a given vessel type. The first option is to employ numerical methods and tools to generate RAOs early in the design phase. The second method is to conduct seakeeping tests in a basin, which is frequently done to verify the conclusions of numerical calculations

For the S-bos platform, RAOs have been generated by using ANSYS-AQWA for the Heave (Z), Roll (Rx) and Pitch (Ry) as they are the most important degrees of freedom for the platform. Surge, sway, and yaw responses are not included in this chapter since they are controlled by the mooring system, which is not taken into account in this research.

RAO only includes radiation damping because they are directly extracted from ANSYS-AQWA and in OrcaFlex the additional linear/quadratic damping will be added. Normally, RAOs include only radiation damping and the intention is their peaks usually matches with natural periods and if all sources of damping are included then the values of the RAOs should decrease. Unmoored structures have no uncoupled resonance times in surge, sway, or yaw, but moored structures have times in the minutes. [21].

#### 4.6.2 Heave

In this section the heave motion can be seen in Figure 25. The RAO for heave motion in waves propagating in the negative 180 degree direction is illustrated. The normal period for heave reaction can be noticed at around 19.3 seconds. In practice, incorporating the Morison model causes drag on the structure, dampening the response and lowering the amplitude at resonance. The shape of this RAO is typical of a semi-submersible and matches Faltinsen's description [21].

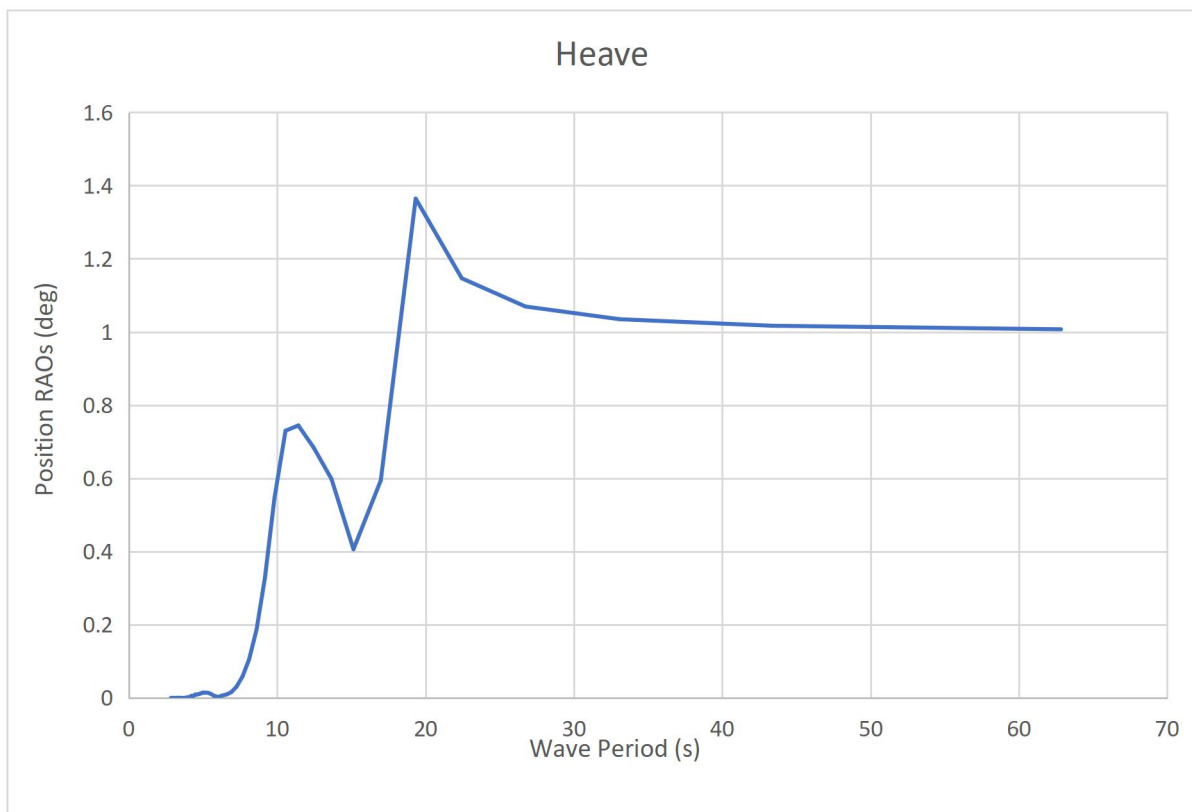


Figure 25: RAO for heave motion of waves with -180 degree direction

The response decreases just before the natural period, which is viewed as a cancellation effect. Because of the viscous forces created by the morison model, the response is not totally cancelled out. In heave, the maximum response occurs after about 19.3 seconds. The X-axis indicates the wave period and it is not a time duration, and Y-axis indicates the value of the parameter per unit wave amplitude/position in degrees. The heave response converges towards one for longer durations, and for long waves, the structure will move in heave with an amplitude equal to the wave amplitude.

### 4.6.3 Roll

For waves encountering the structure at a 90 degree angle, the RAO for roll motion of the structure is given in the Figure 26. This refers to wave's periods in the positive X- and positive Y-direction and is related to the rotation angle. A natural period of around 22.4 seconds can be detected in roll which can be seen in Figure 26:

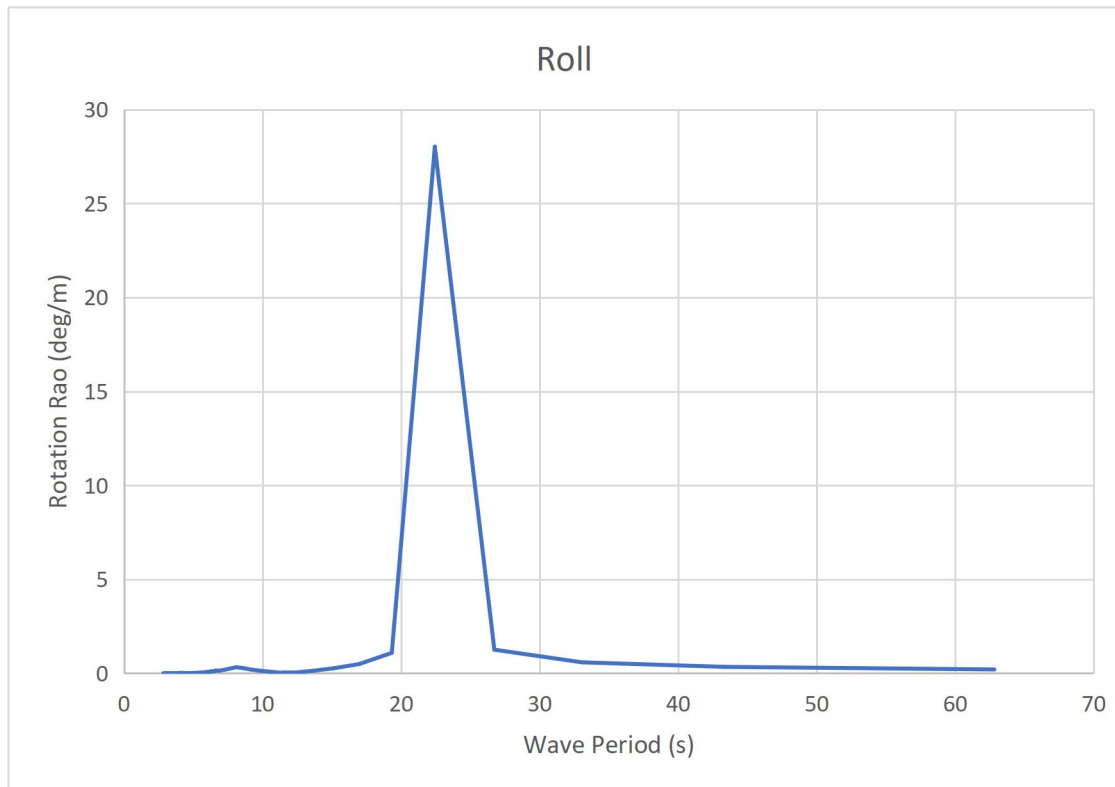


Figure 26: RAO for roll motion of waves with 90 degree direction

Waves hitting the structure from the side will cause a considerably larger roll response than waves hitting the structure from the front. Following and head waves should not cause any roll motion if they are symmetric about the xz-axis and there is no wave spreading or diffracted waves. However, the roll reaction seen in the Figure 26 at 90 degrees is largely due to coupling. This coupling can be seen by looking at mass inertia, damping, and additional mass in Table 7. Another peak in the roll response may be seen at around an 8 second interval. The highest stimulation from the waves corresponds to this peak.

### 4.6.4 Pitch

The structure's pitch motion has the opposite relationship to the wave direction as the roll motion discussed above. Waves with a negative 180 degree direction have the maximum pitch response, as seen in Figure 27. Pitch has a natural period of approximately 22.3 seconds.

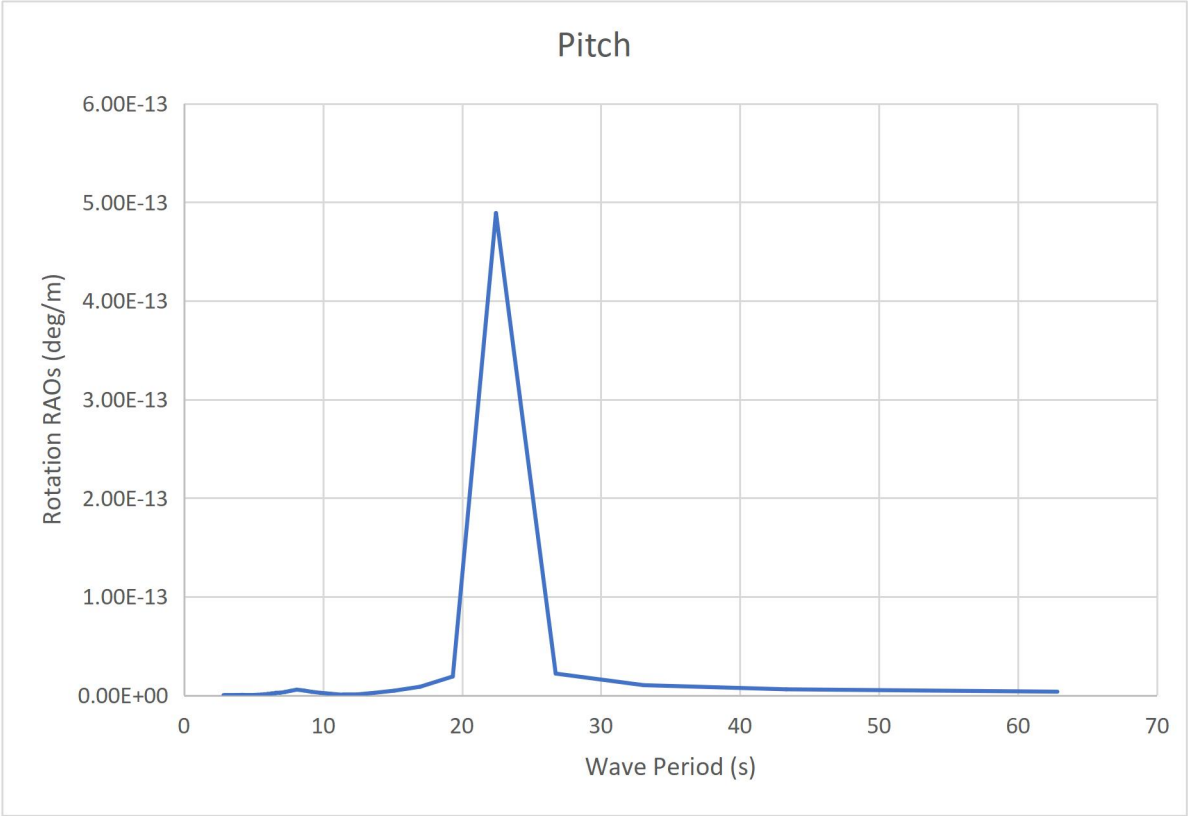


Figure 27: RAO for Pitch motion of waves with -180 degree direction

The size of this resonance peak begs the question of whether the model's damping is enough. The reaction will continue to decay and converge towards zero for longer periods than those depicted in Figure above, as the waves become much longer than the structure's length.

**4.7 First order wave forces**

First order forces are known as wave excitation forces and the sum of Froude Krylov and diffraction forces are known as wave excitation forces. In AQWA, when one uses the drift solver it applies, so AQWA applies directly sum of both forces and it does not distinguish between them. Same scenario for the OrcaFlex. For the Wave excitation forces of S-bos Platform, Wave excitation forces are calculated from AQWA for the Surge, Sway Heave, Roll, Pitch and Yaw Motions and it can be seen in the Figure 28:

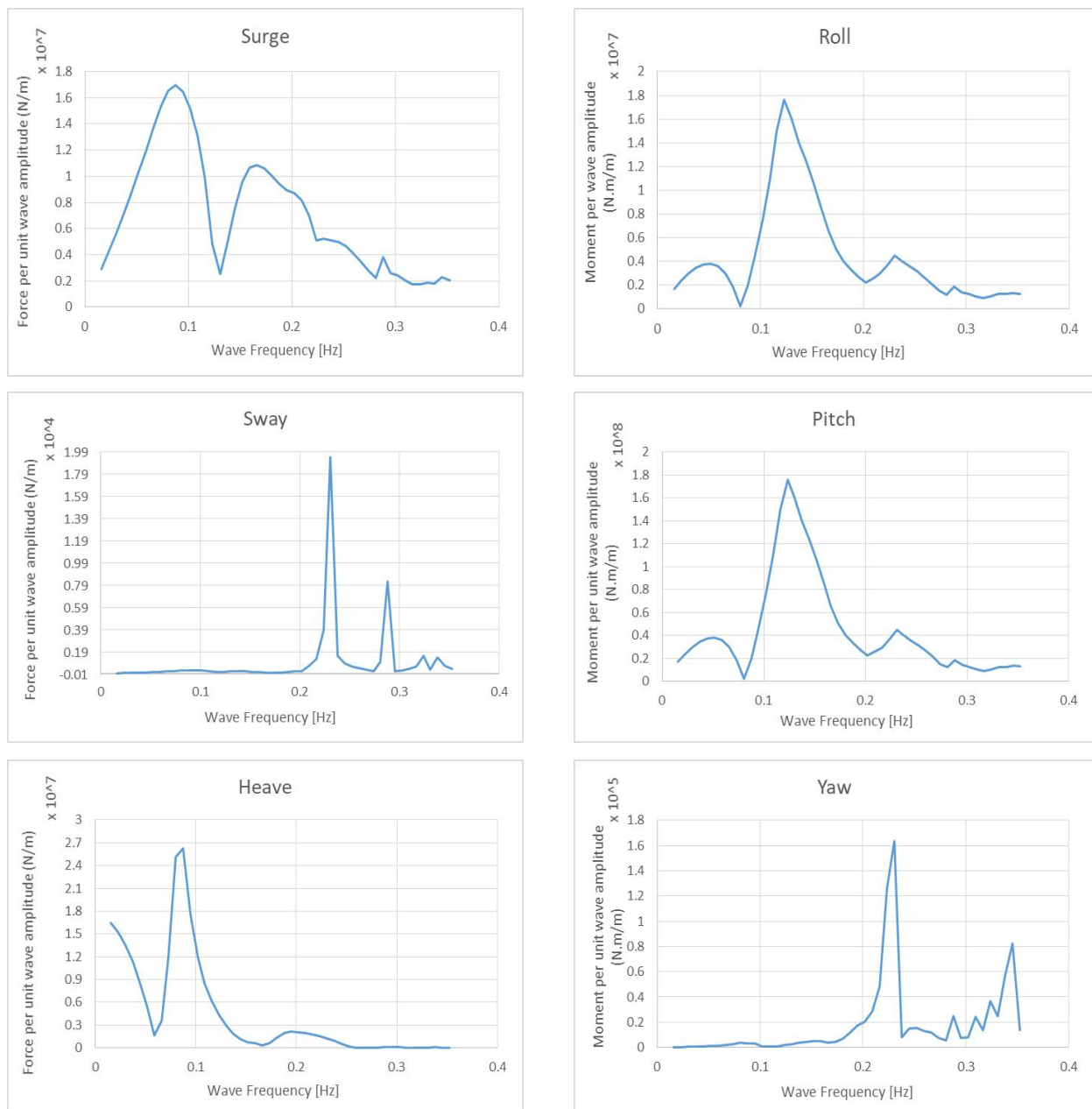


Figure 28: Wave Excitation forces of S-bos

Froude-Krylov force is that force which is related to the incident wave but without taking into account the body. On the other hand diffraction forces are related to the bodies having large structure as compared to the wavelength. The body alters the form of the incident waves over a large area in its vicinity. Wave excitation forces are frequency dependent and also they depend on the wave direction. The force tree on the platform can be seen in Figure 29:

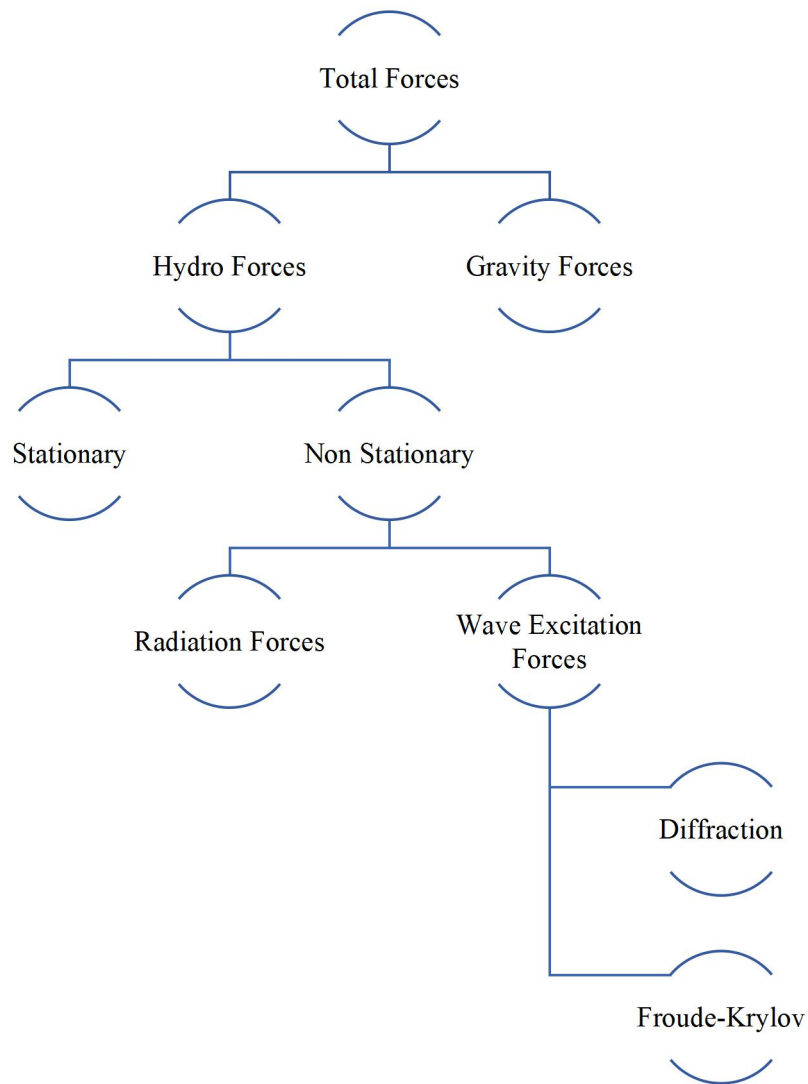


Figure 29: Total forces on the Platform

## 4.8 Radiation damping and Additional Damping

The results for the radiation damping and additional damping was calculated by using Ansys-AQWA. Due to the symmetry, the surge-surge and sway-sway elements, as well as the pitch-pitch and roll-roll parts, have similar magnitudes. Except for the yaw-yaw additional mass, the additional mass in all DOFs peaks in the low wave oscillation frequency. Figure 30 shows the frequency-dependent additional mass and radiation damping coefficients. Only the topmost diagonal matrix elements are visible due to the floater symmetry.

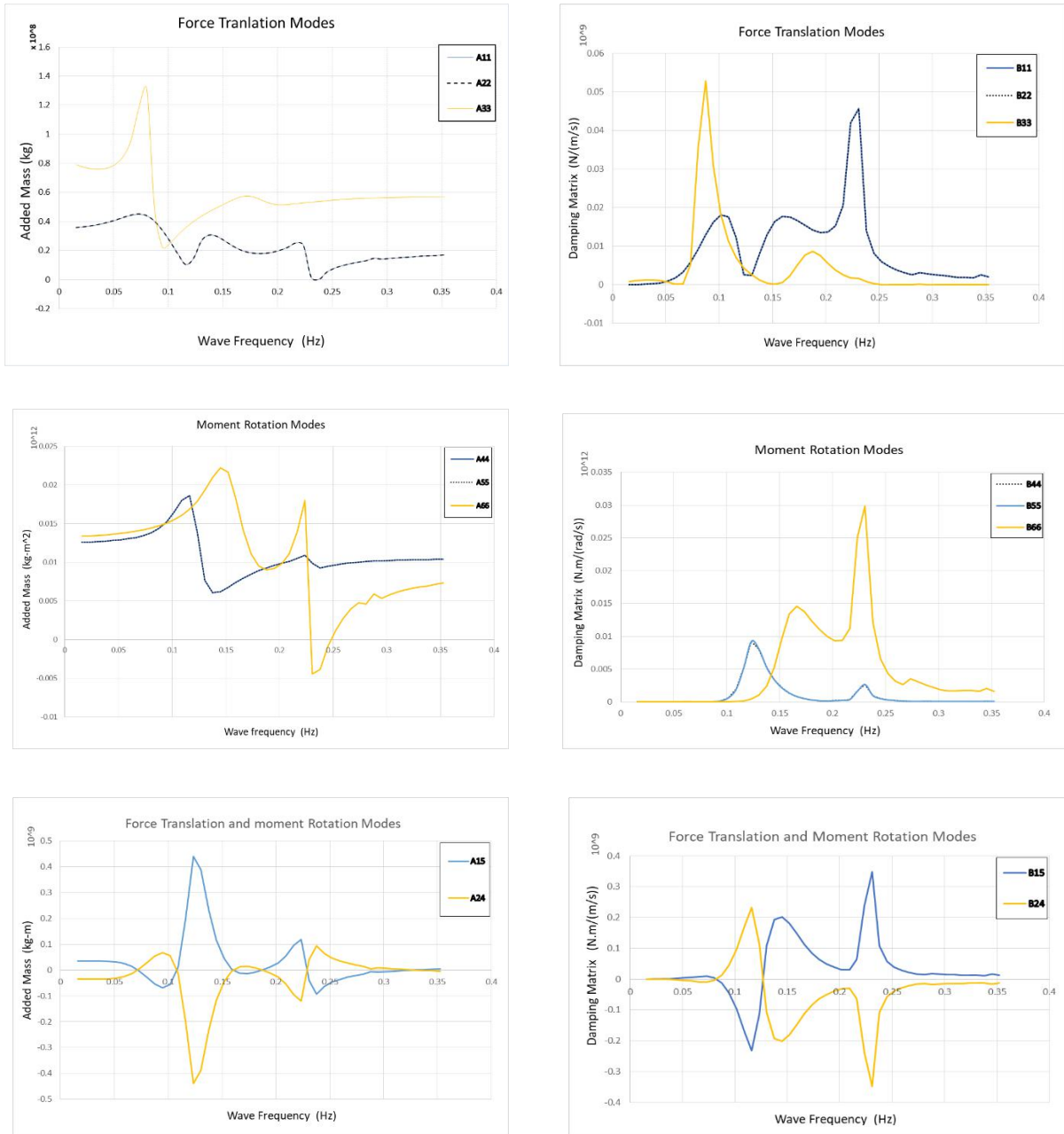


Figure 30: Frequency dependent Added Mass and Radiation Damping matrices

Figure 30 shows the hydrodynamic added mass and radiation damping coefficients in relation to platform response frequency. Only the upper off-axis terms have been reported, as the lower terms are identical, based on previous work with equivalent symmetry in the surge-sway plane (Robertson et al. 2014). In the case of the radiation damping coefficients, an infinity frequency limit is zero by definition, and the peak is seen towards mid-range wave oscillating frequencies.



## 5. Turbine Controller

The goal of a wind turbine controller is to maximize kinetic energy extraction without exceeding design loads. For this, two mechanisms come into play, the torque controller and the blade rotation. The torque controller acts mainly in the region below rated power. Its objective is to follow a predefined relationship between turning speed and wind speed to ensure maximum energy extraction.

The blade rotation controller or pitch modifies the angle of attack of the blades, thus modifying their aerodynamic profile and associated loads, limiting both the torque and the rotation speed of the wind turbine for high wind speeds.

The controller used for this study is compiled using FORTRAN compiler, which is a Dynamic Library (.dll). The functions within the DLL are called by using a python function called Wrapper. The (.dll) reads the controller configuration contained in a .TXT file. This file was inserted into the OrcaFlex to use for the Servo calculations.

The controller used in the project is based on a classic PI (Proportional - Integral) with additional filters to mitigate structural frequency interference in the rotational speed signal. The controller includes the possibility to modify the gain of the blade controller according to its operating point (gain-scheduling). In addition, it is possible to adjust the gains of the torque and blade controller and vary the control strategy in nominal power.

The controller will be based on the one developed by the DTU University and freely accessible and adapted to the 15MW turbine and the S-bos platform. As S-bos is a floating platform, in addition to the aforementioned objectives, another of high importance appears, which is to minimize the known “*negative damping*”. This phenomenon appears due to the speed of the turning action of the blades, causing the turning movements of the platform to be amplified, producing resonance at its natural frequencies.

## 6. Mooring System

A preliminary mooring system is used in this study. The position of the S-bos platform is secured and maintained by the mooring system in order to ensure that it does not vary too much under external force. The mooring lines are connected to fairleads which are situated at the mid of the platform. A quasi-static or dynamic technique is used to implement the mooring model in OrcaFLEX via an external system. To calculate the mooring force, the quasi static multi-segmented mooring method (MSQS) is used in the quasi static mooring model. The pre-tension and linearized mooring force are both components of each mooring force. The sum of all mooring forces equals the total mooring force. Figure 31 is the quasi-static mooring model and its description as follows: (a) the quasi-static model's schematic diagram (b) the catenary solution for each quasi-static mooring line.

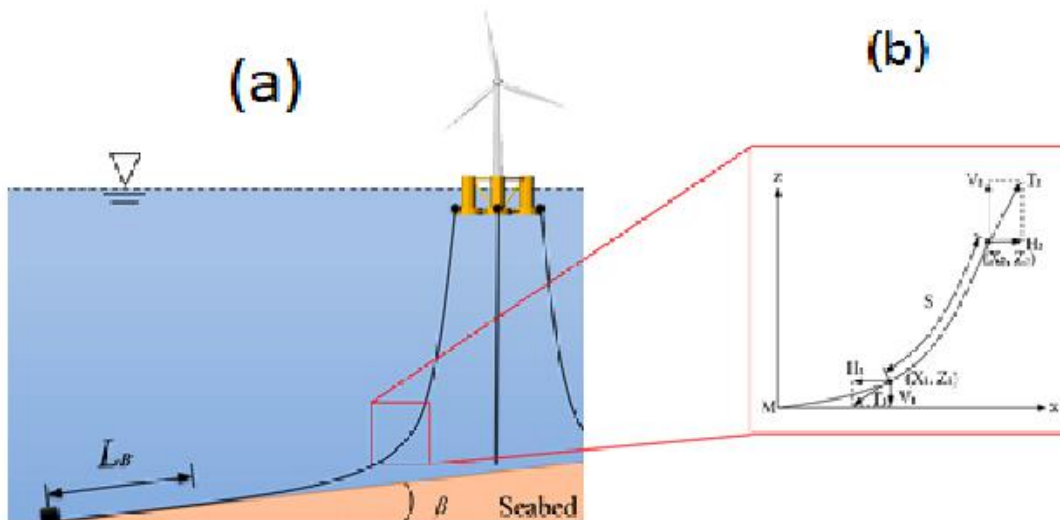


Figure 31: Quasi-static model's schematic diagram (source: MDPI)

The lumped-mass approach [22] is employed in the dynamic mooring model to calculate the dynamic simulation of the interconnected cables, weight, and buoyancy. The mooring cable is divided into  $N$  equal-sized line segments connecting  $N + 1$  node sites in this approach. The index  $i$  begins at the bottom with the anchoring node, which has a value of zero. The line segment between nodes 0 and 1 has an index value of  $1/2$ , and the fairlead node at the top has an index value of  $N$ , as shown in Figure 32:

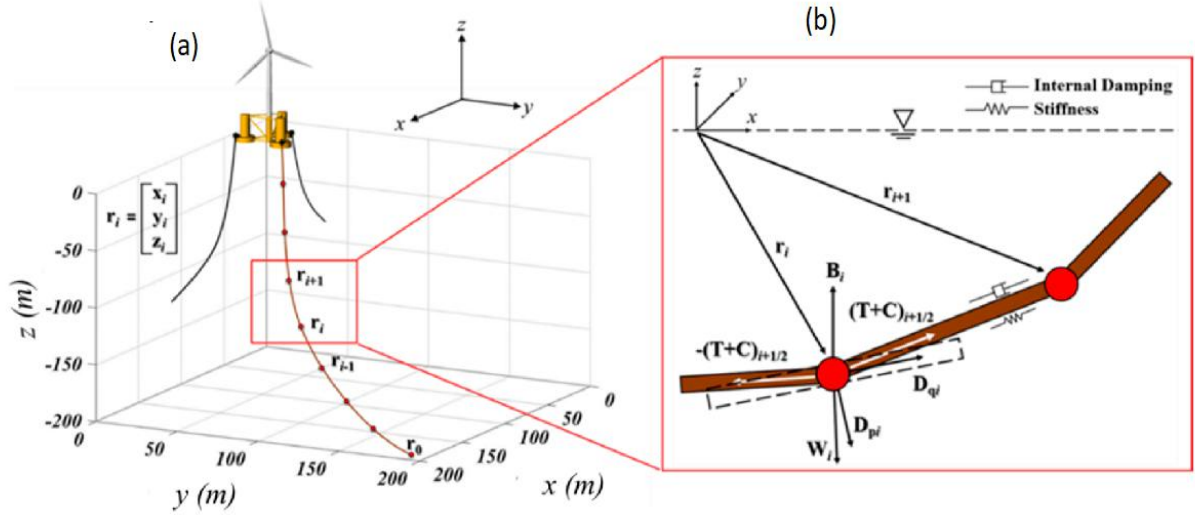


Figure 32: Description of dynamic mooring model

In the description above, section [a] represents the discretization of a mooring cable on the other hand section [b] represents the internal and external forces of a dynamic mooring cable. Using this method, the mass of the mooring cable is discretized into point masses at each node using the lumped-mass (LM) approach, which assigns each node half the total mass of the two neighboring line segments. For node I the 3x3 mass matrix is represented in Eq. (6.1):

$$m_i = \frac{\pi}{4} d^2 L \rho I \quad (6.1)$$

Whereas  $I$  is the identity matrix and  $\rho$  is the density of the mooring cable. The findings of comparing the fully dynamic mooring system methodology outlined in this paper to the quasi-static MIMOSA code from MARINTEK [23] also the MDPI [24] revealed that the adoption of a fully dynamic mooring line had no effect on the blade extreme or fatigue loads.

The mooring lines situated at the upwind corner of the base columns prevent the floating platform from capsizing and maintain its place in the waves. The mooring lines system is made up of four catenary mooring lines that are radially spaced at 90 deg. Two lines are set on each side as it can be seen in the Figure 33:

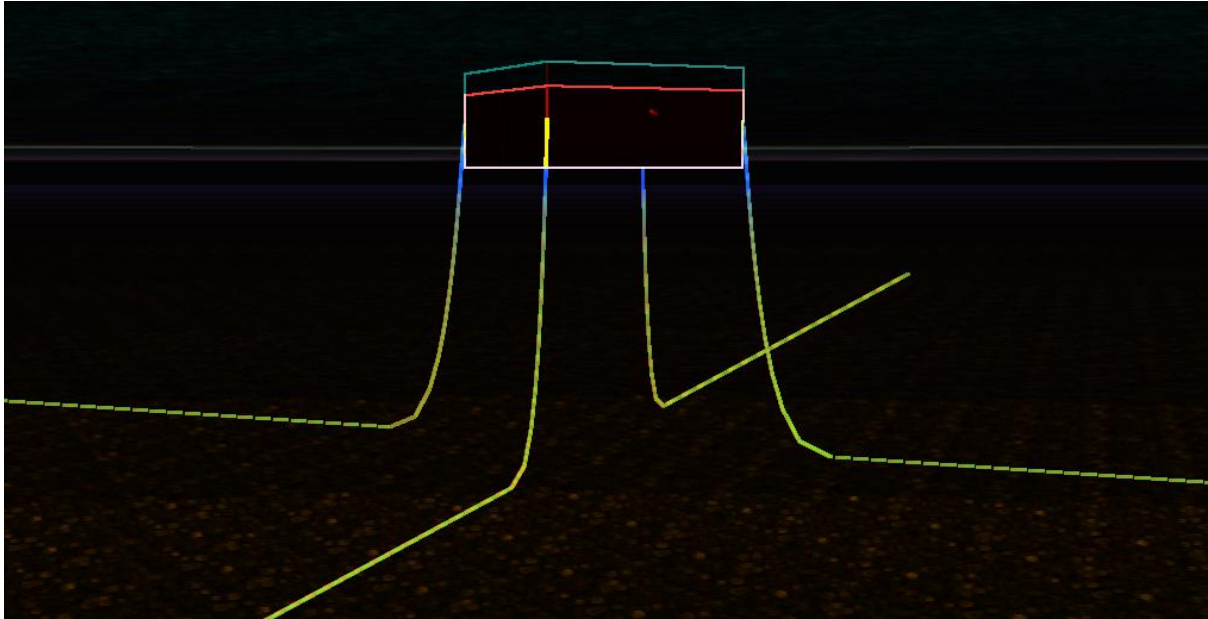


Figure 33: Mooring lines configuration schematic from OrcaFlex

For the S-bos platform, the mooring lines are attached to the concrete base (in static equilibrium) at a depth of 5 meters and to the anchors on the seabed at a depth of 100 meters. The length of the line is 515 meters, and the radius of the footprint is 500 meters.

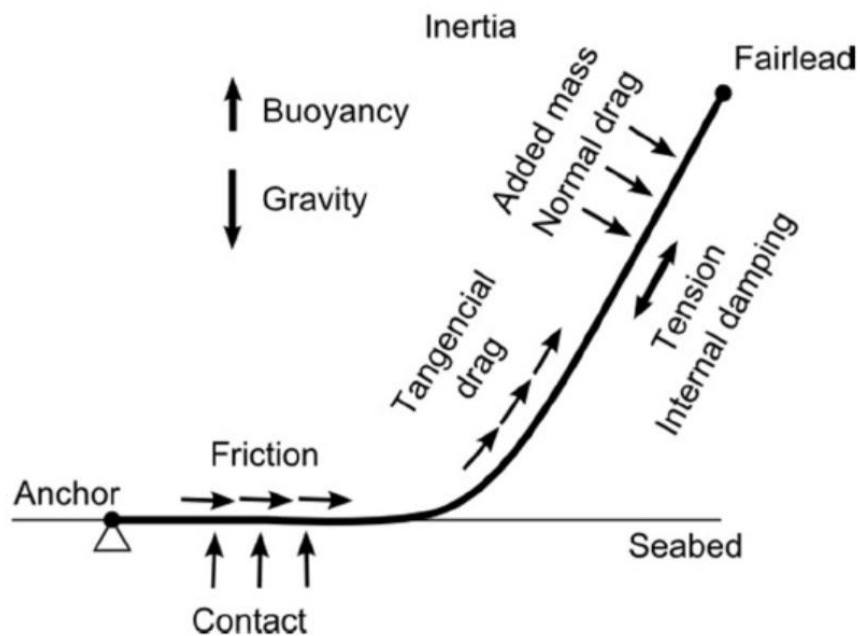


Figure 34: Mooring Line analysis diagram (Source: CENER)

The possible characteristics to be considered for the dynamic mooring analysis are shown in the Figure 34. The length of line in static equilibrium on the seabed is projected to be 282.6

meters, ensuring that uplifting forces on the anchors are minimal. To accurately represent the interaction between the wave loading, the mooring lines and the floating platform, it is concluded that the usage of a dynamic mooring system is required. The mooring line parameters and properties are explained in the Table 6:

Table 6: Mooring lines configuration main parameters and properties

PARAMETERS	DESCRIPTION	VALUE	UNIT
$N$	Number of Mooring Lines	4	[-]
$L$	Line Length	515	[m]
$FPR$	Foot print Radius	500	[m]
$\alpha$	Angle between two adjacent lines	90	[Deg]
$\beta$	Angle of lines at fairlead with vertical axis	21.4	[Deg]
$D$	Link Diameter	0.16m	[mm]
$G$	Grade (quality) of steel	R3	[-]
$W_d$	Dry weight per lines unit length	4.9959	[kN/m]
$W_w$	Wet weight per lines unit length	4.34108	[kN/m]
$A$	Effective steel area	1914109	[mm <sup>2</sup> ]
$EA$	Stiffness	2.186E6	[kN]
$BL$	Breaking Load	15.65E3	[kN]
$C_a$	Added mass coefficient	0.5	[-]
$C_{DT}$	Transversal drag coefficient	2.4	[-]
$C_{DL}$	Longitudinal Drag coefficient	1.15	[-]
$A_{HEQ}$	Hydrodynamic Eq. Cross- Sectional Area	0.064	[m <sup>2</sup> ]
$D_{HEQ}$	Hydrodynamic Eq. Cross- Sectional Diameter	0.287	[m]

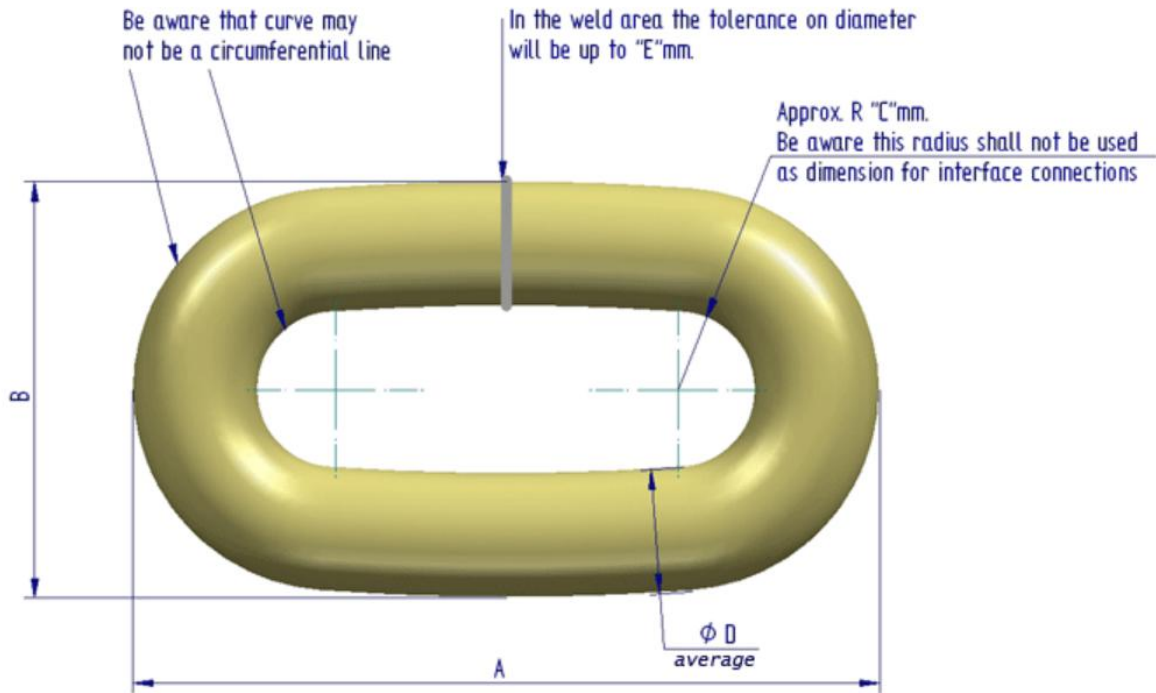


Figure 35: Studless chain link illustration (Source: [www.vicinaycadenas.com](http://www.vicinaycadenas.com))

This mooring chain is considered for the deeper water depths as the design life to withstand is approximately 25 to 30 years for studless chain links. The Chain link diameters are being calculated from the *vicinaycadenas* as shown in Figure 35 for the Mooring chain link diameters and their values and parameters are illustrated in the Table 7:

Table 7: Chain Link Diameters

<i>Parameters</i>	<i>Description</i>	<i>Value</i>	<i>Unit</i>
<i>A</i>	Link Length	960	[mm]
<i>B</i>	Link Width	536	[mm]
<i>C</i>	Link Radius	100	[mm]
<i>D</i>	Link Diameter	160	[mm]
<i>E</i>	Maximum Link Diameter	176	[mm]

## 7. Definition of the Numerical Model

BlueNewables gave a detailed description of all of the platform's components, including their mass, mass moment of inertia, and center of gravity in order to proceed with the calculations in the softwares but they are kept confidential by the BlueNewables. A schematic drawing was also shared, which included all of the required dimensions.

The base or definition of an equivalent OrcaFlex model is the geometrical description of the structure and its structural attributes. Even if OrcaFlex and AQWA are coupled, the bodies of the floating platform must be described in both models using OrcaFlex. The floater bodies are solely defined to model viscous drag in the OrcaFlex-AQWA model; all other hydrodynamic and structural attributes are given by the coupling. OrcaFlex provides for a 3D depiction of structures utilizing multi-element beams, but not for full 3D volumetric modelling and the ASHE illustration modelled in OrcaFlex can be seen in Figure 36:

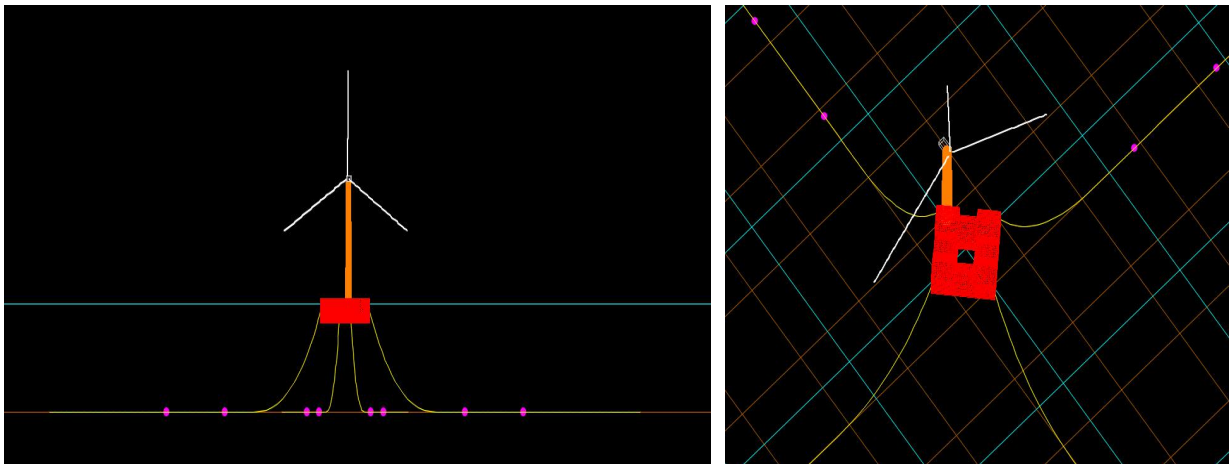


Figure 36: Illustration of ASHE in OrcaFlex Model

As a result, in addition to matching structural properties, the goal was to define a system whose spatial distribution resembled the original structure as closely as possible, because structural and hydrodynamic properties vary with changes in cross-section properties across the length of the bodies.

All of the floater's bodies except for the tower and RNA bodies were modelled as rigid bodies, with mass and mass moments of inertia assigned to their centers of gravity. The tower was

based on the IEA 15MW Reference Wind Turbine tower properties, with the necessary adjustments to match the BlueNewables design's tower height and structural features. The RNA bodies were modeled straight from the IEA 15MW Reference Wind turbine specification model, with minimal changes.

### 7.1 General Arrangement (G.A)

Four rectangular columns are connected to form the substructure which is itself a rectangular concrete structure. There are no connections between the columns since the concrete base to which the columns are fastened is expected to provide adequate support to the columns. In the Figure 37, a top- and side-view sketch of the structure is provided, with the columns and concrete structure designated with a letter and number that are used in the report as labels for the various elements.

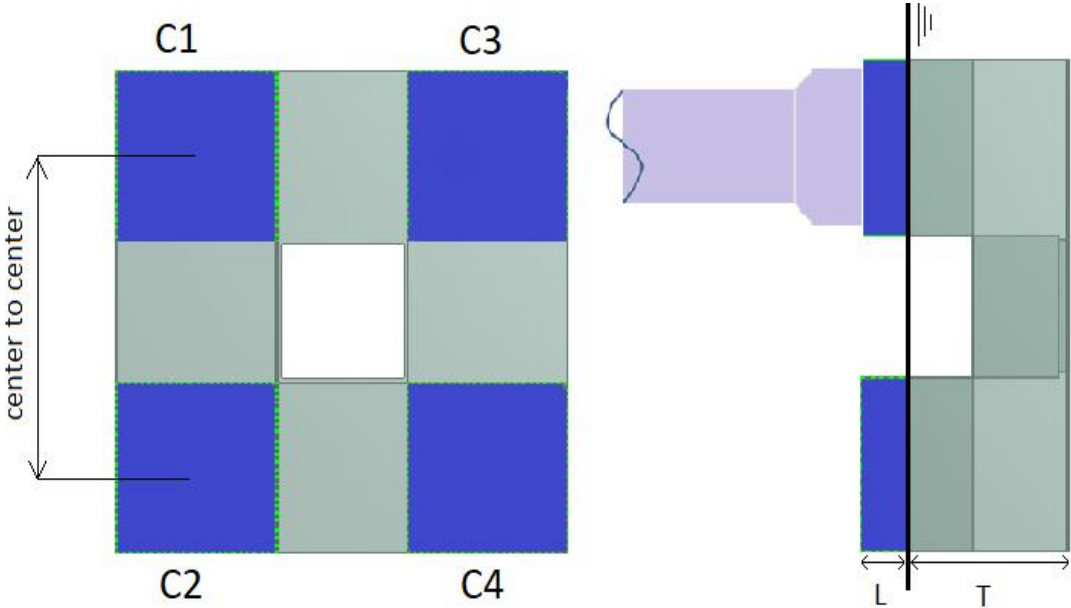


Figure 37: Top-view and Side-view of the S-bos Platform

The distance between the columns is measured from center to center, with L denoting column height and T denoting concrete structure height. These factors are tweaked to obtain the optimal design solution for the task at hand. The turbine is attached to column 1 (C1) as an extension, and the three rectangular elements are concentric and share the same center.

There will be a transition piece between the column and the tower base, allowing the loads from the turbine to be dispersed down to the column and the rest of the support system. The



concrete base, as well as the four columns C1, C2, C3, and C4, are all portrayed as ballast tanks. Although 10% to 12% of their total internal volume is withdrawn for internal structural components, the majority of their internal capacity is meant to be available for ballast water. The base will be filled as much as possible according to their volume in the operational condition. In order to achieve zero trim, the columns are employed for ballast. Zero trim can be obtained by filling C2, C3, and C3 greater than C1 to compensate for the offset mass of the turbine.

### 7.2 S-bos Model Mesh

The S-bos model consists of concrete structure and the four buoyancy columns. Figure 38 shows the S-bos model with the mesh generated in ANSYS-AQWA. The construction is designed as a rectangular closed compartment with four columns that provide sufficient buoyancy to the entire structure. The Structure's upper and lower decks are rectangular, with a rectangular cut-out in the center that is referred to as a moonpool.

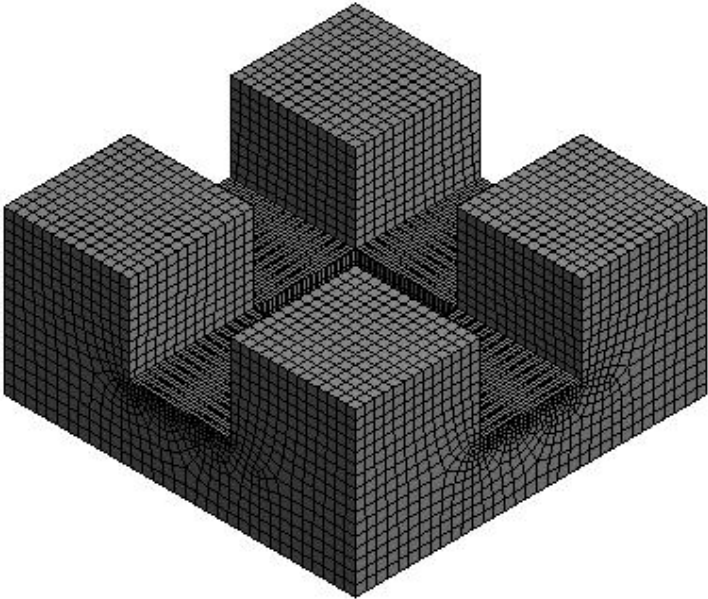


Figure 38: S-Bos model with Mesh

The inner rectangular cut-out is simulated with sharp corners, despite the fact that, in order to reduce stress concentrations, it should be created with a radius when built in reality. These edges are sharply sculpted in order to provide a better mesh in this area. Small radii corners necessitate a significant number of elements to be appropriately represented, which might cause mesh generating issues with ANSYS-AQWA.

The maximum length of each element is defined in the S-bos model, which uses second order elements. It has been set to program controlled and the mesh size is kept modest for the accuracy of the hydrostatic and hydrodynamic studies. Table 8 lists the mesh parameters for the S-bos model.

Table 8: Mesh parameters in AQWA for S-bos Model

<b>Parameters</b>	<b>Values</b>
No. of Nodes	9456
Diffracting Nodes	8048
No. of Elements	9456
Diffracting Elements	7948
Mesh Size	3 m
Tolerance	1.5 m

### 7.3 Rotor-Nacelle-Assembly (RNA)

The design and performance of the IEA Wind 15-MW reference wind turbine, developed collaboratively by NREL, DTU, and UMaine, is given for the S-bos Platform. In this project The IEA Wind 15-MW reference wind turbine [25] is used. In a simple and small nacelle layout, it uses a direct-drive layout with a permanent-magnet, synchronous, radial flux generator. Compared to geared drivetrains, direct-drive wind turbine generators have fewer parts, reduced complexity, higher dependability, and more flexibility in designing for particular topologies.

The direct coupling of the generator at very low speeds, on the other hand, necessitates considerable physical dimensions and mass, posing transportation, assembly, and maintenance issues. To address these issues, an appropriate balance of generator position, bearing number, internal or external stator/rotor arrangement, ancillary component interface, and rotor/stator inactive substructure geometries is required. [26]

In this project, once all of the bodies have been constructed, RNA are oriented to their respective initial positions, and a set of constraints is created to determine which degrees of freedom they are allowed to move with regard to one another. Except for the shaft and the blades, all of the bodies are attached to their neighbors. The shaft constraint is modeled as a bearing with its own vertical axis for rotation. At the design tip-speed ratio (TSR), the rotor has a pitch setting of  $0^\circ$ , however at low wind speeds, the rotor has a positive pitch setting to track maximum power while retaining the minimal rotor speed. At the rated wind speed of 10.59 m/s, the rotor begins to pitch. The blades can also revolve around their own vertical axis, which is controlled by the controller, which also controls the pitch angle at each time step. The main parameters used for the IEC 15 MW RNA are shown in the Table 9

Table 9: IEC 15 MW main parameters for RNA used for S-bos

<b>Parameters</b>	<b>Values</b>	<b>Units</b>
Power rating	15	MW
Turbine class	IEC Class 1B	-
Number of blades	3	-
Control	Variable speed	-
Rated wind speed	10.59	m/s
Cut-in wind speed	3	m/s
Cut-out wind speed	25	m/s
Minimum rotor speed	5	rpm
Maximum rotor speed	7.56	rpm
Design tip-speed ratio	9	-
Airfoil series	FFA-W3	-
Rotor diameter	240	m
Specific rating	332	W/m <sup>2</sup>
Blade mass	65	t
Shaft tilt angle	6	deg
Drivetrain	Direct drive	-
Blade prebend	4	m
Hub diameter	7.94	m
Hub overhang	11.35	m
Rotor precone angle	-4	deg

### 7.4 Tower

The S-bos floater is designed to accommodate large-capacity wind turbines, such as the IEA 15MW Reference Wind Turbine [25], in line with industry developments in offshore wind energy. It can, however, be adapted to smaller wind turbines. As this study does not focus on the tower definition but the general study to the reference wind turbine tower IEA 15 MW was conducted.

The original tower stands 150 meters tall, whereas the S-bos floater requires a tower that stands 140 meters tall. The tower was intended to be significantly heavier. In a global coordinate system, the center of gravity is, as expected, in a different location, yet it is in the same location relative to the tower height.

Based on IEA's modeling of the tower, the S-bos tower was modelled as a completely flexible homogeneous line type body in OrcaFlex. The parameters of the original IEA 15 MW Reference Wind Turbine tower do not quite match the properties of the tower necessary to support the RNA with the S-bos floater, so it will need some modification. The mass moments of inertia, and center of gravity of the altered tower must meet the design requirements. The inertia properties are described in Table 10:

Table 10: Inertia properties of the tower

Parameters	Values			Units
Center of Mass	[8.2E-15	0.0	67.3406]	m
Mass moments of Inertia	[1.274E6	0.0	-150E-12	t.m <sup>2</sup>
	0.0	1.274E6	0.0	
	-150E-12	0.0	18.41E3]	

In order to gain any mass, initially, one have to increase the section mass per length and to match both the weight and the position of the center of gravity, one have to disperse the mass. It will result in a higher mass distribution in the first half of the tower. The radii of gyration of each segment can be adjusted to adjust the mass moments of inertia in the z-axis. Once the mass and center of gravity have been matched, the S-bos tower's natural frequencies must

match with the IEA 15 MW Reference wind turbine tower. The main parameters used for the S-bos tower are given in Table 11

Table 11: IEC 15 MW main parameters for reference Tower used for S-bos

<b>Parameters</b>	<b>Values</b>	<b>Units</b>
Total Length	140	m
Total weight in air	8866.35	kN
Total Displacement	8.33E+04	kN
Total wet weight	-7.45E+04	kN
Total Mass	904.11	t
Material of tower	Steel	-
Volume	8289.58	m <sup>3</sup>

## 8. Time Domain Simulations

In order to analyze the natural periods and their damping's in the time domain simulations, decay tests were undertaken. In order to fully validate the model, wave tests will have to be performed in future. The natural frequencies and damping level of the system can be studied using the decay tests for all degrees of freedom. The time in which a freely oscillating systems completes one cycle of oscillation, is known as natural period. The estimated values of the natural periods for this project were calculated by using the following equations:

$$T = 2\pi \sqrt{\frac{M}{k}} \quad (8.0)$$

$$T_D = \frac{T}{\sqrt{1 - \xi^2}} \quad (8.1)$$

$$T_{33} = 2\pi \sqrt{\frac{M + A_{33}}{\rho g A_{waterplane}}} \quad (8.2)$$

$$T_{44} = 2\pi \sqrt{\frac{I_{44} + A_{44}}{\rho g VGM_t}} \quad (8.3)$$

$$T_{55} = 2\pi \sqrt{\frac{I_{55} + A_{55}}{\rho g VGM_t}} \quad (8.4)$$

Eq. (8.1) is used to calculate the dampened period and on the other hand Eq. (8.2) calculate the heave natural periods which is estimated around 18s referred as T33 in Table 12 and Eq. (8.3) and Eq. (8.4) are used to calculate the roll and pitch natural periods which was around 22.5s which are referred as T44 or T55 in Table 12 and it describes the calculated natural periods in order to compare with the natural periods from AWQA-ORCA models:

Table 12: Calculated Natural periods for S-bos

Natural Period	Values	Units
T33	18.0	s
T44 or T55	22.5	s

The decay tests in OrcaFlex are performed in order to compare against AQWA decay tests. The ASHE (Coupled Assessment) is complex and for this model the decays are without tank tests camping so, the only way to compare is against AQWA rigid model. On the other hand, one can also compare the Orca-AQWA natural periods with the hands on calculations. In the OrcaFlex, the first step was to run decay tests for the numerical models for Heave, Pitch, and Roll, with the goal of fine-tuning the Full OrcaFlex natural frequencies by adjusting the added mass modeling based on the OrcaFlex-AQWA linear damping coefficients in Roll and Pitch, and the Quadratic Damping coefficient for Heave.

The comparison to estimated data was the final step in order to validate the procedure for this study. The results revealed that, on comparison, both models from ANSYS-AQWA and OrcaFlex, the models had excellent agreement in terms of natural periods with the estimated results and moderate agreement in terms of damping levels. The decay tests can be seen in Figure 39, Figure 40 and Figure 41:

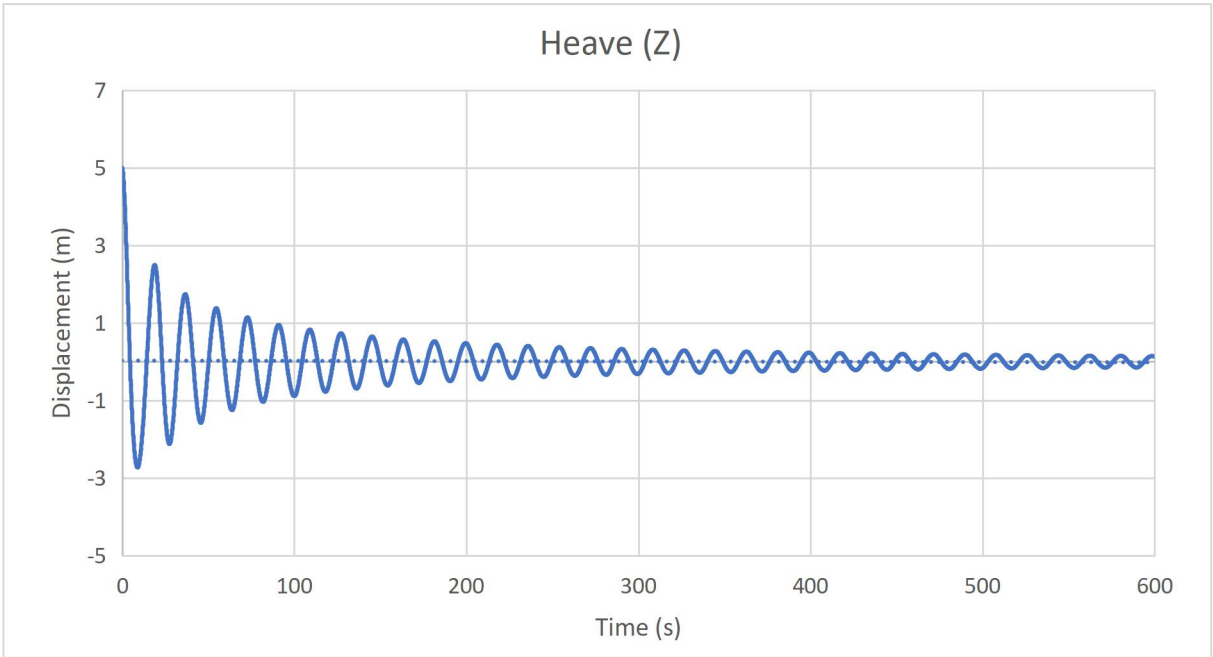


Figure 39: Decay test for the Heave

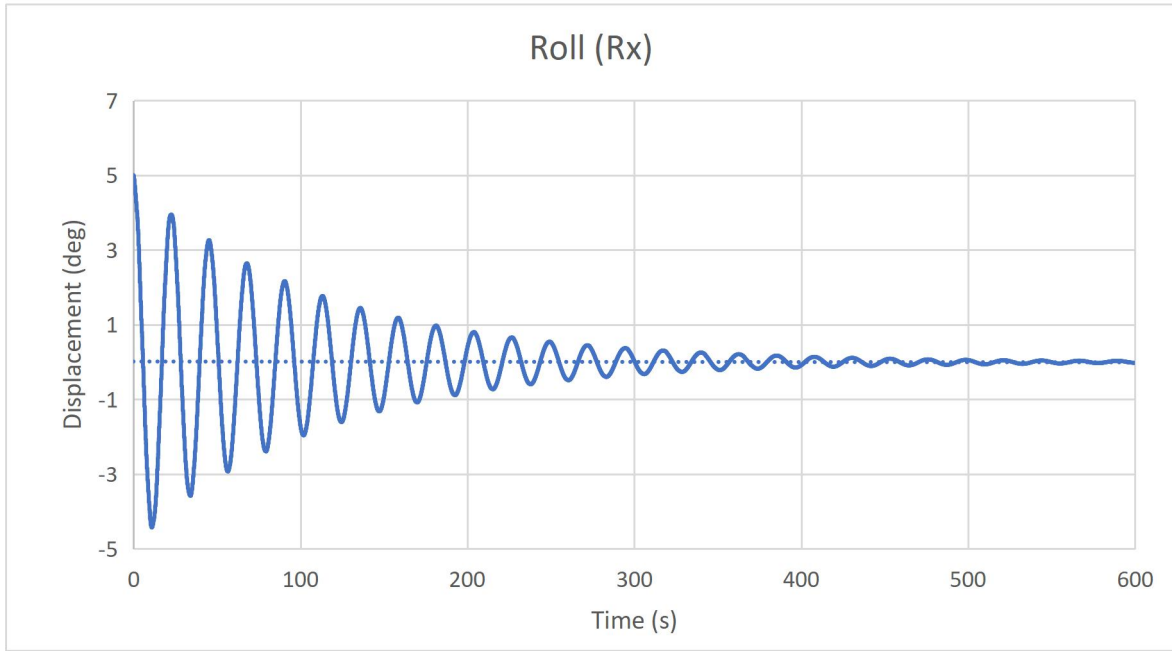


Figure 40: Decay test for the Roll

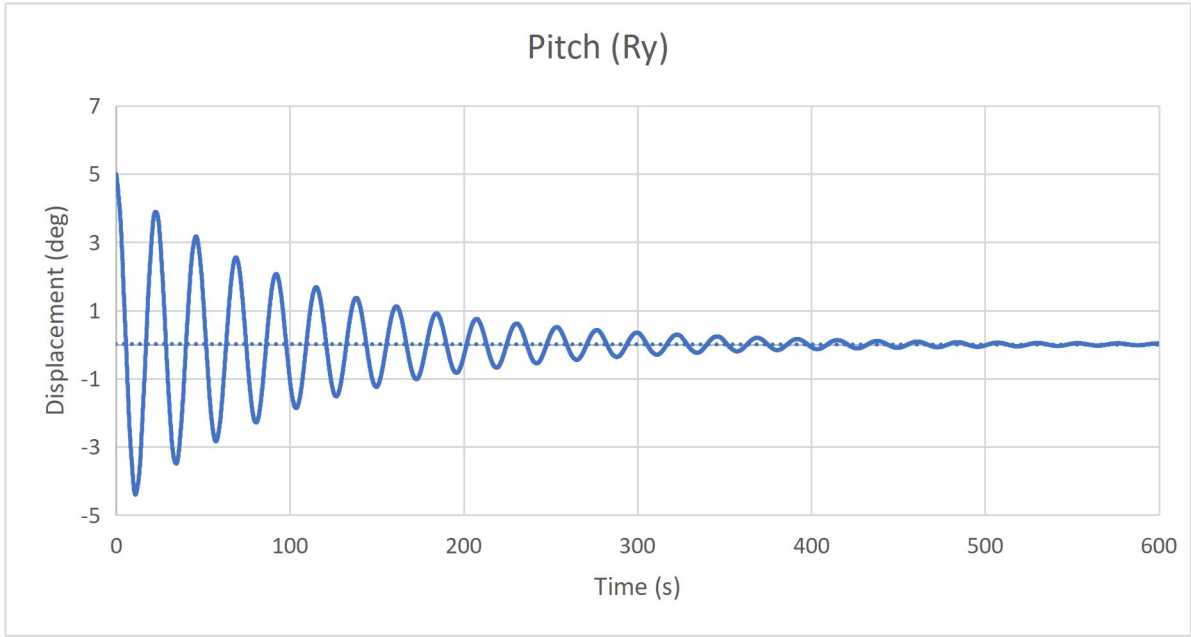


Figure 41: Decay test for Pitch

For the three analyzed DOFs, the natural frequencies are in excellent agreement. The moment in OrcaFlex and Aqwa set for the rotation in Roll and Pitch was 5 degrees and in Heave was set to 5 meters. In comparison to the OrcaFlex-AQWA model, there is only a 1.67% change in Heave, 0.89% in Pitch and a 2.27% of difference in Roll (see Table 13).



Table 13: Natural period comparison of the Estimated Values and OrcaFlex-AQWA models for the degrees of freedom of heave, pitch, and roll using decay tests

Natural Periods	ORCA-AQWA decay tests	Estimated Values	Difference
Heave	18.3 s	18.0 s	1.67 %
Pitch	22.3 s	22.5 s	0.89 %
Roll	23.0 s	22.5 s	2.27 %

The difference was initially represented with the identical values in both models, determining the damping level. At this time, the only comparison that can be made is to ensure that it is identical in both models and that the impact of radiation damping in the OrcaFlex-AQWA model is minimal. The Orca-AQWA natural periods with the hands on calculations matched after comparison which means that one can start the coupled assessment by calculating the DLCs.

The damping level is determined to be in the same order in all three circumstances, and the influence of radiation damping is small. This is not to say that radiation damping is not important in any case; it just means that it is not important for the specific instance of decaying motion observed in free decay testing. By computing RAOs curves in section 4.6, these impacts were adequately examined. Differences in the concrete tank effect the natural periods the most, while variations on the former bodies affect the heave natural period the most. Variations on the later bodies, on the other hand, have the greatest impact on the natural pitch period. Because of the column's placement on the base, they give extra buoyancy to the whole structure.

## 8.1 Coupled Analysis

Before starting the coupled analysis in OrcaFlex, one must check that the linear damping coefficients and quadratic damping coefficients are taken into account correctly and also one must check whether the structure is in equilibrium state or not. Initially, some cases with regular and irregular waves were computed in order to check the structure's behavior. Also,

some other cases including only the wind and only the waves were being determined in order to see how the structure behaves in different conditions.

The case for regular waves were calculated using Airy Waves and irregular waves were calculated using JONSWAP spectrum in OrcaFlex using 300 seconds to 600 seconds of transient which is also called Stage 0 and 3600 seconds for stage 1. The transient stage is the start of the simulation and it is the time which the numerical model takes to behave normally. On the other hand Stage 1 is the real simulation. The time 3600s (equivalent to one hour) was chosen initially to see the behavior in OrcaFlex before starting the real simulation for the DLCs (Design Load Cases) for almost 10800s (equivalent to three hours). The statistics do not change considerably over a three-hour period, and the seastate can be defined by significant wave height (Hs) and mean zero crossing period. According to DNV-RP-C205, "three hours has been imposed as a typical duration between registrations of sea states for monitoring waves". However, the period of stationary can range from 30 minutes to 10 or 12 hours.

DNV-RP-H103 also states three hours. So, after three hours, one can witness a maximum wave height that is statistically similar to that observed using 4 hour, 8 hour, and 12 hour, and so on of storm data. It's in order to capture all of the possible extreme values of sea. In most cases, three hours is statistically sufficient; any more than that is a waste of project time. However, for specific analyses (such as fatigue analysis), if one can show that a time length of less than three hours will yield statistically acceptable findings, then one must accept it but for this studies, complete three hours simulation yields acceptable results.

## **8.2 Design Load Cases**

In order to start the coupled analysis, one must understand what are the DLCs? In general, the strength of a wind turbine, its whole structure and platform designs are investigated in terms of both fatigue and ultimate loads during verification. Ultimate loading limits the design of various components. Extreme wind speeds with a parked rotor, lower wind speeds during operation where the influence of gusty wind is paired with a substantial periodic response, or specific occurrences such as start-up, shutdown, or during yawing can all result in ultimate loading [27].

For the S-bos structure, the DLCs 1.2, 1.6 and 6.1 are taken into account. This is a simplification since a complete set of DLCs are time consuming and it is not the purpose of the thesis. The DLC 1.2 is important to check the production, and 1.6 and 6.1 are the most common to easily check most of the parameters. The DLC 1.2 and 1.6 will require at least 10800s simulations, and the 50 year return wave data will be used. For the DLC 6.1, the turbine is parked and subjected to a 50-year return wind speed and wave specific height and period. For these simulations, a time of 10800s will be used. The Design load case consideration can be seen in the following Table 14

Table 14: DLCs (Design Load Cases) consideration for the Sbos Structure

Design Situation	DLC	Wind Condition V10min @147	Marine Condition				JONSWAP SPECTRA PARAMETERS
			Waves	Wind and wave directionality	Sea Currents	Water level	Gamma
1. Power Production	1.2	NTM 7.50 m/s	$H_s=1,5m$	180	No Currents	MSL	2.0
			$T_p=8$	180		MSL	2.0
		NTM 10.59 m/s	$H_s=1,5m$	180		MSL	2.0
			$T_p=8$	180		MSL	2.0
	NTM 14.00 m/s	$H_s=1,5m$	180	MSL		2.0	
		$T_p=8$	180	MSL		2.0	
1.6	NTM 10.59 m/s	$H_s=5.11m$ and $T_p=11.08s$	180	0.57	MSL	2.0	
6. Parked (standing still os idilling)	6.1	EWM 37.41 m/s	$H_s=5.11m$ and $T_p=11.08s$	180	0.57	MSL	2.0

In the Table 17, the significant wave height ( $H_s$ ) and peak period ( $T_p$ ) for DLC 1.2 is taken into account by interpolating the data used in chapter 3. The wind speed for DLC 1.2 are taken as 7.50 m/s a speed below rated wind speed. 10.59 m/s rated wind speed, 14.00 m/s above rated wind speed. On the other hand the significant wave height ( $H_s$ ) and peak period ( $T_p$ ) in DLC 1.6 and 6.1 for Extreme sea state of 50 yr. return period, with Current speed which is obtained from Flotant [28].

### 8.3 Parameters and Calculation for the DLCs

For the DLC 1.2, it is very important that the significant wave height ( $H_s$ ) and peak period ( $T_p$ ) for Normal Turbulent Model (NTM) are calculated perfectly. After that one must interpolate the value of wind speed in order to get the best result. As wind speed profiles have been calculated in accordance with the recommendations of ISO 19901 by using Eq. (8.5),

$$U(z) = U(o). [1 + C. \ln\left(\frac{z}{10}\right)] \quad (8.5)$$

Whereas:

$$C = 5.73 \cdot 10^{-2} \cdot (1 + 0.5 \cdot U(o))^{0.5} \quad (8.6)$$

And  $U(o)$  is the one hour mean speed at 10m. For all the DLCs the values for the wind speed are interpolated from this equation and calculated values can be seen in the Table 15 for the DLC 1.2 at NTM for the wind speeds 7.5 m/s, 10.59 m/s, 14 m/s, for the DLC 1.6 NTM for the wind speed 10.59 m/s and for the DLC 6.1 EWM 37.41 m/s:

Table 15: Ref. mean wind speed calculation for all considered DLCs

Ref. Mean Wind Speed at NTM 7.5 m/s for DLC 1.2	6.02 m/s
Ref. Mean Wind Speed at NTM 10.59 m/s for DLC 1.2	8.35 m/s
Ref. Mean Wind Speed at NTM 14 m/s for DLC 1.2	10.86 m/s
Ref. Mean Wind Speed at NTM 10.59 m/s for DLC 1.6	8.35 m/s
Ref. Mean Wind Speed at EWM 37.41 m/s for DLC 6.1	26.56 m/s

These ref. mean wind speed values, significant wave height and Peak period values are then input in the OrcaFlex environment section by using Jonswap spectrum to start the simulation which lasts for three hours (10800s). For the DLCs 1.6 and 6.1, one must consider the currents as the current is important for the excursion of the platform and the value for the current speed is taken from this document publically available [28]. Also, to calculate the value for the current force applied on the S-bos platform, one must calculate the submerged area for the platform as it has been shown in Figure 42:

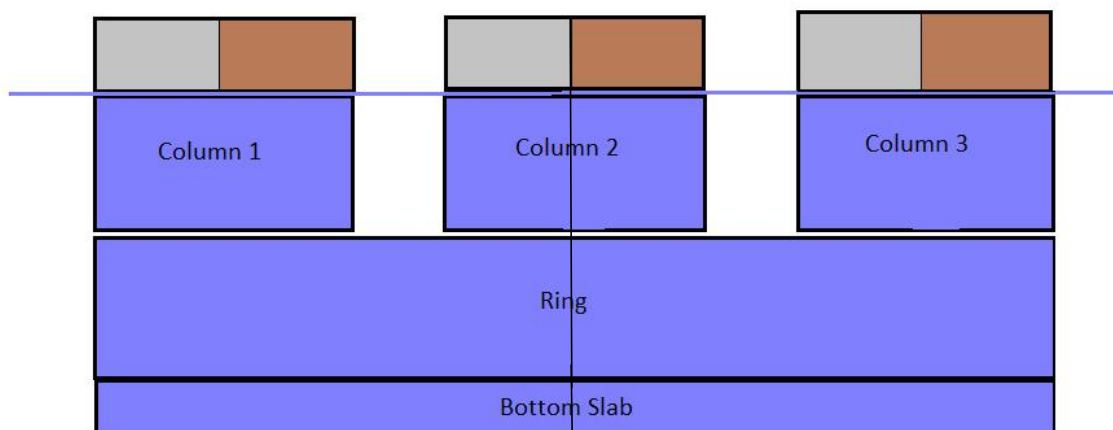


Figure 42: Submerged area consideration for S-bos Platform corner view

The Total submerged area calculated is 1752 m<sup>2</sup> and current speed is 0.57 m/s. The drag coefficient is calculated as an inclined square at 45° which is 2.4 as shown in the Figure 42:

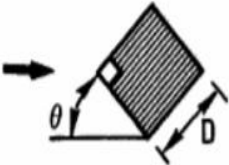
5. Inclined square 	$\theta$	0	5	10	15	20	25	30	35	40	45
	$C_D$	2.2	2.1	1.8	1.3	1.9	2.1	2.2	2.3	2.4	2.4
	$R_e \sim 4.7 \times 10^4$										

Figure 43: Drag coefficient consideration (Source: DNV-RP-C205)

The force applied on the S-bos platform by currents for the DLCs 1.6 and 6.1 is calculated using the Eq. (8.7)

$$F_{Current} = \frac{1}{2} \cdot A \cdot C_d \cdot \rho \cdot V^2 \tag{8.7}$$

The parameters and the calculation for the total force induced by the currents on the S-bos platform is shown in the Table 16:

Table 16: Calculation of the force applied on the S-bos platform induced by currents for the DLCs 1.6 and 6.1

Parameters	Values	Units
Water density ( $\rho$ )	1.025	t/m <sup>3</sup>
Current speed (V)	0.57	m/s
Drag Coefficient (Cd)	2.4	-
Submerged Area (A)	1752	m <sup>2</sup>
<b>Total Force applied by Currents</b>	700.15	kN

The current force is applied at the corner on the platform as illustrated in the Figure 42 for the calculation of DLCs 1.6 and 6.1, the value for the current force applied on the structure will then be input in OrcaFlex as one have to mention currents as well but for the DLC 1.2 this step is not required.

## 8.4 Results and Discussions

For each DLC the simulation time was given 10800s (equivalent to three hours) and it was calculated for each DLC separately in order to achieve the best result. . In order to analyze the results, there are some parameters which are to be analyzed which are Mean Pitch, MPME Pitch (MPME referred as Most Probable Maximum value at Extreme condition), MPME Heave, Mean Surge, MPME Surge, Hub Acceleration, Mean Bending moment (Tower base), MPME Bending Moment (Tower Base), Mean Line tension, MPME Line Tension and Mean Generator Power and here MPME means most probable maximum value at extreme. In the following sections all the calculated DLCs are well explained and discussed.

### 8.4.1 DLC 1.2 NTM 7.5 m/s Hs 1.5m and Tp 8s

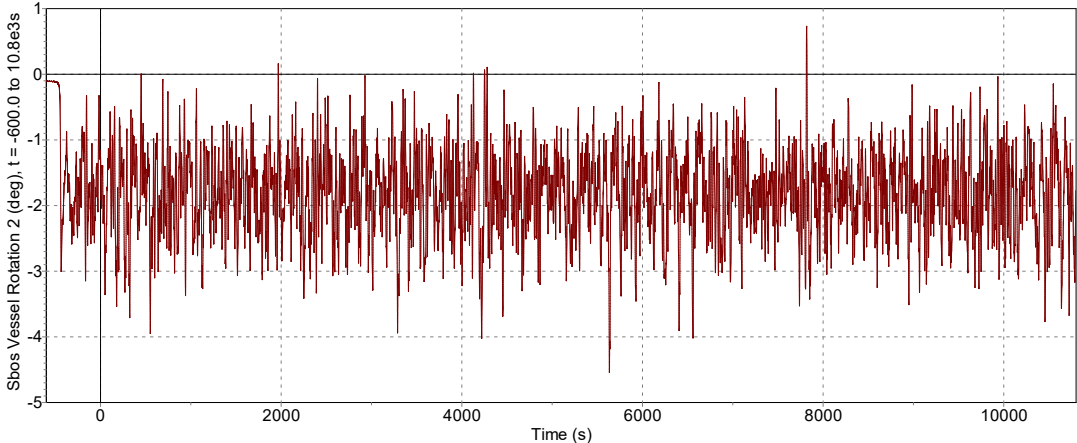


Figure 44: PITCH for DLC 1.2 NTM 7.5 m/s, Hs 1.5m and Tp 8s

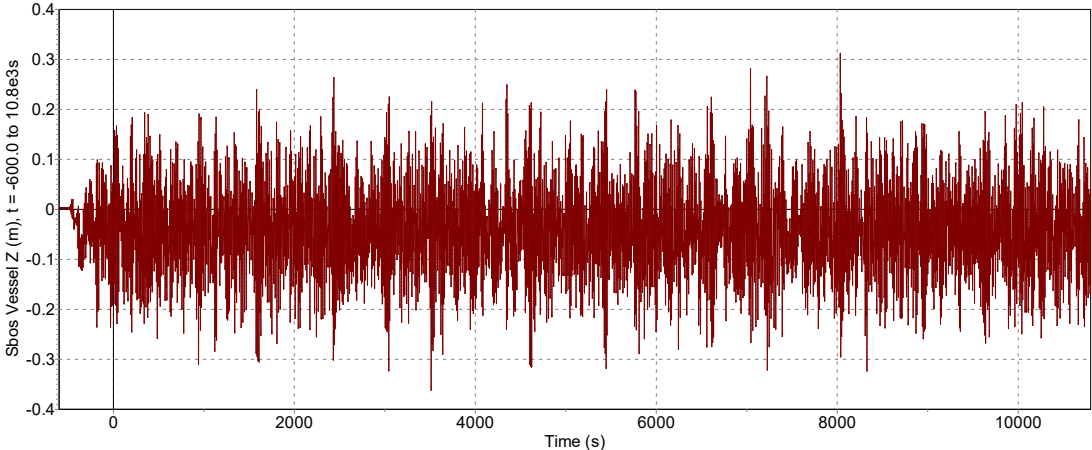


Figure 45: MPME Heave for DLC 1.2 NTM 7.5 m/s, Hs 1.5m and Tp 8s

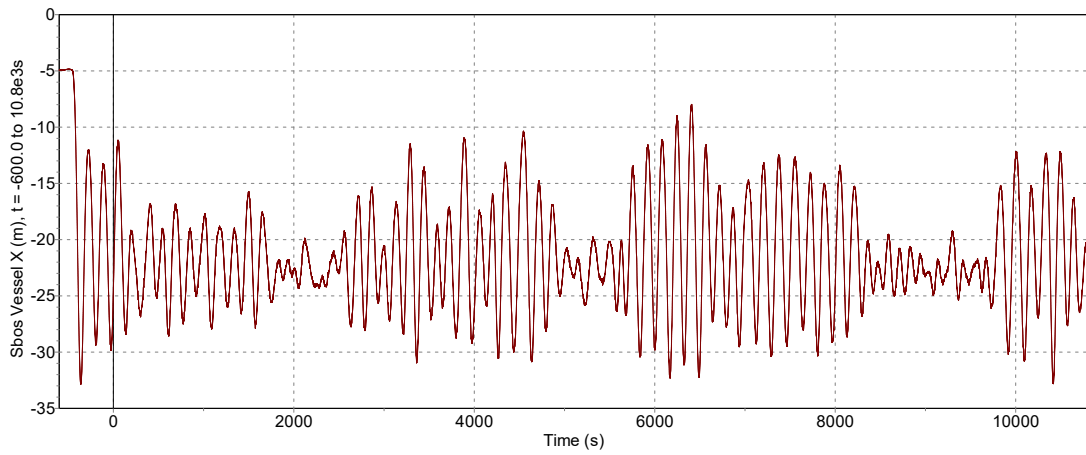


Figure 46: MPME Surge for DLC 1.2 NTM 7.5 m/s, Hs 1.5m and Tp 8s

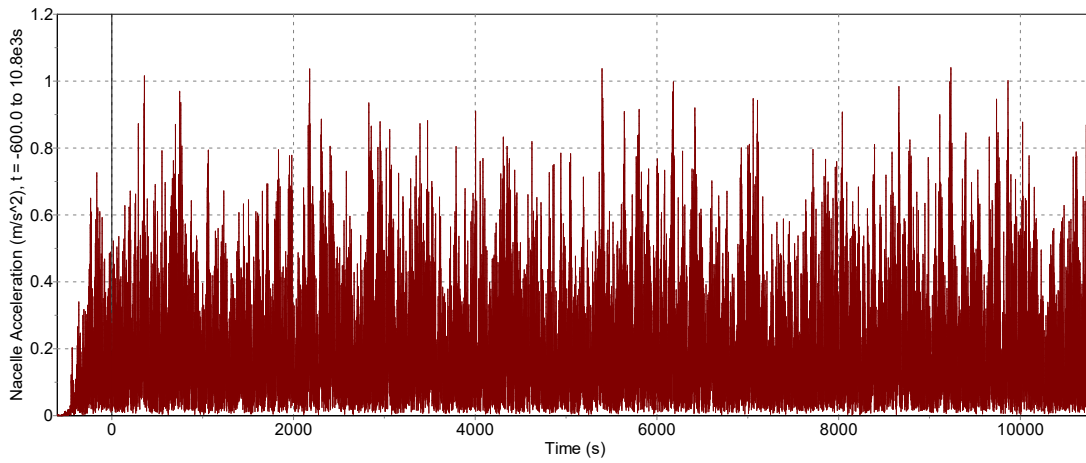


Figure 47: Hub Acceleration for DLC 1.2 NTM 7.5 m/s, Hs 1.5m and Tp 8s

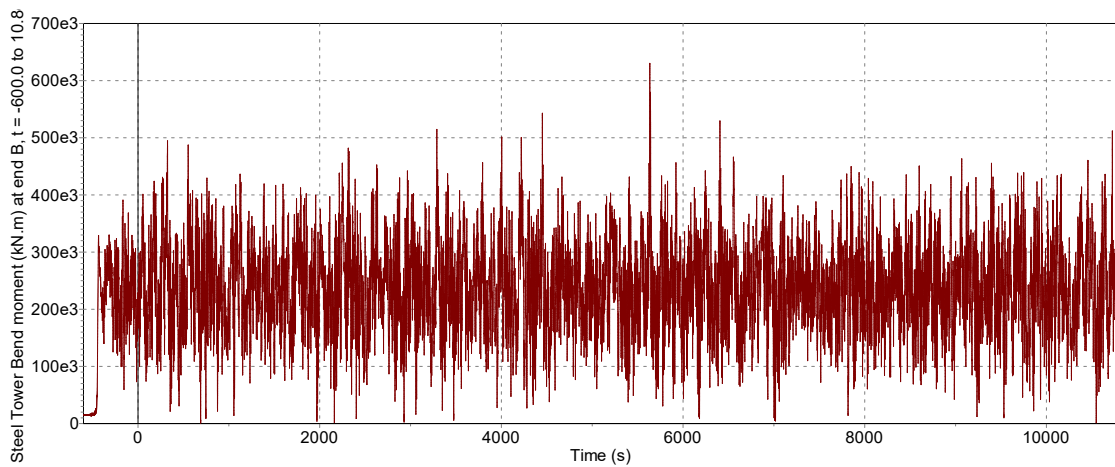


Figure 48: MPME Bending Moment (Tower Base) for DLC 1.2 NTM 7.5 m/s, Hs 1.5m and Tp 8s

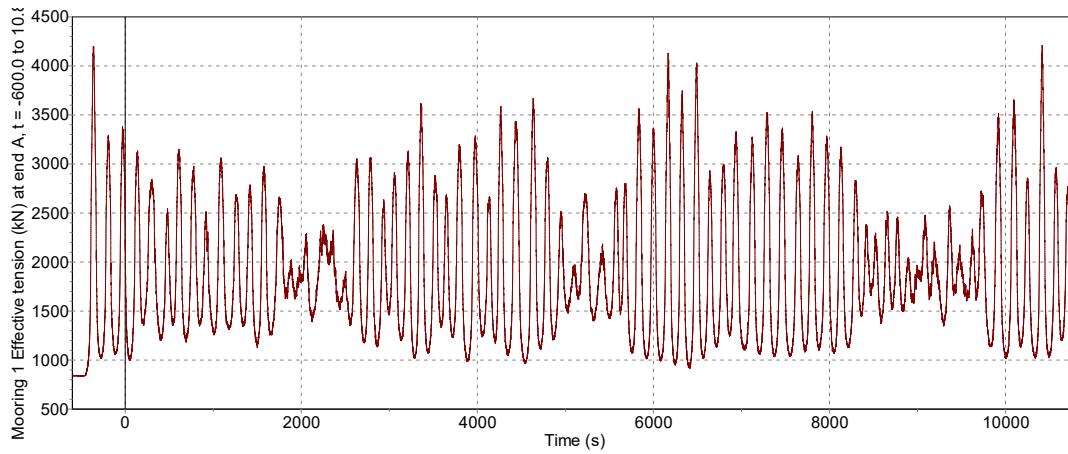


Figure 49: MPME Line Tension for DLC 1.2 NTM 7.5 m/s, Hs 1.5m and Tp 8s

Table 17: Parameters calculated for DLC 1.2 NTM, 7.5 m/s, Hs 1.5m and Tp 8s

Parameters	Value	Unit
Mean Pitch	-1.81	[deg]
MPME Pitch	-4.07	[deg]
MPME Heave	0.28	[m]
Mean Surge	-21.67	[m]
MPME Surge	-35.85	[m]
Hub Acceleration	0.90	[m/s <sup>2</sup> ]
Mean Bending moment (Tower base)	2.37E+05	[kNm]
MPME Bending Moment (Tower Base)	5.38E+05	[kNm]
Mean Line tension	1884.18	[kN]
MPME Line Tension	4003.90	[kN]
Mean Generator Power	5819.04	[kW]



8.4.2 *DLC 1.2 NTM 10.59 m/s, Hs 1.5m and Tp 8s*

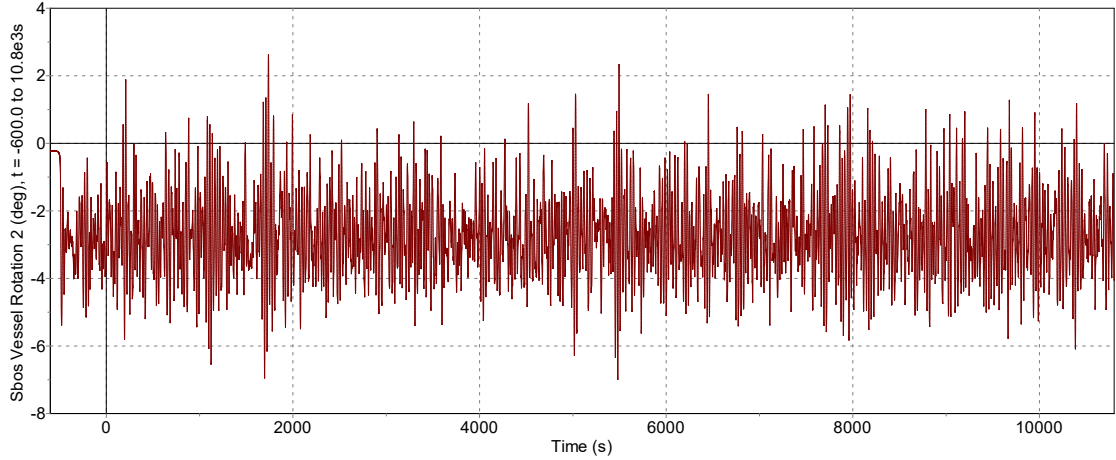


Figure 50: MPME Pitch for DLC 1.2 NTM 10.59 m/s, Hs 1.5m and Tp 8s

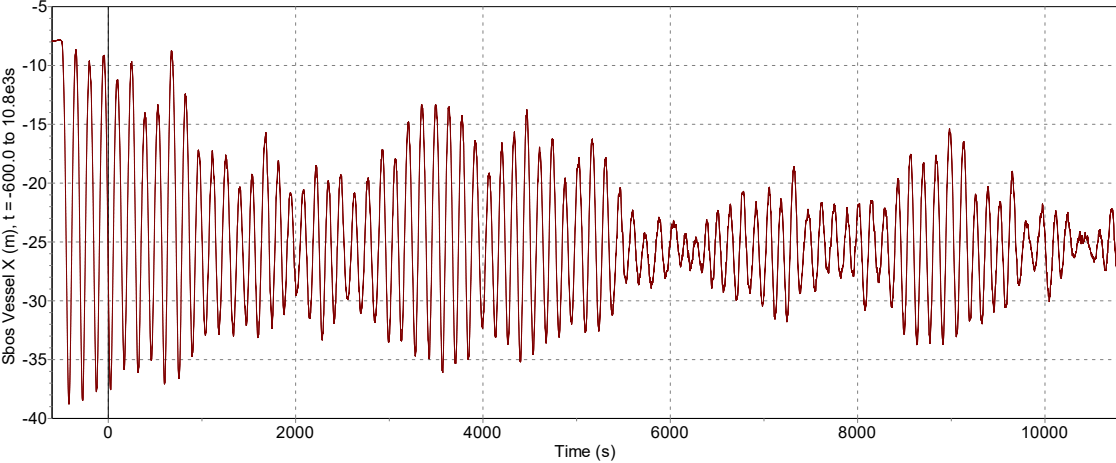


Figure 51: MPME Surge for DLC 1.2 NTM 10.59 m/s, Hs 1.5m and Tp 8s

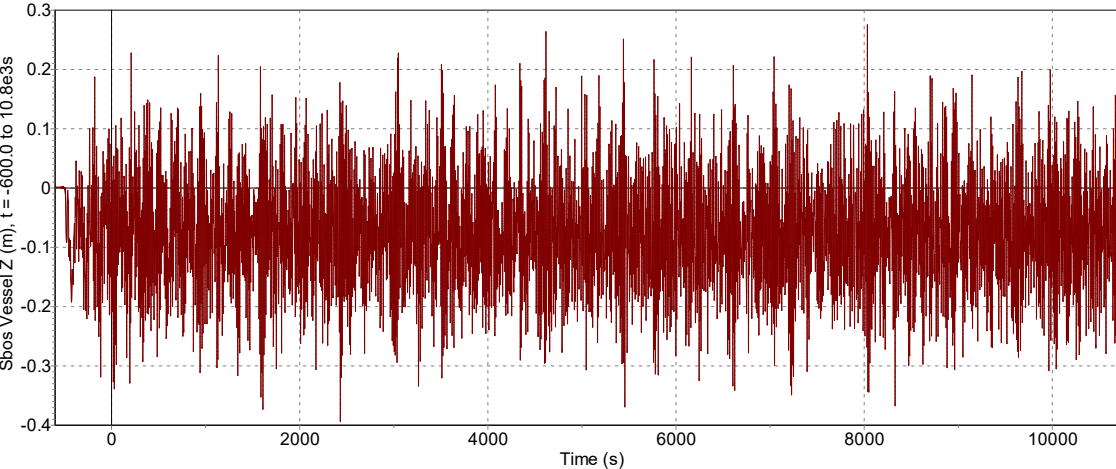


Figure 52: MPME Heave for DLC 1.2 NTM 10.59 m/s, Hs 1.5m and Tp 8s

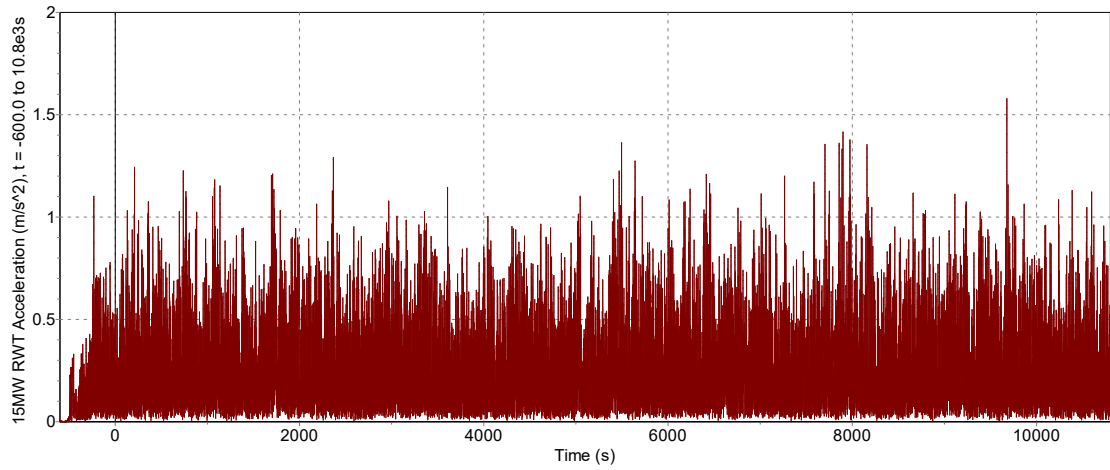


Figure 53: Hub Acceleration for DLC 1.2 NTM 10.59 m/s, Hs 1.5m and Tp 8s

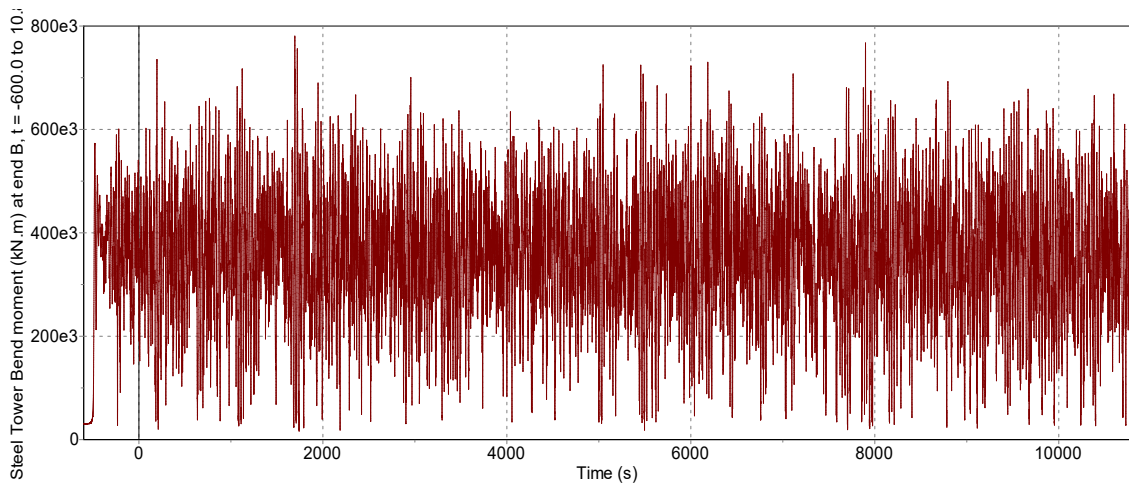


Figure 54: MPME Bending Moment (Tower Base) for DLC 1.2 NTM 10.59 m/s, Hs 1.5m and Tp 8s

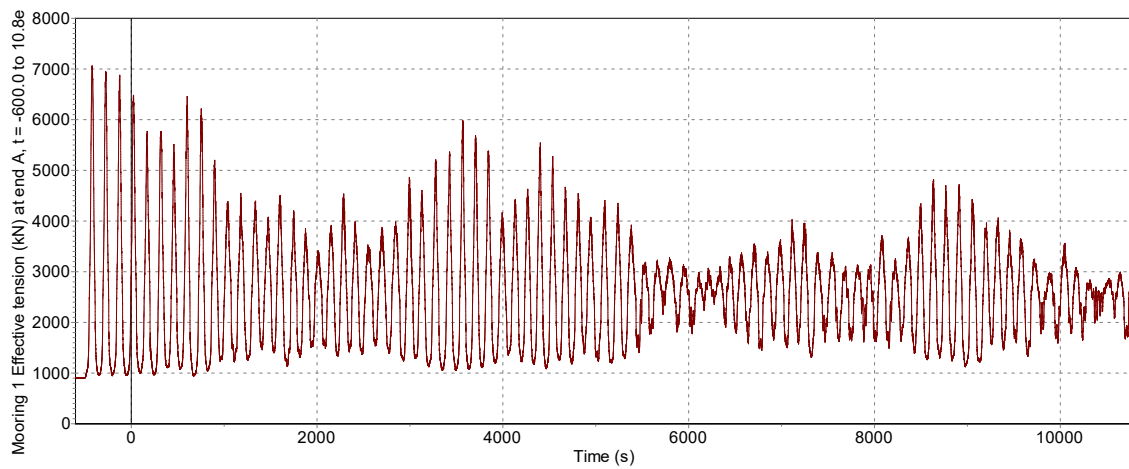


Figure 55: MPME Line Tension for DLC 1.2 NTM 10.59 m/s, Hs 1.5m and Tp 8s

Table 18: Parameters calculated for DLC 1.2 NTM 10.59 m/s, Hs 1.5m and Tp 8s

Parameter	Value	Unit
Mean Pitch	-2.70	[deg]
MPME Pitch	-7.08	[deg]
MPME Heave	0.26	[m]
Mean Surge	-25.01	[m]
MPME Surge	-41.38	[m]
Hub Acceleration	1.13	[m/s <sup>2</sup> ]
Mean Bending moment (Tower base)	3.55E+05	[kNm]
MPME Bending Moment (Tower Base)	8.17E+05	[kNm]
Mean Line tension	2553.45	[kN]
MPME Line Tension	5811.72	[kN]
Mean Generator Power	1.36E+04	[kW]

#### 8.4.3 DLC 1.2 NTM 14.00 m/s, Hs 1.5m and Tp 8s

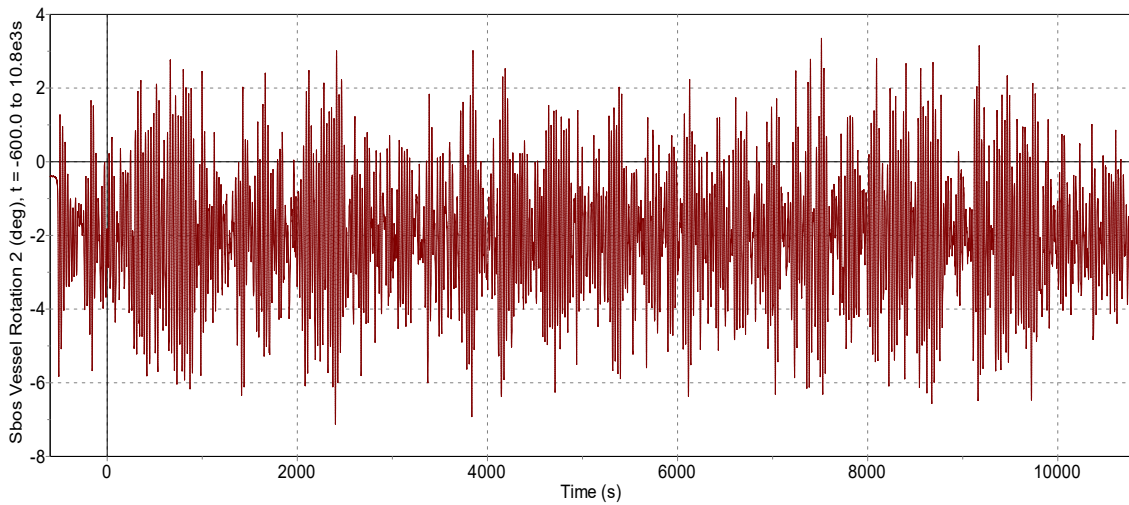


Figure 56: MPME Pitch for DLC 1.2 NTM 14 m/s, Hs 1.5m and Tp 8s

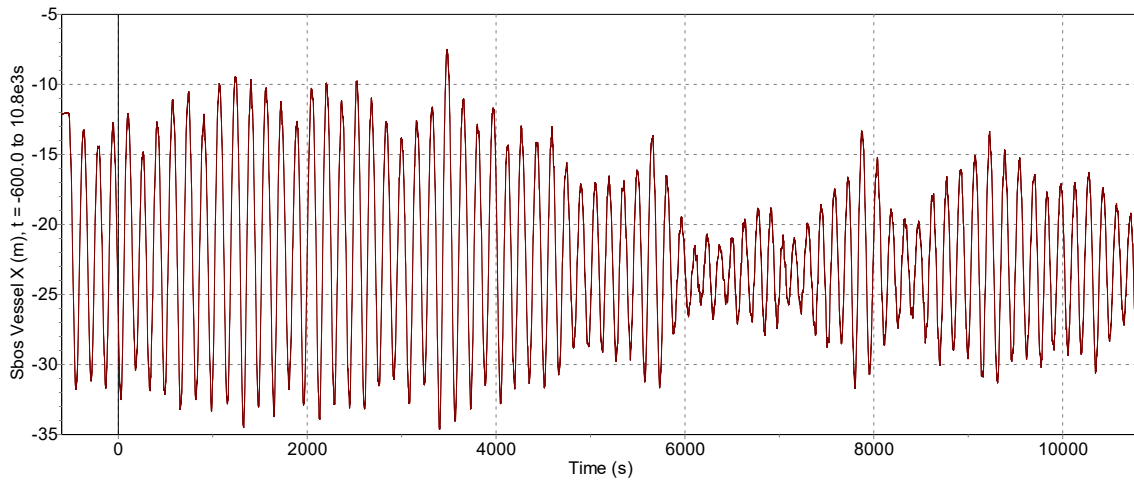


Figure 57: MPME Surge for DLC 1.2 NTM 14 m/s, Hs 1.5m and Tp 8s

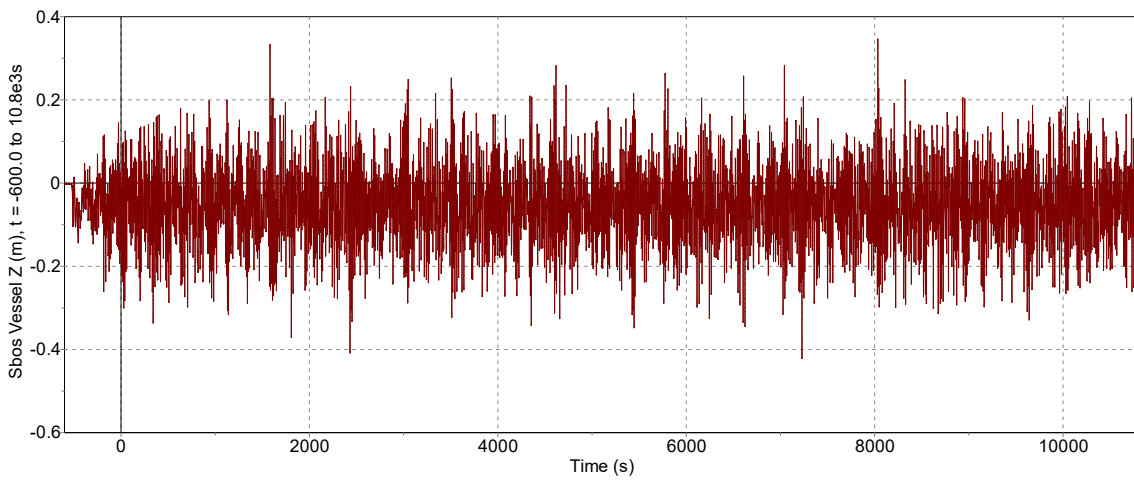


Figure 58: MPME Heave for DLC 1.2 NTM 14 m/s, Hs 1.5m and Tp 8s

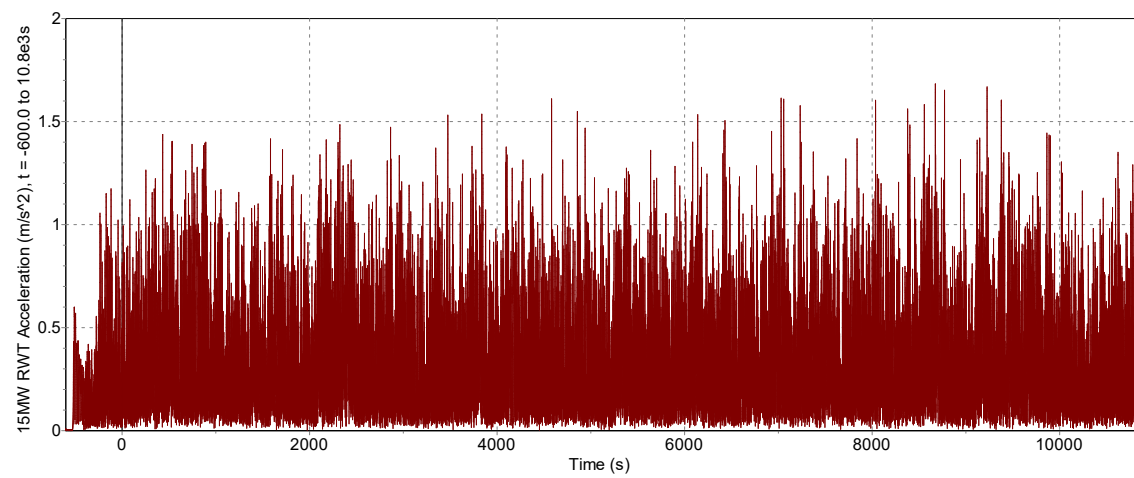


Figure 59: Hub Acceleration for DLC 1.2 NTM 14 m/s, Hs 1.5m and Tp 8s

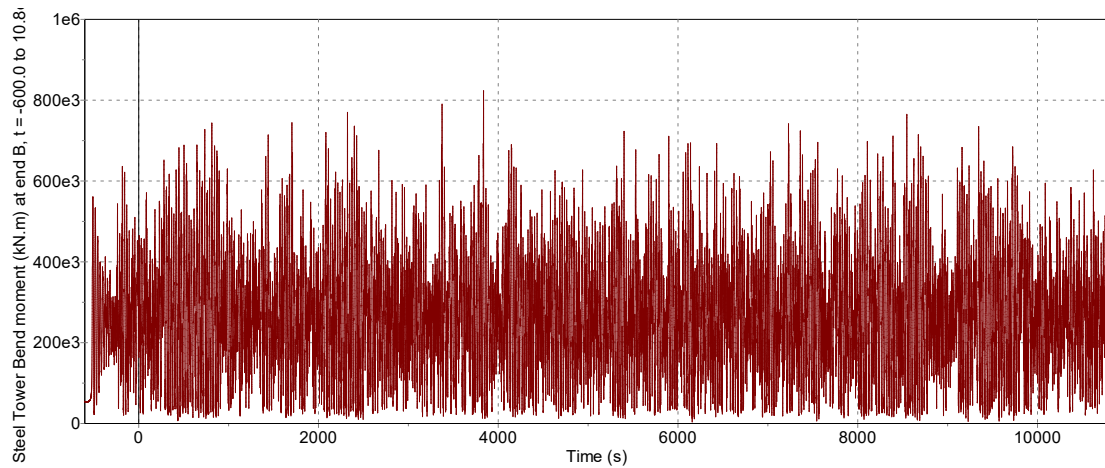


Figure 60: MPME Bending Moment (Tower Base) for DLC 1.2 NTM 14 m/s, Hs 1.5m and Tp 8s

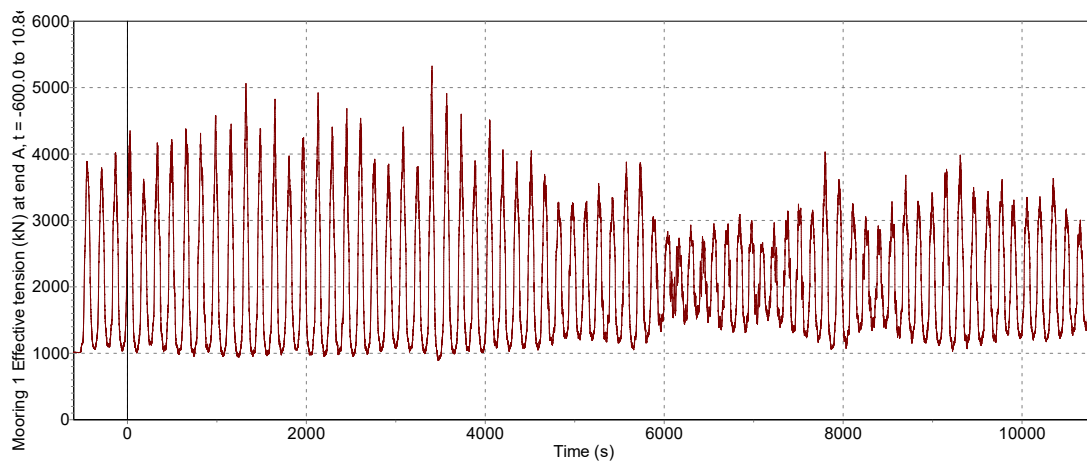


Figure 61: MPME Line Tension for DLC 1.2 NTM 14 m/s, Hs 1.5m and Tp 8s

Table 19: Parameters calculated for DLC 1.2 NTM 14 m/s, Hs 1.5m and Tp 8s

Parameter	Value	Unit
Mean Pitch	-2.00	[deg]
MPME Pitch	-7.90	[deg]
MPME Heave	0.29	[m]
Mean Surge	-22.25	[m]
MPME Surge	-39.42	[m]
Hub Acceleration	1.42	[m/s <sup>2</sup> ]
Mean Bending moment (Tower base)	2.71E+05	[kNm]
MPME Bending Moment (Tower Base)	8.13E+05	[kNm]
Mean Line tension	2088.81	[kN]
MPME Line Tension	4920.45	[kN]
Mean Generator Power	1.49E+04	[kW]

8.4.4 *DLC 1.6 NTM 10.59 m/s, Hs 5.11m and Tp 11.08s*

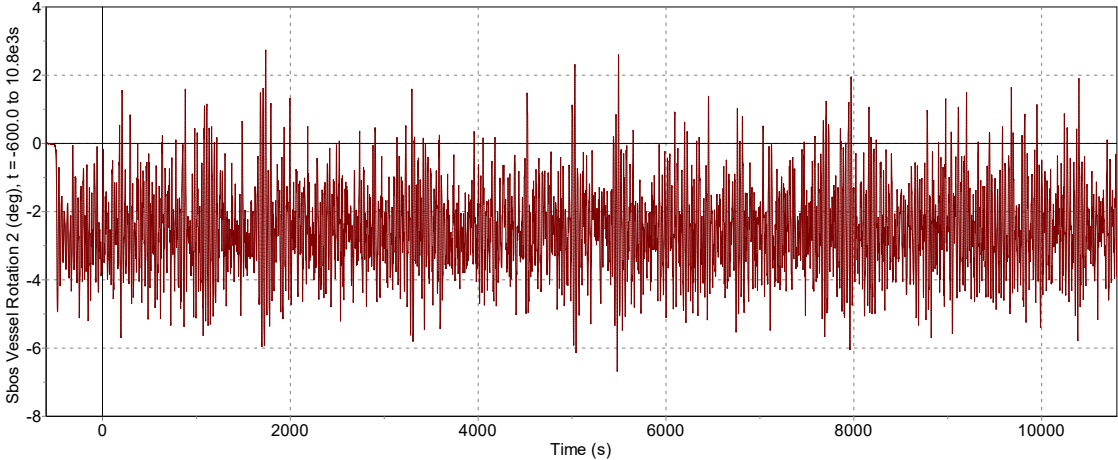


Figure 62: MPME Pitch for DLC 1.6 NTM 10.59 m/s, Hs 5.11m and Tp 11.08s

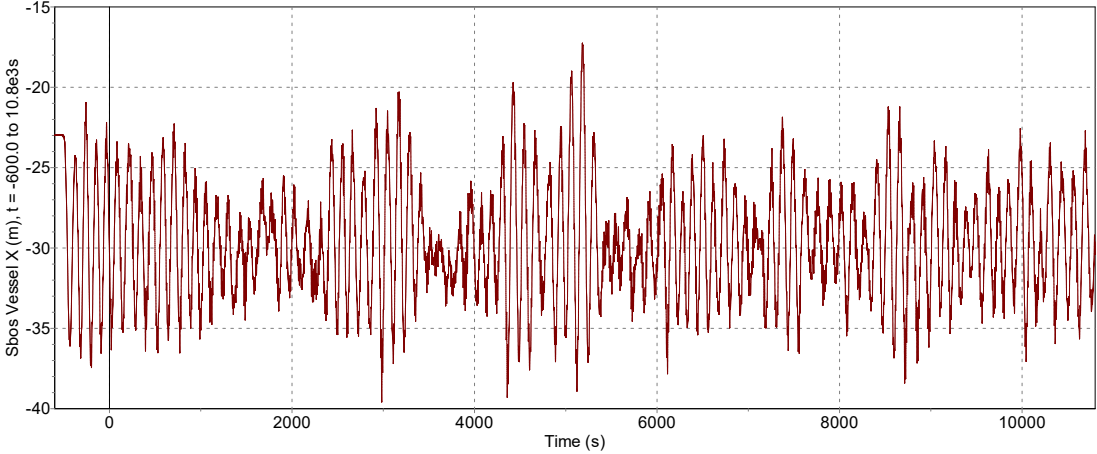


Figure 63: MPME Surge for DLC 1.6 NTM 10.59 m/s, Hs 5.11m and Tp 11.08s

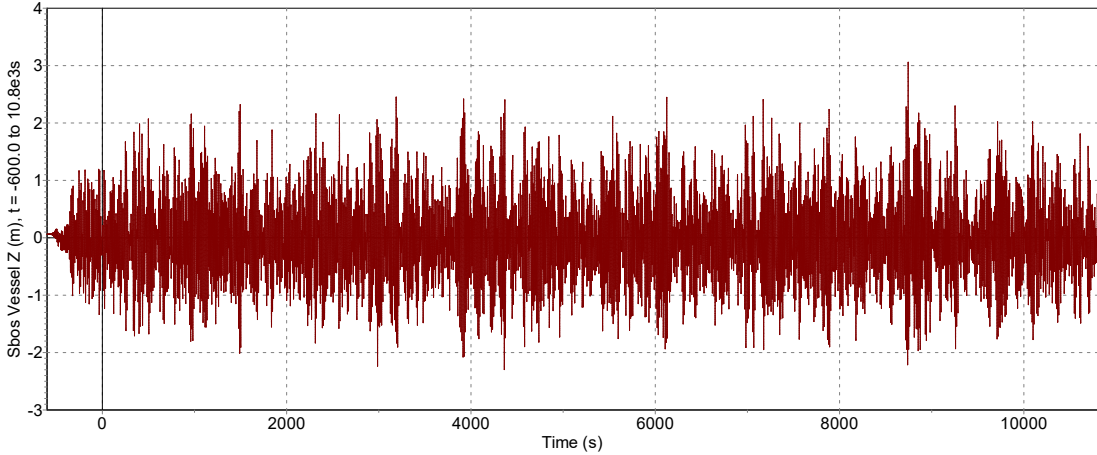


Figure 64: MPME Heave for DLC 1.6 NTM 10.59 m/s, Hs 5.11m and Tp 11.08s

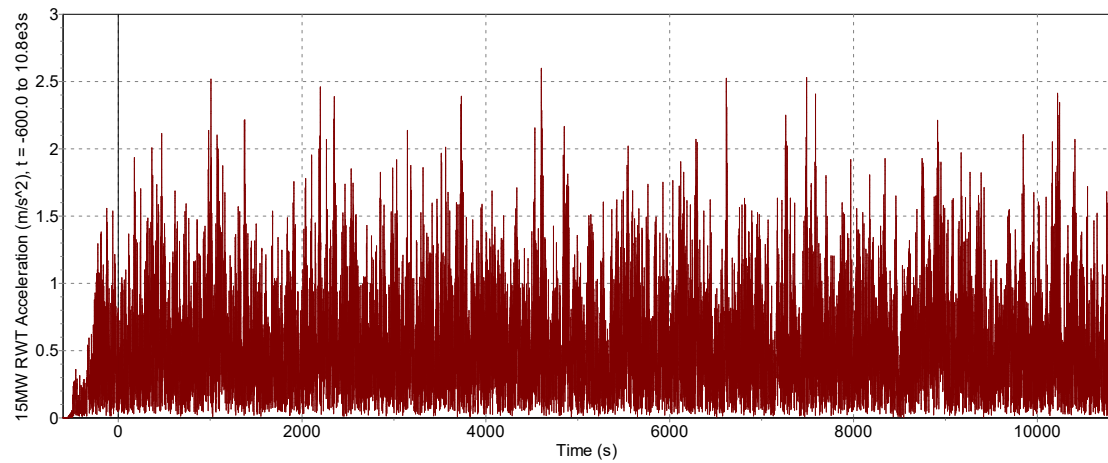


Figure 65: Hub Acceleration for DLC 1.6 NTM 10.59 m/s, Hs 5.11m and Tp 11.08s

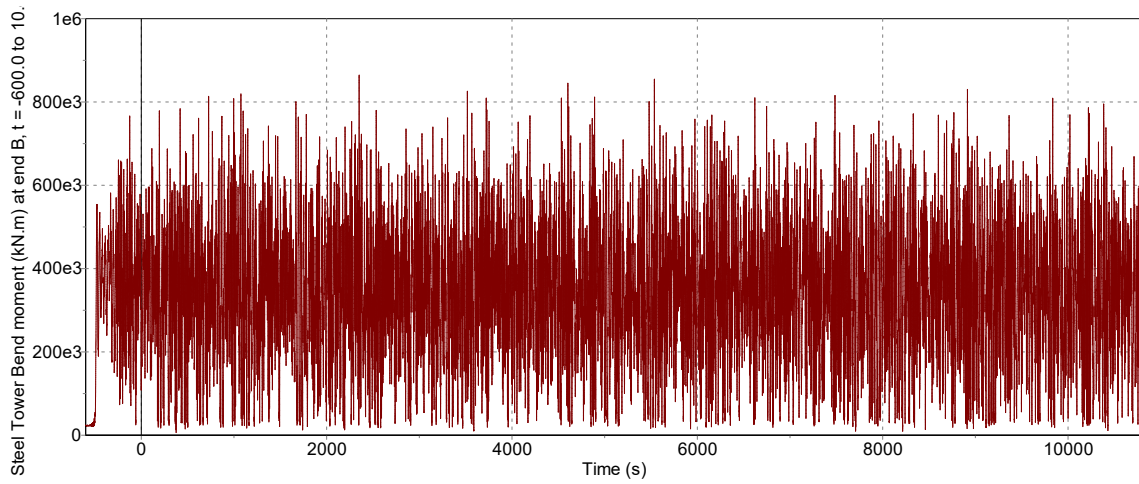


Figure 66: MPME Bending Moment (Tower Base) for DLC 1.6 NTM 10.59 m/s, Hs 5.11m and Tp 11.08s

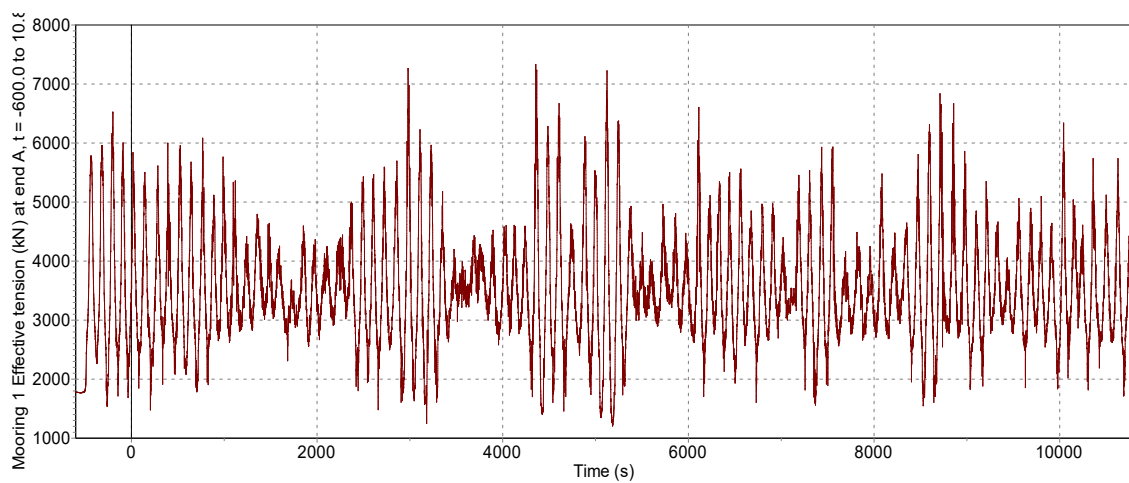


Figure 67: MPME Line Tension for DLC 1.6 NTM 10.59 m/s, Hs 5.11m and Tp 11.08s

Table 20: Parameters calculated for DLC 1.6 NTM 10.59 m/s, Hs 5.11m and Tp 11.08s

Parameters	Value	Unit
Mean Pitch	-2.50	[deg]
MPME Pitch	-7.05	[deg]
MPME Heave	2.65	[m]
Mean Surge	-29.68	[m]
MPME Surge	-40.88	[m]
Hub Acceleration	2.03	[m/s <sup>2</sup> ]
Mean Bending moment (Tower base)	3.49E+05	[kNm]
MPME Bending Moment (Tower Base)	9.48E+05	[kNm]
Mean Line tension	3533.52	[kN]
MPME Line Tension	6704.90	[kN]
Mean Generator Power	1.36E+04	[kW]

#### 8.4.5 DLC 6.1 EWM 37.41 m/s, Hs 5.11m and Tp 11.08s

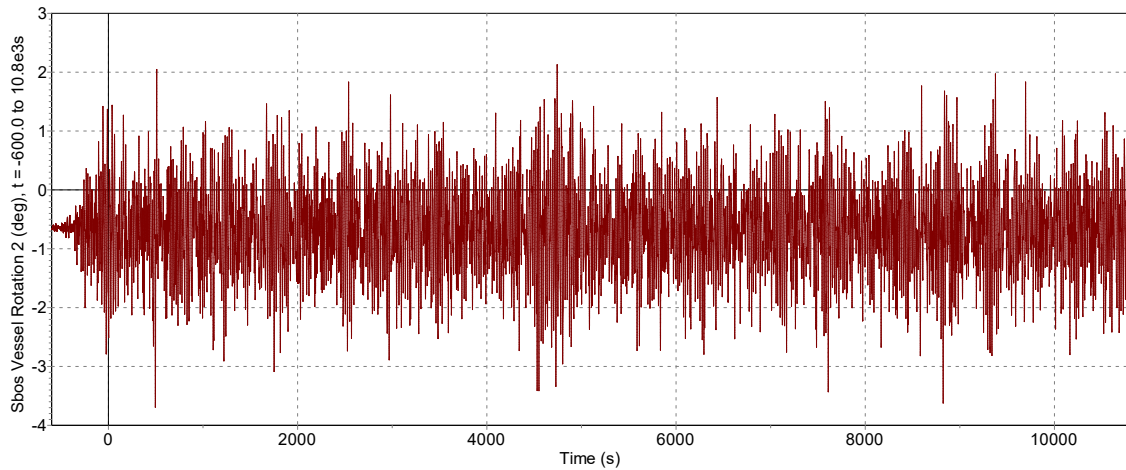


Figure 68: MPME Pitch for DLC 6.1 EWM 37.41 m/s, Hs 5.11m and Tp 11.08s



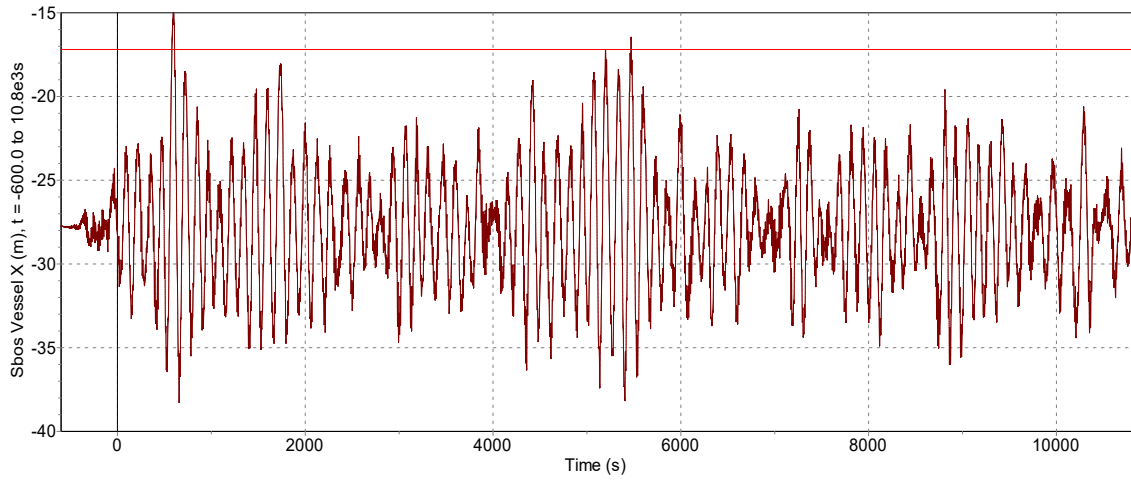


Figure 69: MPME Surge for DLC 6.1 EWM 37.41 m/s, Hs 5.11m and Tp 11.08s

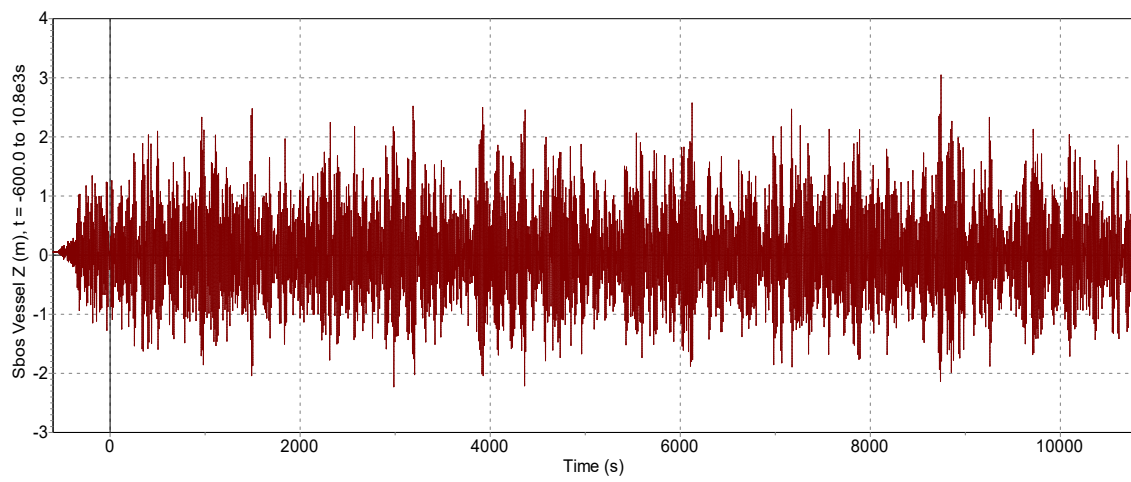


Figure 70: MPME Heave for DLC 6.1 EWM 37.41 m/s, Hs 5.11m and Tp 11.08s

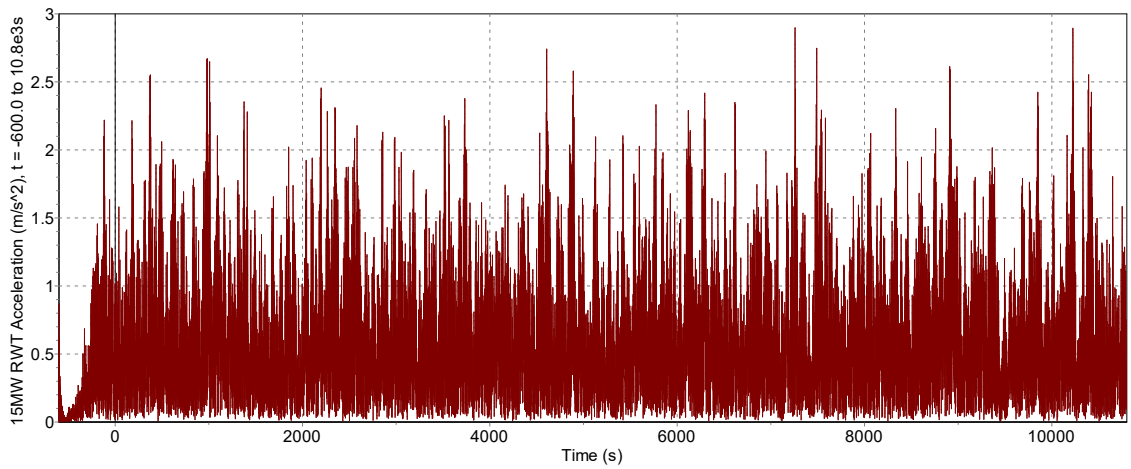


Figure 71: Hub Acceleration for DLC 6.1 EWM 37.41 m/s, Hs 5.11m and Tp 11.08s

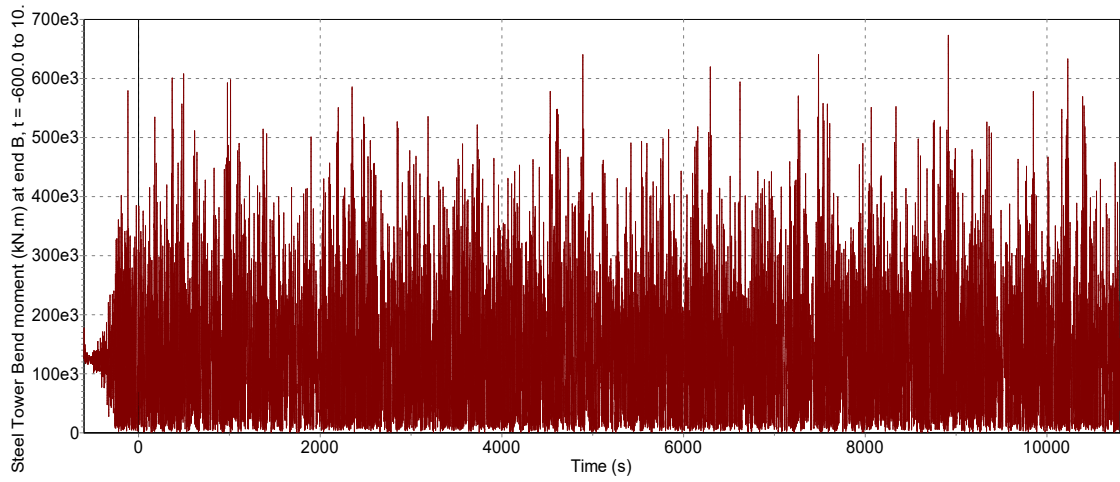


Figure 72: MPME Bending Moment (Tower Base) for DLC 6.1 EWM 37.41 m/s, Hs 5.11m and Tp 11.08s

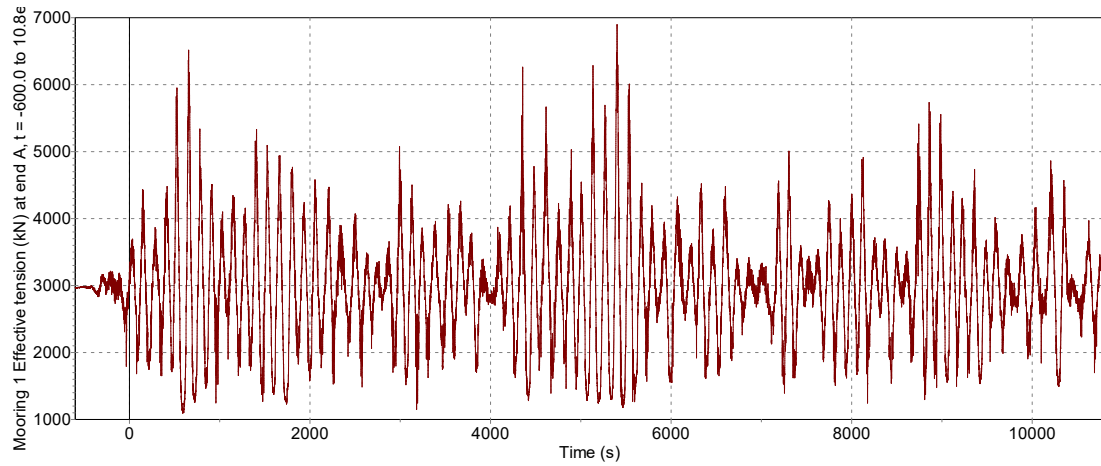


Figure 73: MPME Line Tension for DLC 6.1 EWM 37.41 m/s, Hs 5.11m and Tp 11.08s

Table 21: Parameters calculated for DLC 6.1 EWM 37.41 m/s, Hs 5.11m and Tp 11.08s

Parameter	Value	Unit
Mean Pitch	-0.68	[deg]
MPME Pitch	-3.42	[deg]
MPME Heave	2.72	[m]
Mean Surge	-27.76	[m]
MPME Surge	-38.24	[m]
Hub Acceleration	2.20	[m/s <sup>2</sup> ]
Mean Bending moment (Tower base)	1.54E+05	[kNm]
MPME Bending Moment (Tower Base)	5.60E+05	[kNm]
Mean Line tension	2980.64	[kN]
MPME Line Tension	5740.49	[kN]
Mean Generator Power	0	[kW]

#### **8.4.6 Discussion of the Results**

The first thing to notice is that from -600s to 0s is the stage 0 which is also referred as transient zone. Mean pitch is important as it is the effect of wind on the turbine that can result in tower inclination and also decrease in energy productivity that is why this parameter is taken into account. Among the six degrees of freedom motions, the mean surge and mean pitch motions have the most influence. Mean Bending moment was also an important parameter to find the bending moment at any critical cross section in order to take into account the shear also, if not, the platform or the tower can collapse. On the other hand line tension was considered as snap loads dominate the extreme tension in the mooring lines of a light displacement platform in shallow water. This is because the line's light pre-tension requirements may be insufficient to keep the mooring lines from being exposed to wave motion-induced slack and shock events. The wind turbine will be designed to be shut down if the hub acceleration exceed a safety tolerance. As this parameter is important for the control of the RNA. That is why it is also included for the analysis.

For that purpose it was noticed that the time given from 0s to 10800s was the real simulation time which is referred as stage 1. In order to analyze the results, static pitch value lies between -1.81 deg to -2.50 deg for DLC 1.2 and 1.6 as it can be seen in the Table 17, Table 18, Table 19 and Table 20. On the other hand the static pitch for the DLC 6.1 is -0.68 deg and it can be seen in Table 21. In OrcaFlex, as the pitch is negative in all the cases, so one must select lower tail in OrcaFlex instead of upper tail for the Rayleigh distribution to analyze MPME Pitch (MPME referred as Most Probable Maximum value at Extreme condition) as Rayleigh distribution is the commonly used parameter in this industry. While accessing the results in OrcaFlex, if upper tail value is included, one cannot get the maximum value of the pitch as pitch in this case is negative so lower tail is considered.

The three hours most probable maximum value of Pitch for DLC 1.2 is varying for all the wind speeds but it shows a great contradiction and for the DLC 6.1 it shows almost the same behavior in the DLC 1.2 and 1.6 which is -4.07 deg to -7.05 deg, can be seen in Table 17, Table 18, Table 19 and Table 20 and it is a good result as it shows the structure is behaving as expected.

For the Heave, the statics mean value is almost zero for all considered DLCs as the platform is continuously moving up and down. For the Heave at extreme condition in order to analyze most probable maximum value at extreme of heave, the calculated value varies for all DLCs from 0.26 m to 2.72 m. The Figure 45, Figure 52, Figure 58, Figure 64 and Figure 70 represents the center of gravity position at heave moment for the considered DLCs.

The mean for the surge varies from -21.67 m to -29.68 m for the DLC 1.2 and 1.6 referred in Table 17, Table 18, Table 19 and Table 20. But for the DLC 6.1 the mean of the surge decreases at extreme condition and the value is -27.76 m, see Table 21. The values for the surge are negative because the system of reference makes the moments with the waves in negative direction as this reference was set in OrcaFlex. The three hours most probable maximum value (MPME) for Surge for DLC 1.2 and 1.6 is varying for all the wind speeds from -35.85 m to -40.88 m but it shows a good result at extreme condition and for the DLC 6.1 which is -38.24 m.

In case of Hub Acceleration, the statics mean value is almost zero for all considered DLCs as the nacelle is moving with respect to platform and it is also continuously moving up and down. In the current simulation the maximum accelerations occur further into the simulation time. The value for the hub acceleration for the DLC 1.2, 1.6 and 6.1 varies from  $0.90 \text{ m/s}^2$  to  $2.20 \text{ m/s}^2$  as shown in Table 17, Table 18, Table 19, Table 20 and Table 21. This shows that the hub acceleration represents absolute values as the Figure 47 and Figure 71 doesn't represents in which direction is the acceleration effects that is why every datum in the Figure 47, Figure 53, Figure 59, Figure 65 and Figure 71 is positive which represents that the values are absolute. Also these graphs shows the absolute acceleration of the rotor for each moment.

For the bending moment of the S-bos platform, initially it is to be observed at which end the tower is placed on the platform in the OrcaFlex. After that the static mean value is calculated which is varying from  $2.37\text{E}+5 \text{ kNm}$  to  $3.49\text{E}+5 \text{ kNm}$  for the DLC 1.2 and 1.6 for all wind speeds as shown in Table 17, Table 18, Table 19 and Table 20 but for the DLC 6.1 in Table 21, it shows very good result as the bending moment is perfect in extreme condition. The three hours most probable maximum value (MPME) for mean bending moment at Tower base for DLC 1.2 is varying for all the wind speeds from  $5.38\text{E}+5 \text{ kNm}$  to  $9.48\text{E}+5 \text{ kNm}$  but it shows a good result and for the DLC 6.1 which is  $5.60\text{E}+5 \text{ kNm}$ .

In order to analyze the line effective tension at mooring lines, initially it is to be observed at which end the mooring is placed on the fairlead in the OrcaFlex. The results are analyzed for the 1<sup>st</sup> mooring line as it is the in-line mooring and it is in the direction of the forces. For the mean static result in Table 17, Table 18, Table 19 and Table 20 the value of effective line tension for the DLC 1.2 and 1.6 lies between 1884.18 kN to 3533.52 kN and for the DLC 6.1 it gives 2980.64 kN, see Table 21. The three hours most probable maximum value (MPME) for line effective tension for DLC 1.2 and 1.6 is varying for all the wind speeds from 4003 kN to 6704 kN but it shows a good result and for the DLC 6.1 which is 5740 kN.

**8.4.7. Generator power for DLCs 1.2, 1.6 and 6.1**

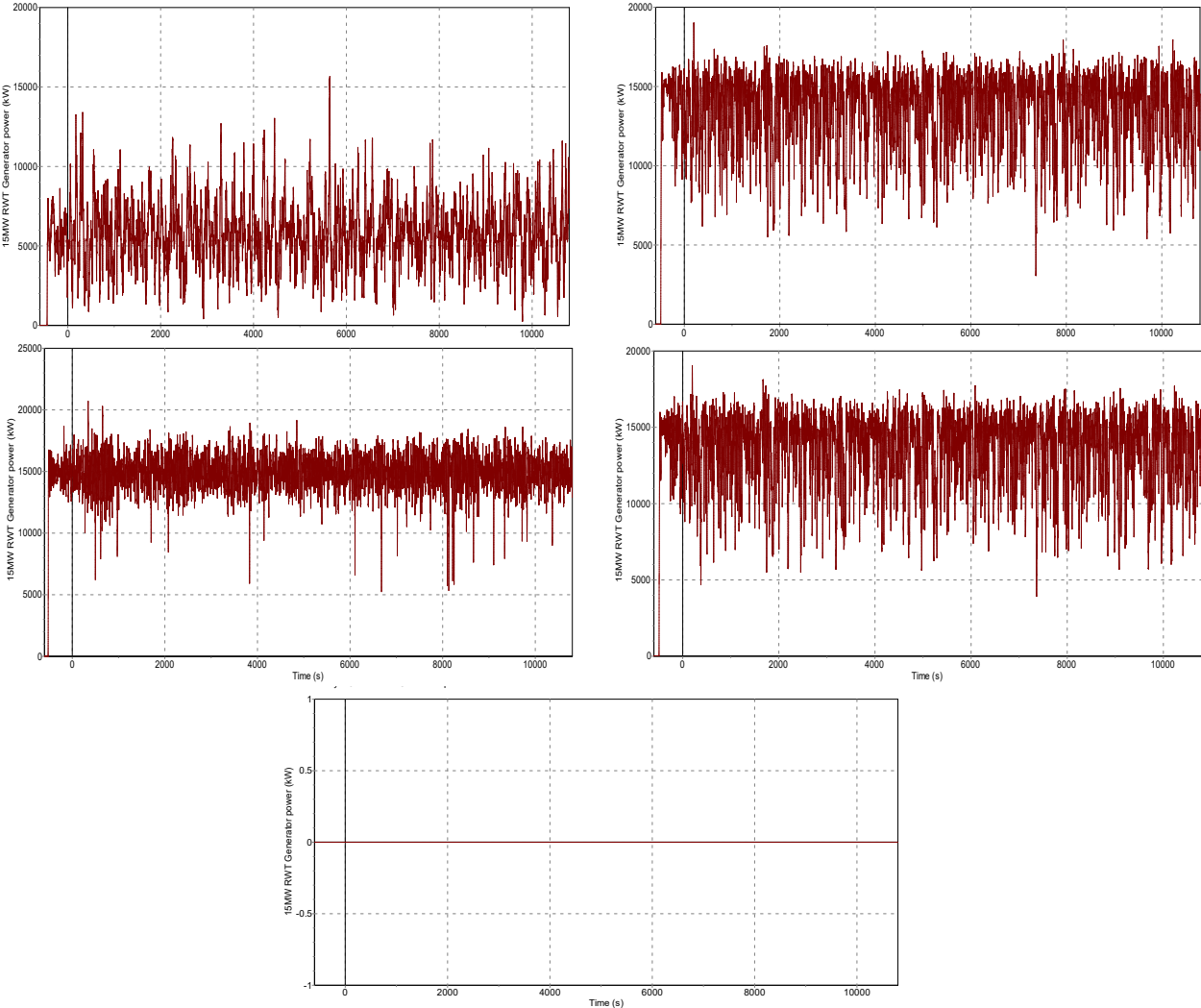


Figure 74: Generator power for DLCs 1.2, 1.6 and 6.1 by showing Generator power

It can be seen in the Figure 74 that the generated power for the S-bos with the reference turbine IEA 15MW is providing an output of an average around 2000 kW. The contribution of S-bos platform with IEA 15MW turbine gives good results in extreme conditions as well as in the normal conditions but it does not considers electrical losses. It can be observed that in all the loading conditions the turbine gives complete required output when analyzing generator power but for the DLC 6.1 it shows 0 as it is in parked condition and it is not generating power, the reason is because the DLC 6.1 is an external load condition and the platform is not operating in this condition.

## 9. Future Work

The geometry of the S-bos platform is not yet finalized. In the future, further shape choices will be examined. The next step in this project would be to do a full set-up and testing of the wind turbine controller to ensure that stability is maintained under various loading circumstances.

Tank testing have not yet been completed, and the numerical model will be calibrated based on those results. After that, the entire set of DLCs will be completed. The controller set-up analysis performed thus far is in no way complete. This study, on the other hand, should be viewed as a preliminary assessment of wind turbine control strategies for this wind turbine and floating platform system. The mooring system used in this study is also a preliminary system. Therefore, a complete mooring analysis is also required for the future.

To recalculate the platform's mass properties, a structural check is required. Because the geometry and design will vary in the future, the controller will need to be re-tuned. Only then the design loop will be completed for the S-bos to enter in the real-time industry.

## 10. Conclusion

The Aero-Hydro-Servo-Elastic numerical modeling (Coupled analysis) of the system composed of the IEA 15MW Reference Wind Turbine mounted on the S-bos platform was the subject of this work. The numerical models were evaluated against estimated outcomes using two hydrodynamic methodologies and then implemented them using ANSYS-AQWA for frequency domain analysis and OrcaFlex for the time domain analysis and their comparison with the estimated values computed in order to validate the AQWA-ORCA numerical model.

The primary issues of a semi-submersible platform was designing a robust enough structure to withstand wave stresses and cost-effective structure for transportation and installation purposes. The S-bos platform is designed to float semi-submerged on the water surface and uses buoyancy stabilization with the help of its four columns. It is simple to transport and install, even in shallow water conditions, because of the low draft. The movements of the platform had an impact on the wind turbine. The cause of wave loading was assumed to be regular sinusoidal waves. To compute the motion of a floating structure in irregular waves, linearly superimposing the data from several normal waves was employed to produce realistic findings on sea states.

In order to conclude the moments for the S-bos structure, after around 19 seconds in Heave, the greatest response in x-axis in the wave period and this period was very close to the natural period calculated which was 18 seconds and it shows a good comparison. For longer durations, the heave response converged to one, and the structure will move in heave with an amplitude equal to the wave amplitude for long waves. The heave reaction does not amplify or diminish over time.

The project's controller is a conventional PI (Proportional- Integral) with additional filters to reduce structural frequency interference in the rotational speed data. In order to gain-schedule, the controller has the ability to alter the blade controller's gain based on its operating point.

The mooring model is implemented in OrcaFlex via an external system using a quasi-static or dynamic approach. The quasi static multi-segmented mooring method (MSQS) is utilized in the quasi static mooring model to compute the mooring force. It was concluded that the use of



a dynamic mooring system is essential to adequately reflect the interplay between wave loading, mooring lines, and the S-bos floating platform.

Estimated values for the natural periods were calculated by hand calculation. Natural periods were checked and added masses were calculated in AQWA. On the other hand the free decay tests for the numerical models for Heave, Pitch, and Roll were computed for the S-bos model, in order to fine-tune the Full OrcaFlex model natural frequencies. Linear damping coefficients in Roll and Pitch, and the Quadratic Damping coefficient in Heave were calculated using the hydrostatics stiffness matrices. Linear damping was calculated as a certain percentage of the critical damping. Quadratic term was calculated by the estimation of certain drag coefficient in a certain degrees on freedom Natural frequencies are in great accord for all three DOFs concentrated for this study. A fine comparison between AQWA-ORCA model and estimated values was seen to initiate the coupled assessment.

The Design load cases (DLCs) 1.2, 1.6, and 6.1 were taken into account for the S-bos platform with 15 MW IEA reference wind turbine with RNA, in order to analyze coupled analysis. The DLC 1.2 was necessary for analyzing the production, and the DLC 1.6 and 6.1 were the most frequent for analyzing the majority of the parameters quickly. But if full set of DLC 1.2 were simulated and analyzed among others, one can analyze other important things such as the fatigue of the mooring. In both extreme and typical situations, the S-bos platform with the IEA 15MW turbine produces good performance. The four columns provides good buoyancy and the structure have good hydrodynamic behavior. The turbine delivers good output in all loading situations.

## References

1. European Wind Energy Association, "86 Million Europeans to get power from the wind by 2010"; News release: October 7, 2003.
2. Walt Musial. Floating wind turbines on the rise, NREL. 2020. *Technical Report*
3. Eslam Energy, Horns Rev Offshore Wind Farm homepage, www.hornsrev.dk: March **2003**.
4. Bertacchi, P., Di Monaco, A., Gerloni, M., Ferranti, G., "Eolomar - a moored platform for wind turbines"; *Wind Engineering* Vol. **18**, No. 4, p**189** (1994).
5. Esteban, M.D.; López-Gutiérrez, J.S.; Negro, V.; Matutano, C.; García-Flores, F.M.; Millán, M.A. Offshore wind foundation design: Some key issues. *J. Energy Resour. Technol.* **2014**, 137, 1–6.
6. S. Butterfield, W. Musial, J. Jonkman, and P. Sclavounos. Engineering challenges for floating offshore wind turbines wind resource assessment in global climate stabilization scenarios. Technical report, National Renewable Energy Laboratory, 2007.
7. Design of floating offshore wind turbine concepts (International Renewable Energy Agency [IRENA], 2016 and Global energy transformation paper, 2019)
8. Sea-to-land ratios of ultimate loads from DLCs 1.1, 1.3, 1.4 and 1.5 for the MIT/NREL TLP, OC3-Hywind Spar and ITI Energy Barge (Source: NREL)
9. NWTC Certification Committee, *Guideline DG01: Wind Turbine Design Load Analysis*, Golden, CO: National Renewable Energy Laboratory, 2003.
10. Sclavounos, P., **13.022** *Surface Waves and Their Interaction with Floating Bodies, Lecture Notes*, Cambridge, MA: Massachusetts Institute of Technology, 2002.

11. Review of modelling challenges associated with floating wind turbines see Matha, M Schlipf, et al. (2011)
12. Manwell, J. F., McGowan, J. G., Rogers, A. L., *Wind Energy Explained*, New York, NY: John Wiley & Sons, 2002.
13. A.N. Robertson, F. Wendt, J.M. Jonkman, W. Popko, H. Dagher, S. Gueydon, J. Qvist, F. Vittori, J. Azcona, and E. Uzunoglu. Oc5 project phase ii: Validation of global loads of the deepcwind floating semisubmersible wind turbine. Technical report, Technical University of Denmark, 2017.
14. J. R. Morison, M. P. O'Brien, J. W. Johnson, and S. A. Schaaf. The force exerted by surface waves on piles. Technical report, University of California Berkely, 1950.
15. Michael Borg and Henrik Bredmose. Qualification of innovative floating substructures for 10mw wind turbines and water depths greater than 50m. Technical report, Technical University of Denmark, 2015
16. Torben J. Larsen, Anders Yde, David Verelst, Mads M. Pedersen, Anders M. Hansen, and Hans Fabricius Hansen. Benchmark comparison of load and dynamics of a floating 5mw semi-sub wind turbine, using three different hydrodynamic approaches. Technical report, Technical University of Denmark, 2014.
17. By R. C. MacCamy and R. A. Fuchs. Wave forces on piles: A diffraction theory. Technical report, Beach Erosion Board Corps of Engineers, 1954.
18. Maija A. Benitz, David P. Schmidt, Matthew A. Lackner, Gordon M. Stewart, Jason Jonkman, and Amy Robertson. Comparison of hydrodynamic load predictions between reduced order engineering models and computational fluid dynamics for the OC4-deepcwind semi-submersible. Technical report, American Society of Mechanical Engineers, 2014.

19. H.Aa.Madsen, N N Srensen, C Bak, N Troldborg, and G Pirrung. Measured aerodynamic forces on a full scale 2mw turbine in comparison with ellipsys3d and HAWC2 simulations. Technical report, Technical University of Denmark, 2018.
20. OrcaFlex-Vessel theory: RAOs and phases, Displacements RAOs (Orcina), 2021
21. Faltinsen, O. M. Sea Loads on Ships and Offshore Structures. Cambridge University Press, 1990.
22. Michael Olivier Chrolenko, Dynamic Analysis and Design of Mooring Lines, Norwegian University of Science and Technology, Technical report, Department of Marine Technology, 2013
23. Hall, M.; Goupee, A. Validation of a lumped-mass mooring line model with DeepCwind semisubmersible model test data. *Ocean Eng.* **2015**, 104, 590–603.
24. Yu-Hsien Lin \* and Cheng-Hao Yang, Hydrodynamic Simulation of the Semi-Submersible Wind Float by Investigating Mooring Systems in Irregular Waves, Technical report, 2020
25. Evan Gaertner<sup>1</sup>, Jennifer Rinker<sup>2</sup>, Latha Sethuraman, Definition of the IEA Wind 15-Megawatt Offshore Reference Wind Turbine, Technical Report
26. Johan N. Stander, Gerhard Venter, and Maarten J. Kamper. “Review of direct-drive radial flux wind turbine generator mechanical design.” In: *Wind Energy* 15.3 (2012), pp. 459–472. DOI: 10.1002/we.484.
27. Peter Hauge Madsen, Kirk Pierce† and Marshall Buhl†, PREDICTING ULTIMATE LOADS FOR WIND TURBINE DESIGN, AIAA-99-0069, pp. 1, American Institute of Aeronautics and Astronautics.
28. Lara Cerdán (EST), Carlos Cortés (EST), D.4.1 – STRUCTURAL AND NAVAL ARCHITECTURE DESIGN BASIS, pp 51, Technical report of Floatant